D-33192
Version 5.0

# Earth Observing System (EOS)
# Tropospheric Emission Spectrometer (TES)

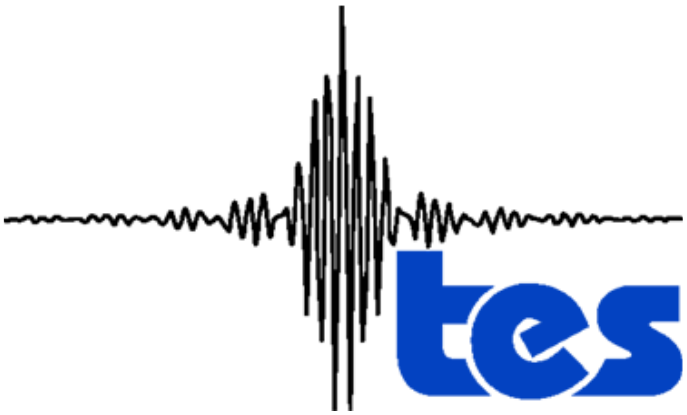


# Data Validation Report
## (Version F06_08, F06_09 data)


### Editors:

Robert Herman and Gregory Osterman

### Contributors:

Christopher Boxe, Kevin Bowman, Karen Cady-Pereira, Tony Clough, Annmarie Eldering, Brendan Fisher, Dejian Fu, Robert Herman, Daniel Jacob, Line Jourdain, Susan Kulawik, Michael Lampel, Qinbin Li, Jennifer Logan, Ming Luo, Inna Megretskaia, Ray Nassar, Gregory Osterman, Susan Paradise, Vivienne Payne, Hank Revercomb, Nigel Richards, Mark Shephard, Dave Tobin, Solene Turquety, Felicia Vilnrotter, Kevin Wecht, Helen Worden, John Worden, Lin Zhang


April 8, 2012


**JPL**
Jet Propulsion Laboratory
California Institute of Technology
Pasadena, California

# Earth Observing System (EOS)
# Tropospheric Emission Spectrometer (TES)

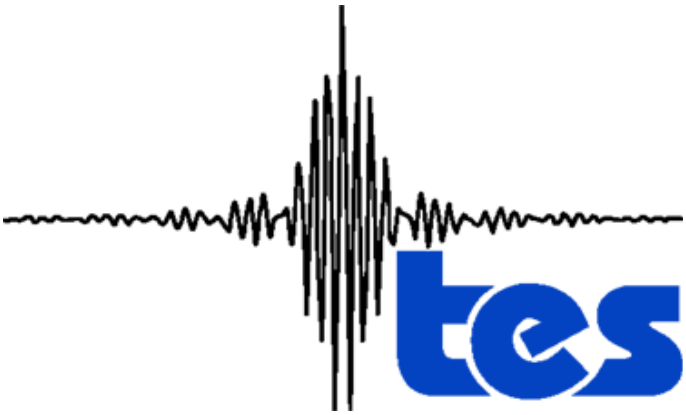


# Data Validation Report
# (Version F06_08, F06_09 data)

**Approved by:**

| | |
|---|---|
| John Worden<br>TES Principal Investigator<br>Jet Propulsion Laboratory | Douglas Shepard<br>TES Ground Data Systems Manager<br>Jet Propulsion Laboratory |

## Revision History:

| Version | Date | Description/Comments |
|---|---|---|
| 1.0 | 8/15/2005 | Initial Version of Validation Report for time frame "launch + 1 year" |
| 2.0 | 1/4/2007 | Validation Report for F03_03 data |
| 3.0 | 11/5/2007 | Validation Report for F04_04 data |
| 4.0 | 11/23/2011 | Validation Report for F05_05, F05_06, F05_07 data |
| 5.0 | 4/8/2012 | Validation Report for F06_08, F06_9 data |

## TABLE OF CONTENTS

## LIST OF FIGURES

## LIST OF TABLES

# 1. Overview or TES Product Validation

This document is intended to provide our best determination of the quality of the TES data products based on detailed comparisons between TES L2 data products and other independent data sets.

Validation is defined, for purposes of this report, as comparison between quantities measured by TES and other data products that represent the state of the atmosphere. This definition will evolve as the validation effort matures. Data used in these figures come from processing at the TES Science Computing Facility and are all publicly available.

The TES L2 nadir products have undergone extensive quality control and validation testing. Table 1-1 shows the definitions of data maturity developed by the Terra-MISR (Multi-angle Imaging SpectroRadiometer) team and adopted by the TES team (http://eosweb.larc.nasa.gov/PRODOCS/misr/Quality_Summaries/maturity_def.html).

Using these definitions, the current validation status of the TES L2 data products are given in Table 1-2. Currently, all the TES L2 nadir products are ready for scientific use with the exception of the emissivity reported over land surfaces. TES methane products should be used in a manner similar to that outlined in Payne et al. 2009 (see section 11). The TES limb products are provisionally validated but should not be used without working with the TES team. Limb data was taken only for the first 9 months of the TES mission and some special observations in 2006. The TES limb data is provisionally validated, but should be used only in collaboration with the TES science team at JPL. This validation report does not include analysis of the limb data validation.

**Table 1-1 Definitions of Data Maturity based on those used by the EOS-Terra MISR Team**

| Term | Definition |
|---|---|
| Beta | Early release products for users to gain familiarity with data formats and parameters. |
| Provisional | Limited comparisons with independent sources have been made and obvious artifacts fixed. |
| Validated Stage 1 | Biases are estimated from independent measurements at selected locations and times. |
| Validated Stage 2 | Biases are estimated from more widely distributed independent measurements. |
| Validated Stage 3 | Biases are estimated from independent measurements representing global conditions. |
| Note: TES L2 retrievals include fully characterized internal error estimates and do not obtain error estimates from external sources. Uncertainty in the TES validation work describes biases when compared to other data sources. | |

**Table 1-2 Current Validation Status of TES L2 Data Products**

| Species | Validation Status |
|---|---|
| Nadir Ozone | Validated Stage 3 |
| Nadir Carbon Monoxide | Validated Stage 3 |
| Nadir Temperature | Validated Stage 3 |
| Nadir Water (Lower/Middle Troposphere) | Validated Stage 3 |
| Nadir Water (Upper Troposphere) | Validated Stage 2 |
| Sea Surface Temperature | Validated Stage 3 |
| Nadir Methane | Validated Stage 2 |
| Sea Surface Temperature | Validated Stage 3 |
| Cloud Properties | Validated Stage 2 |
| Note: TES L2 limb products (Nitric Acid, Ozone, Temperature and Water) are provisionally validated but are not included in this report. | |

In order to compare TES profile data with other measurements, vertical smoothing and sensitivity must be accounted for by applying the appropriate averaging kernels (such as those supplied with the TES data products). The error estimates included in the L2 data products are meaningful based on the current validation analysis.

## 1.1 Applicable Documents

Note: All TES documentation are available online at the TES website, http://tes.jpl.nasa.gov/documents/ and at the NASA (National Aeronautics and Space Administration) Langley Atmospheric Science Data Center (ASDC) http://eosweb.larc.nasa.gov/PRODOCS/tes/table_tes.html . All TES related publications are available at the TES web site http://tes.jpl.nasa.gov/documents/publications/

[1] Lewicki, S., D. Shepard, M. Madatyan and S. Gluck (2009), TES Science Data Processing Standard and Special Observation Data Products Specifications, Version 11.9, JPL Internal Report D-22993, May 26, 2009, for public released data, software release 11.3.

[2] Robert Herman and Gregory Osterman (editors), Christopher Boxe, Kevin Bowman, Karen Cady-Pereira, Tony Clough, Annmarie Eldering, Brendan Fisher, Dejian Fu, Robert Herman, Daniel Jacob, Line Jourdain, Susan Kulawik, Michael Lampel, Qinbin Li, Jennifer Logan, Ming Luo, Inna Megretskaia, Ray Nassar, Gregory Osterman,

Susan Paradise, Vivienne Payne, Hank Revercomb, Nigel Richards, Mark Shephard, Dave Tobin, Solene Turquety, Felicia Vilnrotter, Helen Worden, John Worden, Lin Zhang (2011), Earth Observing System (EOS) Tropospheric Emission Spectrometer (TES) Data Validation Report (Version F05_05, F05_06, F05_07 data), Version 4.0, JPL Internal Report D-33192, November 23, 2011.

[3] Osterman, G., (editor), K. Bowman, A. Eldering, B. Fisher, R. Herman, D. Jacob, L. Jourdain, S. Kulawik, M. Luo, R. Monarrez, G. Osterman, S. Paradise, V. Payne, S. Poosti, N. Richards, D. Rider, D. Shepard, M. Shephard, F. Vilnrotter, H. Worden, J. Worden, H. Yun and L. Zhang (2009), Earth Observing System (EOS) Tropospheric Emission Spectrometer (TES) Level 2 (L2) Data User's Guide (Up to & including Version 4 data), Version 4.0, JPL Internal Report D-38042, May 20, 2009.

# 2. An Overview of the TES Instrument and Data Products

This section provides information about the TES instrument and the L2 data products. More detailed information on the TES data products is available in the TES L2 Data User's Guide (Osterman et al., 2009) and the TES Data Product Specification Document (Lewicki et al., 2009).

## 2.1 Instrument Description

The Tropospheric Emission Spectrometer (TES) on EOS-Aura was designed to measure the global, vertical distribution of tropospheric ozone and ozone precursors such as carbon monoxide (Beer et al., 2001; Beer, 2006). TES is a nadir and limb viewing infrared Fourier transform spectrometer (FTS) (http://tes.jpl.nasa.gov/instrument/). The TES spectral range is from 650 to 3250 $cm^{-1}$. The apodized resolution for standard TES spectra is 0.10 $cm^{-1}$, however, finer resolution (0.025 $cm^{-1}$) is available for special observations. The footprint of each nadir observation is 5 km by 8 km, averaged over detectors. Limb observations (each detector) have a projection around 2.3 km x 23 km (vertical x horizontal).

TES is on the EOS-Aura platform (http://aura.gsfc.nasa.gov/) in a near-polar, sun-synchronous, 705 km altitude orbit. The ascending node equator crossings are near 1:45 pm local solar time.

## 2.2 TES Observation Modes

### 2.2.1 Global Surveys

TES makes routine observations in a mode referred to as the "global survey". A global survey is run every other day on a predefined schedule and collects 16 orbits (~26 hours) of continuous data. Each orbit consists of a series of repetitive units referred to as a sequence. A sequence is further broken down into scans. Global surveys are always started at the minimum latitude of an Aura orbit. Table 2-1 provides a summary of the initial and modified versions of the TES Global Surveys from Launch to the present day.

**Table 2-1 Description of TES Global Survey Modifications**

| Start Date/ First Run ID | Scans | Sequences | Maximum Number of TES L2 Profiles | Along-Track Distance between Successive Nadir Scan Locations | Description |
|---|---|---|---|---|---|
| August 22, 2004 / First GS Run ID 2026<br>(First 4 GS runs were 4 orbits only)<br>(First full GS is Run ID 2147/Sep 20, 2004) | 3 Limb/ 2 Nadir | 1152 sequences (72 per orbit) | Maximum of 4608 L2 profiles<br>(1152 sequences x (3 Limb Scans+ 1 Nadir Scan)) | ~544 km | • At-launch Global Survey (Aura launched on July 15, 2004)<br>• Each sequence composed of 2 calibration scans, 2 nadir viewing scans and 3 limb scans.<br>• The two nadir scans were acquired at the same location on the spacecraft ground track. Their radiances were averaged, providing a single TES L2 profile. |
| May 21, 2005 / Run ID 2931 | 3 Nadir | 1152 sequences (72 per orbit) | Maximum of 3456 L2 profiles<br>(1152 sequences x 3 nadir scans) | ~182 km | • Global survey was modified to conserve instrument life.<br>• Three limb scans were eliminated and replaced by an additional nadir scan.<br>• The 3 Nadir scans were acquired at locations equally spaced along the spacecraft ground track. The radiances of individual scans are not averaged. |
| January 10, 2006 / Run ID 3239. | 3 Nadir | 1136 sequences (71 per orbit) | Maximum of 3408 L2 profiles<br>(1136 sequences x 3 nadir scans) | ~182 km | • The last sequence in each orbit was replaced with an instrument maintenance operation. |
| June 6, 2008 / Run ID 7370. | 3 Nadir | 960 sequences (60 per orbit) | Maximum of 2880 L2 profiles<br>(960 sequences x 3 nadir scans) | ~182 km | • Global survey was modified to conserve instrument life.<br>• No measurements poleward of 60°S latitude. |
| July 30, 2008 / Run ID 8187. | 3 Nadir | 768 sequences (48 per orbit) | Maximum of 2304 L2 profiles<br>(768 sequences x 3 nadir scans) | ~182 km | • Global survey was further modified to conserve instrument life.<br>• No measurements poleward of 50°S, 70°N latitude. |

| Start Date/ First Run ID | Scans | Sequences | Maximum Number of TES L2 Profiles | Along-Track Distance between Successive Nadir Scan Locations | Description |
|---|---|---|---|---|---|
| April 7, 2010 / Run ID 11125 | 3 Nadir | 512 sequences (32 per orbit) | Maximum of 2048 L2 profiles<br><br>(512 sequences x 4 nadir scans) | Spacing regular, but no longer uniform<br><br>(56, 195, 187, 122 km) | • Global survey was further modified to conserve instrument life.<br>• No measurements poleward of 30°S, 50°N latitude.<br>• Blackbody calibrations reduced: no calibrations within the GS, only one pre-GS and one post-GS. |

### 2.2.2 Special Observations

Observations are sometimes scheduled on non-global survey days. In general these are measurements made for validation purposes or with highly focused science objectives. These non-global survey measurements are referred to as "special observations". Eight special observation scenarios have been used to date and are summarized in Table 2-2.

**Table 2-2 Description of TES Special Observation Modes**

| Name | Dates | Pointing | Sequences | Scans per Sequence | Distance Between Scans | Comments |
|---|---|---|---|---|---|---|
| Step and Stare | Sep 2004 through Aug 6, 2005 | Nadir | 6 | 25 | 40 km | Continuous along-track nadir views, ~45 degrees of latitude. |
| Step and Stare | July 1, 2007 through present | Nadir | 1 | 165 | 45 km | Along track nadir observations spanning 65 degrees of latitude |
| Step and Stare | Jan 17, 2006 – Oct 8, 2006 and Spring 2008 | Nadir | 1 | 125 | 45 km | Continuous along-track nadir views, ~50 degrees of latitude. |
| Note: In 2008 both the 125 and 165 scan Step and Stare macros were used | | | | | | |
| Transect | Jan 16, 2006 through present | Near Nadir | 1 | 40 | 12 km | Hi density along-track or off nadir views. |
| Transect | Aug 20, 2005 – Sept 2, 2005 | Near Nadir | 1 | 68 | 25 km | Hi density along-track or off nadir views. |

| Name | Dates | Pointing | Sequences | Scans per Sequence | Distance Between Scans | Comments |
|---|---|---|---|---|---|---|
| Stare | Launch through present | Near Nadir | 1 | 32 | 0 km | All measurements at a single location. |
| Limb Only | Jan 31, 2006 – May 20, 2006 | Limb | 1 | 62 | 45 km | Continuous along-track limb views, 25 degrees of latitude. |
| Limb HIRDLS | Feb 13, 2006 Only | Limb | 142 | 3 | 182 km | 2 orbits of continuous limb measurements for HIRDLS (High Resolution Dynamics Limb Sounder) comparison |

## 2.3 TES Scan Identification Nomenclature

Each TES scan is uniquely identified by a set of three numbers called the run ID, the sequence ID and the scan ID. Each major unit of observation is assigned a unique run ID. Run IDs increase sequentially with time. The first on-orbit run ID is 2000. The sequence ID is assigned to repetitive units of measurements within a run. They start at 1 and are automatically incremented serially by the TES flight software. The scan ID is also incremented by the flight software each time a scan is performed. Each time the sequence is set to 1, the scan ID is reset to 0.

Each time TES makes a set of measurements, that data set is assigned an identification number (referred to as a "run ID"). A calendar of the TES run IDs for global surveys and a list of all TES run IDs (including observation data, time and date) can be found at http://tes.jpl.nasa.gov/data/datacalendar/ )

## 2.4 Where to Obtain TES Data

There are two locations for obtaining TES data. Links to both locations are available from the TES site at the Langley Atmospheric Science Data Center (ASDC) http://eosweb.larc.nasa.gov/. The supporting documentation necessary to use TES data is also available at the Langley ASDC site.

- The primary location for obtaining TES data is the Earth Observing System (EOS) Data Gateway https://wist.echo.nasa.gov/api/. This site makes available earlier versions of the TES data.
- A secondary location for obtaining TES data is the Langley ASDC data pool. The data pool has space limitations that make it somewhat dynamic, therefore older versions of TES data may not be available there.

The TES data files are listed in different ways for the different sites. The naming convention will be described in Section 2.5.

All TES data products are in HDF-EOS 5 format and are completely documented in the TES Data Product Specification documents referenced at http://tes.jpl.nasa.gov/documents/ . The site also contains links to the TES documentation mentioned in this manuscript.

Routines for reading the TES Level 2 data products, written in IDL, are available at ASDC TES site. We expect to have IDL routines for determining "C-Curve" ozone retrievals (see section 5.1.1.2 of the TES L2 Data User's Guide (Osterman et al., 2009)) available at the ASDC as well.

## 2.5 File Formats and Data Versions

Information about the TES data file content and format versioning can be found in the L2 product filenames. Table 2-3 provides information for differentiating between the TES versions. When ordering the data on the EOS Data Gateway, the TES level 2 products can be initially differentiated by the TES Product (ESDT or Earth Science Data Type) version label shown in the first column of Table 2-3. Once the data is downloaded, more information can be gathered from the TES version string in the filename.

The TES L2 Data Products are provided in files separated out by the atmospheric species being measured. The parts of the product filename are:

<inst.>-<platform>_<process level>-<species>-<TES view mode>_r<run id>_<version id>.he5

The TES Version String (version id), contains the Format and content version:

F<format version>_<science content version>

A change to the format version string corresponds to minor updates to the fields available within the file or minor bug fixes. Changes to the science content string reflect major changes in the science content of certain fields in the data products.

An example file name is:

TES-Aura_L2-O3-Nadir_r000002945_F04_04.he5

This particular file contains TES nadir measurements of ozone for run ID 2945 (000002945).

In addition to the atmospheric products, there are data files with additional (ancillary) data that are important for working with TES data. These ancillary files can be used with any species data file and contain the string "Anc" in the filename.

Table 2-3 provides a way to map the TES version string information to the TES data product version. For example, version F03_03 is the first version to contain limb data and version F03_02 data was a significant upgrade to the science content in the data products and therefore is referred to as version 2 (V002) TES data. When ordering TES Level 2 data products through the EOS Data Gateway, the products will be grouped by the TES version number (ESDT) in a form that looks like:

TES/AURA L2 O3 NADIR V003.

If the TES data is ordered through the Langley ASDC Data Pool using the FTP (File Transfer Protocol) interface, the version 3 nadir ozone data will be listed in the form:

TL2O3N.003.

If the TES data is ordered through the Langley Data Pool using the Web interface, the version 3 nadir ozone data will be listed as:

TL2O3N.3.

While the data may be listed differently for the different sites for downloading the products, the filenames will be identical.

There are six different versions of TES L2 data products. It is currently planned that all TES L2 data products should be processed with V005 by October 2012. Until that time, there will be a mixture of F05_07, F06_08, and F06_09 data products available. Data from versions prior to V003 (F04_04) are no longer publicly available, but the evolution of the product versions and file formats is provided in this document back to V001 (F01_01 and F02_01).

**Table 2-3 Description of the TES L2 Data Product Version Labels**

| TES Product (ESDT) Version | TES Version String | Format Version | Science Content Version | Description |
|---|---|---|---|---|
| V001 | F01_01 | 1 | 1 | The first publicly released L2 data |
| V001 | F02_01 | 2 | 1 | Bug fixes and additional fields |
| V002 | F03_02 | 3 | 2 | Some additional fields but major upgrade to scientific quality of data. |
| V002 | F03_03 | 3 | 3 | Limb data and some bug fixes |
| V003 | F04_04 | 4 | 4 | Improvements to nadir ozone, temperature, methane and to limb products. Fully processed from Sep 2004 through present. |

| TES Product (ESDT) Version | TES Version String | Format Version | Science Content Version | Description |
|---|---|---|---|---|
| V004 | F05_05 or F05_06<br>F05_07 (Final V004) | 5 | 5,6 or 7 | Improvements to temperature and methane retrievals.<br>F05_07 is the final V004 release using retrieval software R11.3 and when available should be used over F05_05 or F05_06.<br>F05_07 differentiates between GMAO* versions used in retrieval by date and TES run ID (see below)<br>F05_05 refers to data processed using GMAO GEOS-5.1.0 products using TES retrieval software release R11.2<br>F05_06 refers to data processed using GMAO GEOS-5.2.0 products using TES retrieval software release R11.2 |
| V005 | F06_08 or<br>F06_09 | 6 | 8 or 9 | F06_08 added $CO_2$ and $NH_3$ to list of Standard Products.<br>F06_09 added $N_2O$ to the list of Standard Products. |

** The TES processing software uses meteorological fields from the NASA Global Modeling and Assimilation Office (GMAO) GEOS (Goddard Earth Observing System) model as inputs to the Level 2 data retrievals.*

## 2.6 TES Standard L2 Products

Currently the TES data products available for any given run ID are listed in Table 2-4. The products are separated by species with an ancillary file providing additional data fields applicable to all species. A description of the contents of the product files, information on the Earth Science Data Type names and file organization can be found in the TES Data Processing Specification (DPS) document (Lewicki, et al., 2009).

**Table 2-4 Description of the TES L2 Data Product Files Currently Available**

| TES L2 Standard Data Product | TES View Mode | Description |
|---|---|---|
| Ozone | Nadir and Limb | TES ozone profiles and some geolocation information |
| Temperature | Nadir and Limb | TES atmospheric temperature profiles and some geolocation information. |
| Water Vapor | Nadir and Limb | TES nadir water vapor profiles and some geolocation information |
| Carbon Monoxide | Nadir | TES nadir carbon monoxide profiles and some geolocation information |
| Carbon Dioxide | Nadir | TES nadir carbon dioxide profiles and some geolocation information |
| Ammonia | Nadir | TES nadir ammonia profiles and some geolocation information |
| HDO | Nadir and Limb | TES HDO (Hydrogen Deuterium Monoxide) profiles and some geolocation information |
| Methane | Nadir | TES nadir methane profiles and some geolocation information |
| Nitric Acid | Limb | TES limb nitric acid profiles and some geolocation information |
| Ancillary | Nadir and Limb | Additional data fields necessary for using retrieved profiles. |
| Summary | Nadir and Limb | Provides information on retrieved volume mixing ratios/temperatures without averaging kernel, error matrices. |
| Supplemental | Nadir and Limb | Provides information on non-retrieved species that are used in the Level 2 retrievals (climatologies, covariance matrices, etc.) |

TES retrieves surface temperature and it is reported in each nadir species file, however the value in the atmospheric temperature file is the one that should be used for scientific analysis.

## 2.7 References

### 2.7.1 TES References

[1] Beer, R., T. A. Glavich, and D. M. Rider (2001), Tropospheric emission spectrometer for the Earth Observing System's Aura satellite, *Applied. Optics, 40 (15),* 2356-2367, May 20, 2001.

[2] Beer, R. (2006), TES on the Aura Mission: Scientific Objectives, Measurements and Analysis Overview, *IEEE Transactions on Geoscience and Remote Sensing, 44 (No.5), Special Issue on Aura,* 1102-1105, May 2006.

[3] Lewicki, S., D. Shepard, M. Madatyan and S. Gluck (2009), TES Science Data Processing Standard and Special Observation Data Products Specifications, Version 11.9, JPL Internal Report D-22993, May 26, 2009, for public released data, software release 11.3.

[4] Osterman, G., (editor), K. Bowman, A. Eldering, B. Fisher, R. Herman, D. Jacob, L. Jourdain, S. Kulawik, M. Luo, R. Monarrez, G. Osterman, S. Paradise, V. Payne, S. Poosti, N. Richards, D. Rider, D. Shepard, M. Shephard, F. Vilnrotter, H. Worden, J. Worden, H. Yun and L. Zhang (2009), Earth Observing System (EOS) Tropospheric Emission Spectrometer (TES) Level 2 (L2) Data User's Guide (Up to & including Version 4 data), Version 4.0, JPL Internal Report D-38042, May 20, 2009.

# 3. Executive Summary

Below is a summary of each data validation section.

- **Section 4 – L1B Radiance:**

Though this report is focused primarily on the TES Level 2 data products, it is important to understand that the L1B radiance products have also undergone a rigorous validation as reported in Shephard et al. (2008) and in the TES Validation Report V003 (Osterman et al., 2007). The fundamental measurement of the Tropospheric Emission Spectrometer (TES) on board the Aura spacecraft is upwelling infrared spectral radiances. Accurate radiances are critical for trace gas profile retrievals for air quality as well as sensitivity to climate processes. For example, any radiometric systematic errors (e.g. calibration) not addressed in the L1B radiances will propagate as errors into the retrieved atmospheric parameters (Bowman et al., 2006, Worden et al., 2004).

In April 2010, TES implemented a new strategy for observing and processing calibration measurements (see Section 4 for details). In order to validate TES spectra processed with the new calibration strategy, and to check comparisons of TES with AIRS over the entire TES data record from 2004 to present, we developed a more automated comparison tool based on the methods used for TES/AIRS comparisons in Shephard et al. (2008). Given the differences in ground footprints for TES and AIRS, comparisons are only meaningful for clear-sky, ocean scenes. Results for April 2009 (old calibration approach) compared to April 2010 (new calibration approach) are not significantly different which suggests the new approach provides the same radiance accuracy as before.

- **Section 5 – Nadir Ozone:**

The retrieval algorithm of TES V005 ozone profiles is nearly identical to that of TES V004. The changes in retrieval algorithm for other trace gases in the TES V005 products are not expected to downgrade the quality of ozone profiles. The TES V004 validation report, a version prior to this one, showed that the percent and absolute biases of TES-sonde are congruent to previous validation studies of TES V001 and V002. Hence, verifying the consistency between the percent and absolute biases of TES V005 and that of TES V004 is sufficient to validate TES V005 nadir ozone profile. TES V005 nadir ozone profiles provide data that were measured in the TES global survey, step-and-stare, transect, and stare observation modes. They were compared with ozonesonde measurements from multiple datasets that have been used in the TES V004 validation. The percent and absolute differences between TES and ozonesonde were investigated in six latitude zones. The seasonal variability of ozone was investigated by using the 904 TES-sonde coincidences in the $35^{o}$ N to $56^{o}$ N latitude zone.

The criteria of ±9 h, a 300 km radius and a cloud optical depth less than 2.0 were applied to search for the TES-sonde coincidence measurements. The flagged TES data were filtered out. 1907 matches were found from those TES measurements that have been processed for V005. Their latitude range is from $72.5^{o}$ S to $81.8^{o}$ N and time spans from 2006 to 2010. The TES averaging kernel and a priori constraint were applied to the ozonesonde data in order to: 1) compare the TES ozone profiles and ozonesonde data in an unbiased quantifiable manner (i.e. not biased by the TES a priori) 2) take TES measurement sensitivity and vertical resolution into account.

In general, TES V005 ozone profiles are positively biased (by less than 15%) from the surface to the upper-troposphere (~ 1000 to 100 hPa) and negatively biased (by less than 20%) from the upper-troposphere to the lower-stratosphere (100 to 30 hPa) when compared to the ozone-sonde data. Both V004 and V005 TES data showed the mean bias is from –14 to +15% and the one standard deviation is from 5 to 20%. The absolute mean percent differences for all seasons for mid-to-lower tropospheric ozone also show an improvement when compared to Nassar et al. (2008). All of these features are consistent with that of Boxe et al. (2010) and TES V004 validation report (Herman et al., 2011).

- **Section 6 – Carbon Monoxide:**

Comparisons have been carried out between TES carbon monoxide retrievals and those from a variety of satellite and aircraft instruments. Global patterns of carbon monoxide as measured by TES are in good qualitative agreement with those seen by MOPITT on the NASA Terra satellite. Comparisons of profiles of CO between TES and MOPITT show better agreement when a priori information is accounted for correctly. TES carbon monoxide agrees to within the estimated uncertainty of the aircraft instruments, including both errors and the variability of CO itself. In the upper troposphere, TES CO are found to bias lower compared to that of MOPITT by a few percent.

- **Section 7 – Nadir Temperature:**

TES V005 nadir temperature (TATM) retrievals have been compared with nearly coincident radiosonde (hereafter sonde) measurements from the NOAA ESRL global sonde database. For TES V005 TATM minus Tradiosonde (with averaging kernel applied), the bias is +0.2 to +0.5 K in the lower troposphere, -0.5 K in the upper troposphere. This is an improvement over previous versions of TES TATM. The rms is less than 1 K in the stratosphere and upper troposphere, but increases to 1.7 K in the lower troposphere. In clear sky conditions (average cloud effective optical depth less than 0.1), the bias improves in the lower troposphere but increases to +0.5 K at 500 hPa pressure level.

To evaluate the retrieval stability the monthly mean and standard deviation of the TATM residual between TES and the Global Modeling and Data Assimilation Office (GMAO) GEOS-5 model, which provides the first guess and a priori for the TATM retrieval, were calculated. The statistics for both Tropical Pacific and Northern Atlantic Ocean regions indicate only minor month-to-month variability and no substantial trends over the entire five-and-a-half year period. The standard deviation of the residual was generally smaller than the standard deviation of the GMAO GEOS-5 but larger than the TES estimated measurement error. Overall, based on this analysis it appears that the TES retrieval quality has remained stable from 2006 - 2011.

- **Section 8 – Sea Surface Temperature:**

TES retrievals of sea surface temperature rely on validation of previous data versions, as described in detail in the TES Validation Report V003 (Osterman et al., 2007).

- **Section 9 – Water Vapor:**

TES uses an optimal estimation non-linear least squares retrieval (Bowman et al., 2006). The latest version V005 uses a wide band retrieval (1100 to 1330 $cm^{-1}$) to jointly estimate the mixing ratios of four species: HDO, $H_2O$, $CH_4$, and $N_2O$ (Worden et al., 2012). This new retrieval

dramatically improves the vertical resolution in the lower troposphere for water vapor. Comparisons have been made between TES V005 water vapor profiles and radiosonde profiles, demonstrating greater sensitivity to boundary layer water vapor than previous versions. Comparisons were also made with the NOAA ESRL global radiosonde database for close coincidences of <100 km and -0.5 hours to +1.5 hours. TES V005 water vapor has a small bias of +10% to -12% in the lower troposphere, with a positive bias up to +15% in the middle troposphere at 400 hPa. The rms differences tend to increase from 30% near the surface to 50% in the middle troposphere.

- **Section 10 – HDO/$H_2O$:**

For validation of V4 HDO, we refer the reader to Worden et al. (2011).

V5.1 estimates of HDO/$H_2O$ show considerable more sensitivity to the isotopic composition of water vapor with typically 2 DOFS of freedom in the tropics and ~1 DOF at high latitudes. This increased sensitivity allows the TES estimates to resolve lower tropospheric and mid-tropospheric variability of the HDO/$H_2O$ vapor ratio (see Worden et al., 2012) with the expense of increased uncertainty over tropical oceans.

We find that the HDO/$H_2O$ estimates are consistent with the previous TES release within the altitude range where the sensitivity overlaps. However, the new version is biased higher by approximately 7.5 per mil. Consequently, the estimated bias correction factor for V5.1 should be 5.55% (Worden et al., 2011).

- **Section 11 – Methane:**

The validation of the TES $CH_4$ product described in Section 11 is sufficient to characterize the latitudinal dependence of the mean bias and the instrument error. Work so far suggests that TES $CH_4$ contains useful information when viewed using the "representative tropospheric volume mixing ratio" (RTVMR) approach. TES shows a positive mean bias of 1.0 % - 3.7 % with random instrument error of 1.4 % - 1.6 % with respect to measurements made during the first two HIPPO missions. TES successfully captures the latitudinal gradient observed during HIPPO I and II.

- **Section 12 – Cloud Products:**

TES retrievals of cloud products rely on validation of previous data versions, as described in detail in the TES Validation Report V004 (Herman et al., 2011).

- **Section 13 – Carbon Dioxide:**

TES $CO_2$ is retrieved between 40S and 45N, with average cloud optical depth < 0.5, among other tests, for good quality. On average, TES $CO_2$ has an average of 0.65 degree of freedom for signal (DOFS) – with the most DOFS for daytime land cases (which can be on the order of 1 DOFS) and the least for nighttime or winter land cases (which can be on the order of 0.3 DOFS). Ocean targets (day or night) have intermediate DOFS with about 0.8 DOFS. The averaging kernel indicates sensitivity between the surface to above 100 mb, with the most sensitivity between about 700 and 300 mb, peaking at about 650 mb. Although a profile is retrieved and has been validated, there is very little independent information at the different profile levels and it is critical to utilize the provided averaging kernel when using TES data. TES V005 $CO_2$ has

been compared with aircraft vertical profiles over the Pacific from the HIAPER (High-Performance Instrumented Airborne Platform for Environmental Research) Pole-to-Pole Observation (HIPPO) program (Wofsy et al., 2011) and over land at the SGP Arm site (Riley et al., 2009). Further details of this validation can be found in Kulawik et al. (2012). This validation was done with the prototype code which is nearly identical to the production code (PGE), but has some minor differences due to differences in the altitude grid calculation. The HIPPO analysis can be done with the processed PGE (Product Generation Executive) data, but the SGP analysis requires a full time series of TES at the SGP site and will need to await a more complete V005 dataset. Analysis of the PGE comparisons to HIPPO show about a 1.2 ppm error and an overall -0.7 ppm bias, as compared to the prototype which has about a 1.1 ppm error and an overall bias of +0.5 ppm. There are some outliers in the monthly mean values from both the prototype and the PGE and we are working on additional quality flags to screen these out. A fuller set of TES data needs to be examined before the V005 bias is officially set as different sites and times have relative biases on the order of 0.5 ppm. The single target error for TES $CO_2$ in the mid-Troposphere is on the order of 8 ppm, however averaging over 20 degrees longitude, 10 degrees latitude, and 1 month results in errors on the order of 1 ppm over both ocean and land targets. Through comparisons to validation data, we have found that the errors are underpredicted by a factor of about 1.5, and that the averaging kernel needs be corrected to account for the TES multi-step retrieval. The details of this correction are found in Kulawik et al. (2012) which involves a pressure-dependent scale factor. Although the TES $CO_2$ product is modest both in sensitivity and coverage, Nassar et al. (2011) found that TES added information to the surface flask measurements and was useful for estimating fluxes, both separately, and jointly with flask measurements. We have also recently found (manuscript in preparation) that TES assimilation into GEOS-Chem improves the amplitude of the mid-tropospheric $CO_2$ seasonal cycle as compared with aircraft profiles measured at the SGP-Arm site.

- **Section 14 – Ammonia:**

TES can detect spatial variability and seasonal trends in $NH_3$. The TES $NH_3$ signals appear well correlated with in situ measurements when averaged over time and/or space over regions with not ideal observing conditions, such as eastern China or North Carolina. When there are high concentrations, warm temperatures and few clouds, as in the San Joaquin Valley, it is possible to compare non-averaged TES signals with in situ measurements and show that both present similar spatial variability.

## 3.1 References

### 3.1.1 TES References

[1] Bowman K.W., C.D. Rodgers, S.S. Kulawik, J. Worden, E. Sarkissian, G. Osterman, T. Steck, M. Lou, A. Eldering, M. Shephard, H. Worden, M. Lampel, S.A. Clough, P.D. Brown, C.P. Rinsland, M. Gunson, and R. Beer (2006), Tropospheric emission spectrometer: Retrieval method and error analysis, *IEEE Trans. Geosci. Remote Sens., 44(5)*, 1297-1307, May 2006.

[2] Boxe, C.S., J.R. Worden, K.W. Bowman, S.S. Kulawik, J.L. Neu, W.C. Ford, G.B. Osterman, R.L. Herman, A. Eldering, D.W. Tarasick, A.M. Thompson, D.C. Doughty,

M.R. Hoffmann, S.J. Oltmans (2010), Validation of northern latitude Tropospheric Emission Spectrometer stare ozone profiles with ARC-IONS sondes during ARCTAS: sensitivity, bias and error analysis, *Atmospheric Chemistry and Physics*, doi:10.5194/acp-10-9901-2010, October 20, 2010.

[3] Herman R. and G. Osterman (editors), Christopher Boxe, Kevin Bowman, Karen Cady-Pereira, Tony Clough, Annmarie Eldering, Brendan Fisher, Dejian Fu, Robert Herman, Daniel Jacob, Line Jourdain, Susan Kulawik, Michael Lampel, Qinbin Li, Jennifer Logan, Ming Luo, Inna Megretskaia, Ray Nassar, Gregory Osterman, Susan Paradise, Vivienne Payne, Hank Revercomb, Nigel Richards, Mark Shephard, Dave Tobin, Solene Turquety, Felicia Vilnrotter, Helen Worden, John Worden, Lin Zhang (2011), Earth Observing System (EOS) Tropospheric Emission Spectrometer (TES) Data Validation Report (Version F05_05, F05_06, F05_07 data), Version 4.0, JPL Internal Report D-33192, November 23, 2011.

[4] Kulawik, S.S., J.R. Worden, S.C. Wofsy, S.C. Biraud, R. Nassar, D.B.A. Jones, E.T. Olsen, G.B. Osterman, (2012), Comparison of improved Aura Tropospheric Emission Spectrometer (TES) $CO_2$ with HIPPO and SGP aircraft profile measurements, *Atmospheric Chemistry and Physics Discussions*, *12*, 6283 – 6329, February 29, 2012.

[5] Nassar, R., J.A. Logan, H.M. Worden, I.A. Megretskaia, K.W. Bowman, G.B. Osterman, A.M. Thompson, D.W. Tarasick, S. Austin, H. Claude, M.K. Dubey, W.K. Hocking, B.J. Johnson, E. Joseph, J. Merrill, G.A. Morris, M. Newchurch, S.J. Oltmans, F. Posny, F.J. Schmidlin, H. Vömel, D.N. Whiteman, and J.C. Witte (2008), Validation of Tropospheric Emission Spectrometer (TES) Nadir Ozone Profiles Using Ozonesonde Measurements, *J. Geophys. Res. 113*, D15S17, (doi:10.1029/2007JD008819), May 7, 2008.

[6] Nassar, R., D.B.A. Jones, S.S. Kulawik, J.R. Worden, K.W. Bowman, R.J. Andres, P. Suntharalingam, J.M. Chen, C.A.M. Brenninkmeijer, T.J. Schuck, T.J. Conway, D.E. Worthy (2011), Inverse modeling of $CO_2$ sources and sinks using satellite observations of $CO_2$ from TES and surface flask measurements, *Atmos. Chem. Phys.*, ***11****, (12),* 6029-6047, June 24, 2011.

[7] Osterman, G., (editor), K. Bowman, K. Cady-Pereira, T. Clough, A. Eldering, B. Fisher, R. Herman, D. Jacob, L. Jourdain, S. Kulawik, M. Lampel, Q. Li, J. Logan, M. Luo, I. Megretskaia, R. Nassar, G. Osterman, S. Paradise, V. Payne, H. Revercomb., N. Richards, M. Shephard, D. Tobin, S. Turquety, F. Vilnrotter, H. Worden, J. Worden, and L. Zhang (2007), Earth Observing System (EOS) Tropospheric Emission Spectrometer (TES) Data Validation Report (Version F04_04 data), Version 3.0, JPL Internal Report D-33192, November 5, 2007.

[8] Shephard, M. W., H. M. Worden, K. E. Cady-Pereira, M. Lampel, M. Luo, K. W. Bowman, E. Sarkissian, R. Beer, D. M. Rider, D. C. Tobin, H. E. Revercomb, B. M. Fisher, D. Tremblay, S. A. Clough, G. B. Osterman, and M. Gunson (2008), Tropospheric Emission Spectrometer Nadir Spectral Radiance Comparisons, *J. Geophys. Res.*, *113*, D15S05, (doi:10.1029/2007JD008856), April 22, 2008.

[9] Worden, J., S. S. Kulawik, M. W. Shephard, S. A. Clough, H. Worden, K. Bowman, and A. Goldman (2004), Predicted errors of tropospheric emission spectrometer nadir retrievals from spectral window selection, *J. Geophys. Res., 109, D09308,* May 15, 2004.

[10] Worden, J., D. Noone, J. Galewsky, A. Bailey, K. Bowman, D. Brown, J. Hurley, S. Kulawik, J. Lee, and M. Strong (2011), Estimate of bias in Aura TES HDO/$H_2O$ profiles from comparison of TES and in situ HDO/$H_2O$ measurements at the Mauna Loa observatory, *Atmospheric Chemistry and Physics*, *11*, 4491–4503, 2011, doi:10.5194/acp-11-4491-2011, May 12, 2011.

[11] Worden, J., S. Kulawik, C. Frankenberg, V. Payne, K. Bowman, K. Cady-Peirara, K. Wecht, J.-E. Lee, D. Noone (2012), Profiles of $CH_4$, HDO, $H_2O$, and $N_2O$ with improved lower tropospheric vertical resolution from Aura TES radiances, *Atmospheric Measurement Techniques, 5, 397–411, 2012*, doi:10.5194/amt-5-397-2012, February 20, 2012.

### 3.1.2 General References

[12] Riley, W.J., S.C. Biraud, M.S. Torn, M.L. Fischer,D. P. Billesbach, J.A. Berry (2009), Regional $CO_2$ and latent heat surface fluxes in the Southern Great Plains: Measurements, modeling, and scaling, *Journal of Geophysical Research-Biogeosciences, 114*, G04009, DOI: 10.1029/2009JG001003, 2009.

[13] Wofsy, S.C., the HIPPO Science Team and Cooperating Modellers and Satellite Teams (2011), HIAPER Pole-to-Pole Observations (HIPPO): Fine grained, global scale measurements for determining rates for transport, surface emissions, and removal of climatically important atmospheric gases and aerosols, *Phil. Trans. of the Royal Society A, vol. 369 (no. 1943)*, 2073-2086, May 28, 2011.

# 4. TES L1B Radiance Validation

Though this report is focused primarily on the TES Level 2 data products, it is important to understand that the L1B radiance products have also undergone a rigorous validation as reported in Shephard et al. (2008) and in the TES Validation Report V003 (Osterman et al., 2007). The fundamental measurement of the Tropospheric Emission Spectrometer (TES) on board the Aura spacecraft is upwelling infrared spectral radiances. Accurate radiances are critical for trace gas profile retrievals for air quality as well as sensitivity to climate processes. For example, any radiometric systematic errors (e.g. calibration) not addressed in the L1B radiances will propagate as errors into the retrieved atmospheric parameters (Bowman et al., 2006, Worden et al., 2004).

Recently, Connor et al. (2011) investigated the long-term stability of TES L1B radiances and found no significant trend (variation from 0 values) in the radiance residuals for the years 2005 to 2009. For the V005 data in this validation report, we will discuss the changes to the L1B calibration strategy starting April 1, 2010 and more recent comparisons of TES with the Atmospheric Infrared Sounder (AIRS) on NASA's Aqua satellite (Aumann et al., 2003).

## 4.1 Changes in TES calibration strategy, April 2010

In April 2010, TES implemented a new strategy for observing and processing calibration measurements in response to problems found with the Pointing Control System (PCS) when viewing the on-board blackbody. In order to prevent further degradation of the PCS, views of the calibration blackbody (which use an azimuthal rotation) embedded in TES Global Surveys were removed. We have found that the time variation of the 340 K blackbody signals is slow (weeks to months) and depends mostly on detector contamination (i.e., ice build-up), therefore, a lower frequency of blackbody observations is acceptable for accurate radiometric calibration. We now take scans of the blackbody before and after TES Global Surveys so that we can acquire several scans for averaging with a single azimuthal rotation of the PCS. However, views of cold space (using a pitch rotation that does not appear to stress the PCS) are still taken with every sequence of the Global Survey to provide the instrument background signal, which varies along the orbit. Since TES observations taken in Special Observation mode were already processed with "bracketing" calibrations, no changes were required to implement the new calibration strategy for Global Surveys in the L1B algorithm (Worden et al., 2006), which has remained unchanged from V003. L1B radiance files that include the new calibration strategy are identified with "C01" in the filename, e.g.:
TES-Aura_L1B-Nadir_FP1B_r0000011375-o31632_C01_F03_04.h5

## 4.2 TES/AIRS Comparisons over the TES data record

In order to validate TES spectra processed with the new calibration strategy described above and to check comparisons of TES with AIRS over the entire TES data record from 2004 to present, we developed a more automated comparison tool based on the methods used for TES/AIRS comparisons in Shephard et al. (2008). Given the differences in ground footprints for TES and AIRS, comparisons are only meaningful for clear-sky, ocean scenes.

Results for April 2009 (old calibration approach) compared to April 2010 (new calibration approach) are not significantly different which suggests the new approach provides the same radiance accuracy as before.

### 4.2.1 TES/AIRS Comparisons

The TES-AIRS comparison tool has the following steps:

1) Select TES ocean scenes with average effective cloud OD < 0.05 (clear-sky).
2) Find AIRS spectra within 13 km, 1 hr of each TES scene.
3) Weighted average of 16 TES spectra and NESR (Noise Equiv. Spectra Radiance).
4) De-spike TES spectra using frequencies where NESR < 0.
5) Convolve averaged TES spectra with AIRS spectral response function (SRF).
6) Convert from radiance to brightness temperature (BT) and store frequencies and BT differences where TES NESR > 0 (no spikes) and exclude AIRS channels with a value >= 3 in the ExcludeChans (under "Data Fields") from the AIRS file.

Further selection of compared scenes is required to eliminate the cases where AIRS was viewing clouds or land that TES was not. Based on the distribution of BT (brightness temperature) differences we select only those comparisons where the average BT difference had an absolute value less than 1K and RMS less than 2K for the statistics to characterize each TES run.

### 4.2.2 Results from TES/AIRS comparisons

We show the results for the TES/AIRS comparisons in Table 4-1. We note that the RMS values in Table 4-1 are somewhat higher in than those reported in Shephard et al. (2008) for runs 2147 and 2931. This is likely due to the tighter selection criteria applied by Shephard el al., (2008). However, for this study, it was more important to apply consistent criteria over the time record. The only change that seems significant over the period shown here is the smaller TES-AIRS BT difference in filter 2A1 starting around Feb. 2008, and demonstrated in Figure 4-1. The results for 2A1 did not change with the new calibration approach. This change will be investigated with other radiance comparison approaches (e.g., Connor et al., 2011) and by communication with the AIRS team.

**Table 4-1 TES – AIRS Brightness Temperature (K) Differences: Run average and RMS.**

| TES Run | Date | N_tgt | 2B1 avg (K) | 2B1 rms (K) | 1B2 avg (K) | 1B2 rms (K) | 2A1 avg (K) | 2A1 rms (K) |
|---|---|---|---|---|---|---|---|---|
| 2147 | 20040920 | 248 | -0.23 | 0.80 | 0.02 | 0.67 | 0.43 | 0.55 |
| 2931 | 20050521 | 376 | -0.12 | 0.75 | 0.04 | 0.58 | 0.47 | 0.45 |
| 3194 | 20051127 | 418 | -0.11 | 0.77 | 0.03 | 0.62 | 0.39 | 0.49 |
| 3202 | 20051207 | 484 | -0.09 | 0.77 | 0.01 | 0.59 | 0.42 | 0.45 |
| 3555 | 20060408 | 390 | 0.05 | 0.74 | 0.08 | 0.57 | 0.39 | 0.45 |
| 5311 | 20070407 | 419 | -0.11 | 0.75 | 0.05 | 0.56 | 0.48 | 0.47 |
| 5948 | 20070807 | 479 | -0.19 | 0.73 | 0.07 | 0.60 | 0.37 | 0.46 |
| 6370 | 20071008 | 451 | -0.07 | 0.77 | 0.09 | 0.61 | 0.41 | 0.44 |
| 6485 | 20071207 | 379 | -0.22 | 0.76 | 0.03 | 0.60 | 0.34 | 0.47 |
| 6592 | 20080207 | 386 | -0.13 | 0.72 | -0.02 | 0.54 | 0.20 | 0.40 |
| 6888 | 20080407 | 452 | -0.16 | 0.75 | -0.08 | 0.57 | 0.12 | 0.41 |
| 7378 | 20080608 | 413 | -0.33 | 0.72 | -0.03 | 0.62 | 0.11 | 0.41 |
| 8342 | 20080807 | 473 | -0.27 | 0.70 | -0.09 | 0.55 | 0.08 | 0.39 |
| 9274 | 20081008 | 377 | -0.18 | 0.74 | 0.004 | 0.60 | 0.09 | 0.41 |
| 10115 | 20081207 | 342 | -0.27 | 0.71 | -0.04 | 0.59 | 0.16 | 0.41 |
| 10305 | 20090207 | 339 | -0.26 | 0.73 | -0.07 | 0.57 | 0.08 | 0.42 |
| 10436 | 20090408 | 259 | -0.20 | 0.73 | -0.03 | 0.58 | 0.06 | 0.40 |
| 11125 | 20100407 | 452 | -0.16 | 0.70 | -0.03 | 0.57 | 0.07 | 0.38 |

Notes:

1. N_tgt indicates the number of comparisons used for the run statistics.
2. TES frequency ranges are:
   2B1: 650-920 $cm^{-1}$
   1B2: 920-1160 $cm^{-1}$
   2A1: 1090-1340 $cm^{-1}$

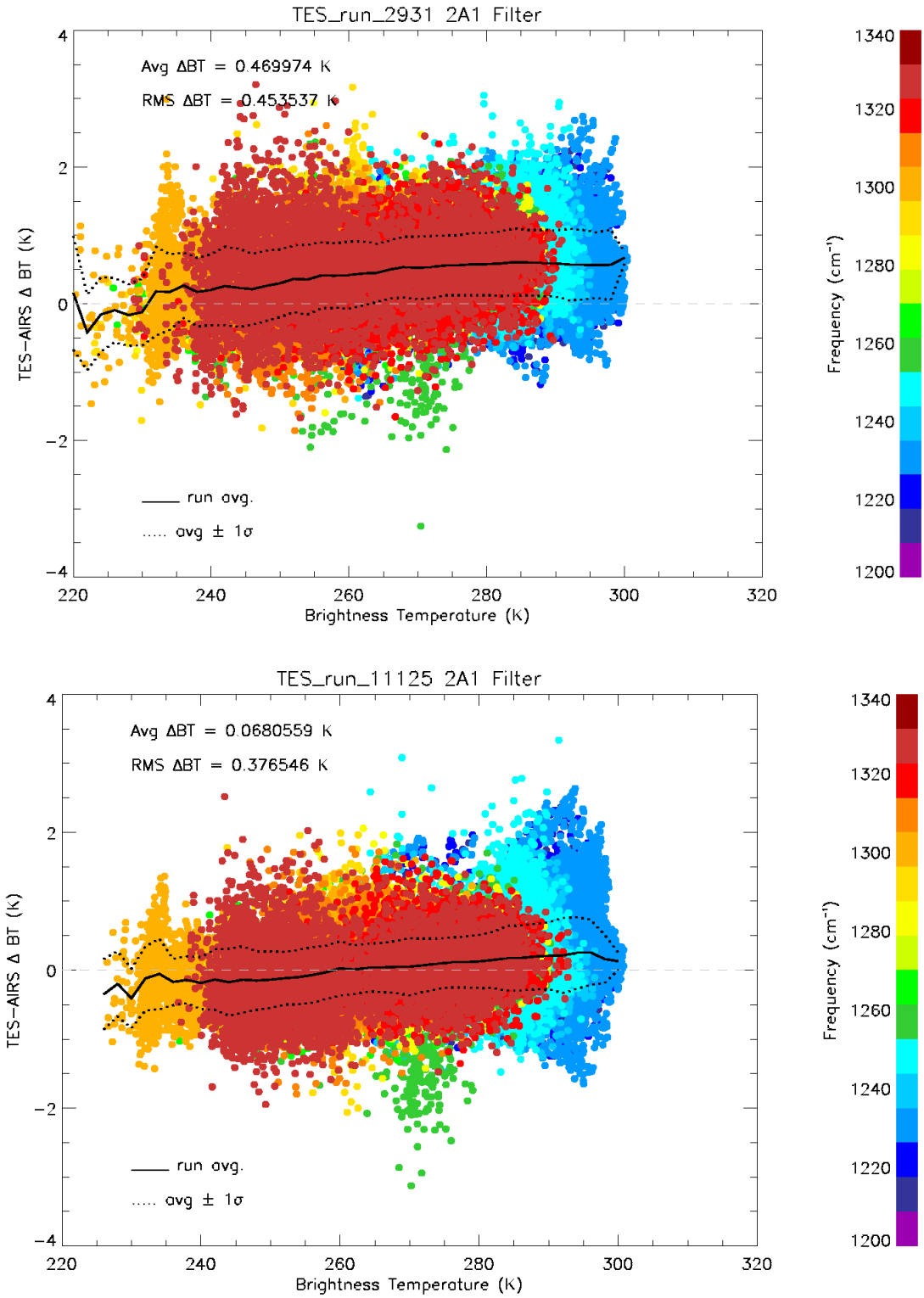


**Figure 4-1** TES-AIRS BT difference vs. BT (colors indicate frequency) for the 2A1 filter for 20050521, TES run 2931 (top) and 20100507, TES run 11125 (bottom).

## 4.3 References

### 4.3.1 TES L1B Radiance Validation Reference

[1] Connor, T.C., M. W. Shephard, V. H. Payne, K. E. Cady-Pereira, S. S. Kulawik, M. Luo, G. Osterman, and M. Lampel (2011), Long-term stability of TES satellite radiance measurements, *Atmospheric Measurement Techniques, 4*, doi:10.5194/amt-4-1481-2011, 1481–1490, July 25, 2011.

[2] Osterman, G., (editor), K. Bowman, K. Cady-Pereira, T. Clough, A. Eldering, B. Fisher, R. Herman, D. Jacob, L. Jourdain, S. Kulawik, M. Lampel, Q. Li, J. Logan, M. Luo, I. Megretskaia, R. Nassar, G. Osterman, S. Paradise, V. Payne, H. Revercomb., N. Richards, M. Shephard, D. Tobin, S. Turquety, F. Vilnrotter, H. Worden, J. Worden, and L. Zhang (2007), Earth Observing System (EOS) Tropospheric Emission Spectrometer (TES) Data Validation Report (Version F04_04 data), Version 3.0, JPL Internal Report D-33192, November 5, 2007.

[3] Shephard, M. W., H. M. Worden, K. E. Cady-Pereira, M. Lampel, M. Luo, K. W. Bowman, E. Sarkissian, R. Beer, D. M. Rider, D. C. Tobin, H. E. Revercomb, B. M. Fisher, D. Tremblay, S. A. Clough, G. B. Osterman, and M. Gunson (2008), Tropospheric Emission Spectrometer Nadir Spectral Radiance Comparisons, *J. Geophys. Res., 113*, D15S05, (doi:10.1029/2007JD008856), April 22, 2008.

### 4.3.2 TES References

[4] Bowman K. W., C. D. Rodgers, S. S. Kulawik, J. Worden, E. Sarkissian, G. Osterman, T. Steck, M. Lou, A. Eldering, M. Shephard, H. Worden, M. Lampel, S. A. Clough, P. D. Brown, C. P. Rinsland, M. Gunson, and R. Beer (2006), Tropospheric emission spectrometer: Retrieval method and error analysis, *IEEE Trans. Geosci. Remote Sens., 44(5)*, 1297-1307, May 2006.

[5] Worden, H., R. Beer, K.W. Bowman, B. Fisher, M. Luo, D. Rider, E. Sarkissian, D. Tremblay, J. Zong (2006), TES Level 1 Algorithms: Interferogram Processing, Geolocation, Radiometric, and Spectral Calibration, *IEEE Trans. Geosci. Remote Sensing, 44*, 1288- 1296, May 2006.

[6] Worden, J., S. S. Kulawik, M. W. Shephard, S. A. Clough, H. Worden, K. Bowman, and A. Goldman (2004), Predicted errors of tropospheric emission spectrometer nadir retrievals from spectral window selection, *J. Geophys. Res., 109*, D09308, May 15, 2004.

### 4.3.3 General References

[7] Aumann, H.H., M.T. Chahine, C. Gautier, M.D. Goldberg, E. Kalnay, L.M. McMillin, H. Revercomb, P.W. Rosenkranz, W.L. Smith, D. H. Staelin, L.L. Strow, and J. Susskind (2003), AIRS/AMSU/HSB on the Aqua mission: Design, Science Objectives, Data Products, and Processing Systems, *IEEE Trans. Geosci. Remote Sensing, 41*, 253-264 (2003).

# 5. Validation of TES V005 nadir ozone profiles using ozonesonde measurements

## 5.1 Overview

The retrieval algorithm of TES V005 ozone profiles is nearly identical to that of TES V004. The changes in retrieval algorithm for other trace gases in the TES V005 products are not expected to downgrade the quality of ozone profiles. TES V004 validation report, a version prior to this one, showed that the percent and absolute biases of TES-sonde are congruent to previous validation studies of TES V001 and V002. Hence, verifying the consistency between the percent and absolute biases of TES V005 and that of TES V004 is sufficient to validate TES V005 nadir ozone profile. TES V005 nadir ozone profiles provide data that were measured in the TES global survey, step-and-stare, transect, and stare observation modes. They were compared with ozonesonde measurements from multiple datasets that have been used in the TES V004 validation. The percent and absolute differences between TES and ozonesonde were investigated in six latitude zones. The seasonal variability of ozone was investigated by using the 904 TES-sonde coincidences in the $35^{o}$ N to $56^{o}$ N latitude zone.

The criteria of ±9 h, a 300 km radius and a cloud optical depth less than 2.0 were applied to search for the TES-sonde coincidence measurements. The flagged TES data were filtered out. 1907 matches were found from those TES measurements that have been processed for V005. Their latitude range is from $72.5^{o}$ S to $81.8^{o}$ N and time spans from 2006 to 2010. The TES averaging kernel and a priori constraint were applied to the ozonesonde data in order to: 1) compare the TES ozone profiles and ozonesonde data in an unbiased quantifiable manner (i.e. not biased by the TES a priori) 2) take TES measurement sensitivity and vertical resolution into account.

In general, TES V005 ozone profiles are positively biased (by less than 15%) from the surface to the upper-troposphere (~ 1000 to 100 hPa) and negatively biased (by less than 20%) from the upper-troposphere to the lower-stratosphere (100 to 30 hPa) when compared to the ozone-sonde data. Both V004 and V005 TES data showed the mean bias is from –14 to +15% and the one standard deviation is from 5 to 20%. The absolute mean percent differences for all seasons for mid-to-lower tropospheric ozone also show an improvement when compared to Nassar et al. (2008). All of these features are consistent with that of Boxe et al. (2010) and TES V004 validation report (Herman et al., 2011).

## 5.2 TES Ozonesonde Comparisons

TES nadir ozone profiles were retrieved using the optimal estimation method (OEM). The OEM combines TES measurements and a priori into the retrieved ozone profiles. An unbiased and quantitative TES-sonde comparison method, which has been applied in the TES V001, V002, V003, V004 and V005 validation, takes the impacts of a priori into account. The method applies the TES operator (i.e., averaging kernel and a priori constraint) to ozonesonde profiles. This approach generated ozonesonde profiles for the TES-sonde comparisons by smoothing the high vertical resolution ozonesonde data with the TES averaging kernels and adding a priori information into the ozonesonde data. TES-sonde percent and absolute differences were calculated using TES nadir ozone profiles and the ozonesonde profiles whose vertical resolution and impacts of a priori profiles are consistent to those TES nadir ozone profiles.

Ozone percent and absolute difference profiles are shown in Figure 5-1 (TES V004 minus sonde) and Figure 5-2 (TES V005 minus sonde) for six latitude zones (Arctic, north midlatitudes, northern subtropics, tropics, southern low- and mid-latitudes, and Antarctic). The number of matches from TES V005 is less than that of TES V004 due to the differences in the amount of data that have been processed between TES V004 and TES V005. The southern low (subtropics) and mid-latitudes were combined as a single zone because of the small number of coincident TES-ozonesonde measurements (122 matches for TES V004 and 90 matches for TES V005). Percent (left panels) and absolute (right panels) difference profiles are shown from the surface up to 10 hPa. In Figure 5-1 and Figure 5-2, all individual profiles are plotted in gray; mean and standard deviation ranges are overlaid in dark blue and broken light blue, respectively. The mean minus standard deviation and mean plus standard deviation (or the one standard deviation ranges) are overlaid in black. *N* is the number of TES-ozonesonde profiles plotted after removing cloudy scenes and flagged TES data.

An overall positive bias in the TES V004 (Figure 5-1) and V005 (Figure 5-2) ozone retrievals, compared to the ozonesondes, are found in all six latitude zones. This positive bias is more apparent in the mean ozone percent and absolute difference profiles. Both TES V004 and V005 mean percent bias in the troposphere is generally within 15% with an exception in the Antarctic region where both TES V004 and V005 ozone profiles showed up to 20% positive bias in the upper troposphere. Figure 5-1 and Figure 5-2 also show that the absolute values of the TES bias generally increase near the tropopause and in the lower stratosphere. However, this translates to a small percent difference because of the higher amount of ozone in that altitude region. Similar to comparison of TES V004 and V005 with ozonesondes, a positive bias in the TES measurements relative to the ozonesondes has been noticed in TES V002 $O_3$ validation report.

In Arctic and Antarctic, both TES V005-ozonesonde and TES V004-ozonesonde comparisons exhibit a positive percent bias. And the variations in the absolute bias are nearly zero as a function of altitude. The exception to the general positive bias in the TES V005-ozonesonde comparisons was found over the Arctic (20 to 70 hPa), the Antarctic (20 to 50 hPa) and the northern subtropics (100 to 400 hPa). They display a negative bias with a peak value about -10%. TES V004-ozonesonde comparisons show same features at the Arctic and Antarctic as TES V005, but TES V004 in the northern subtropics has positive bias, compared to ozonesonde measurements.

Given the fact that an identical algorithm was used for TES V004 and V005 ozone retrievals, we expect a similar quantitative representation for TES V005-sonde comparisons as those for TES V004. The similarity between Figure 5-1 and Figure 5-2 (i.e., the TES V004- and V005-ozonesonde comparisons in the six latitude bins) are overwhelming, specifically the bias of the mean and the standard deviation or root-mean-square error.

The percent and absolute TES-sonde difference of ozone profiles for winter, spring, summer, and fall in northern midlatitudes (35 to 56$^o$ N) are shown in the left and right panels of Figure 5-3 (using 2863 TES V004-sonde coincidences) and of Figure 5-4 (using 904 TES V005-sonde coincidences). Both TES V004 and V005 show a positive mean bias less than 15% when compared to ozonesonde measurements. It is an improvement, compared to TES V002 ozone profiles used by Nassar et al. (2008) to study the seasonal variability of ozone profiles (using 700 coincidence TES-sonde measurements) in northern midlatitudes. Nassar et al. (2008) illustrated that the altitude of the peak in the mean percent difference profiles was lowest in the winter and highest in the summer. It likely relates to the changing tropopause height and variability of ozone

(Logan, 1999). But the altitudes at which the mean percent difference peaks for the winter and summer are not significantly higher or lower compared to the spring and fall. The seasonal division also shows that the low altitudes outliers predominantly occur in the summer and to a lesser degree in the spring and that the summer northern midlatitude bias profiles somewhat resemble the northern subtropics or the tropics in the upper troposphere. With the exception of a small negative bias at ~ 90 to 100 hPa in the summer for V002 mean ozone percent difference, the mean $O_3$ percent and absolute differences generally show a positive bias for all seasons. All of these features are in agreement with Boxe et al. (2010), TES V004 and TES V005 $O_3$.

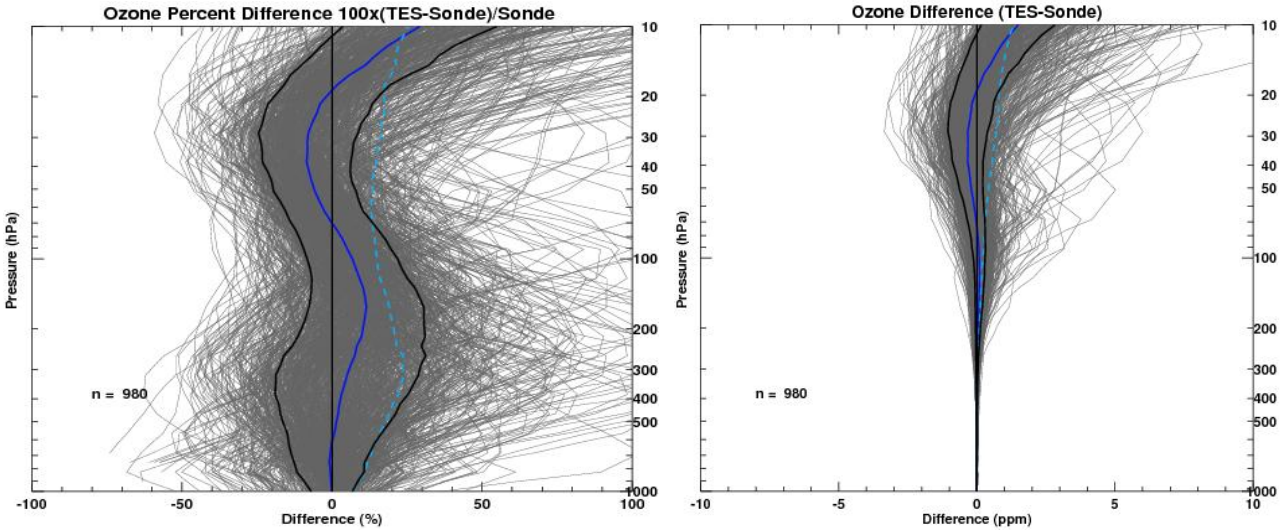


**(A: Arctic 56$^o$ N to 90$^o$ N)**

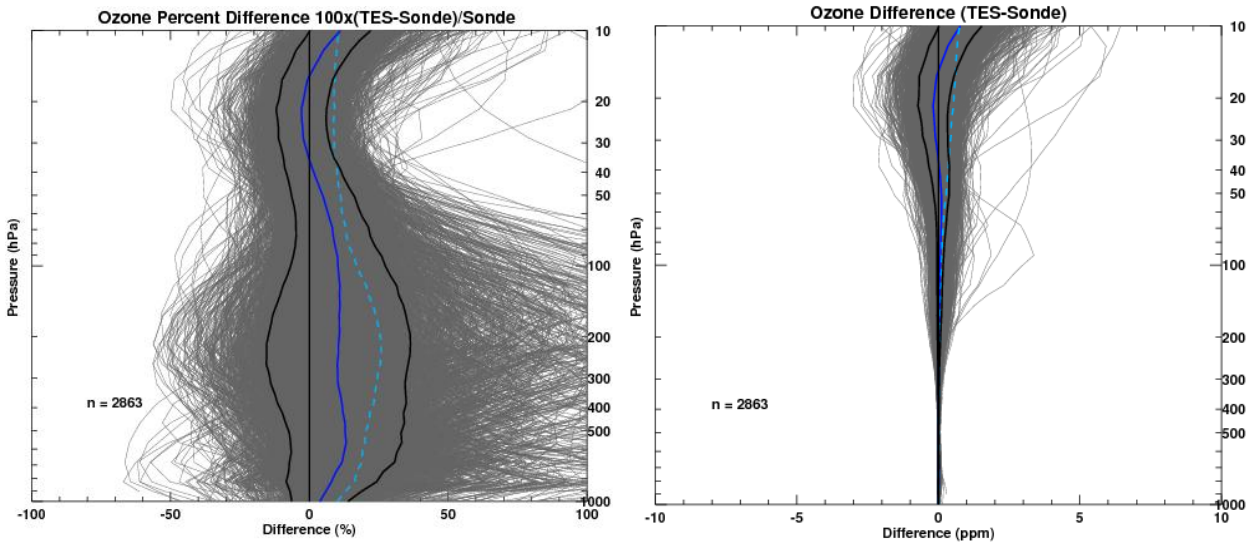


**(B: Northern Midlatitudes 35$^o$ N to 56$^o$ N)**

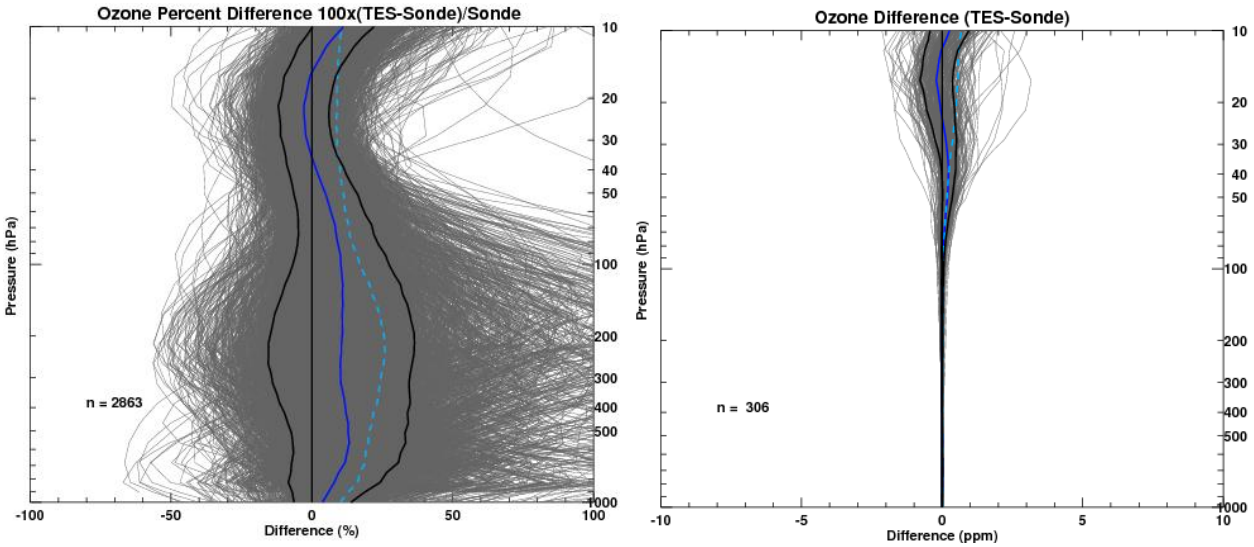


**(C: Northern Subtropics 15$^{o}$ N to 35$^{o}$ N)**

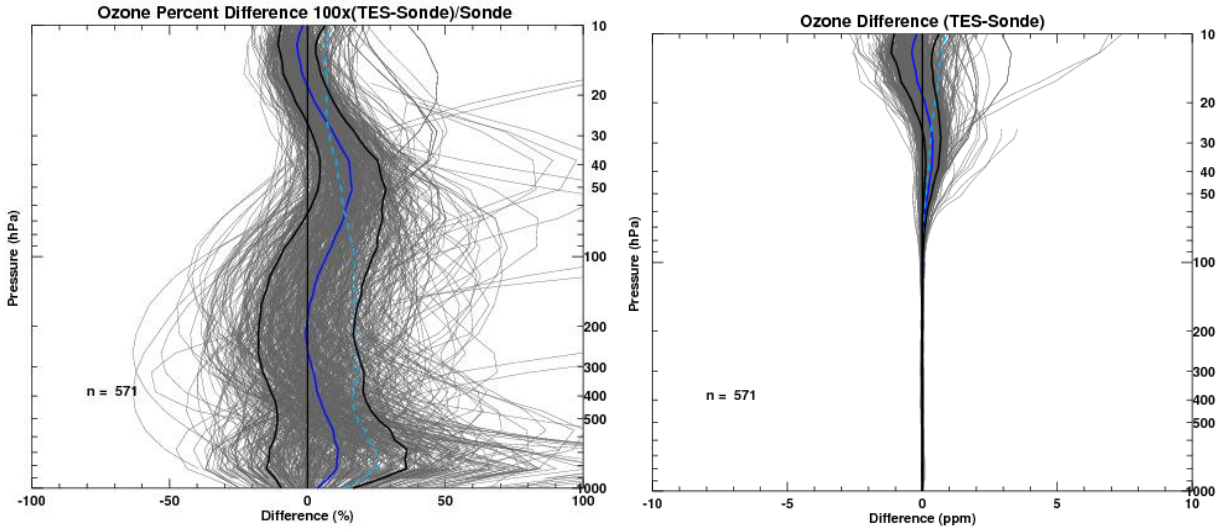


**(D: Tropics 15$^{o}$ S to 15$^{o}$ N)**

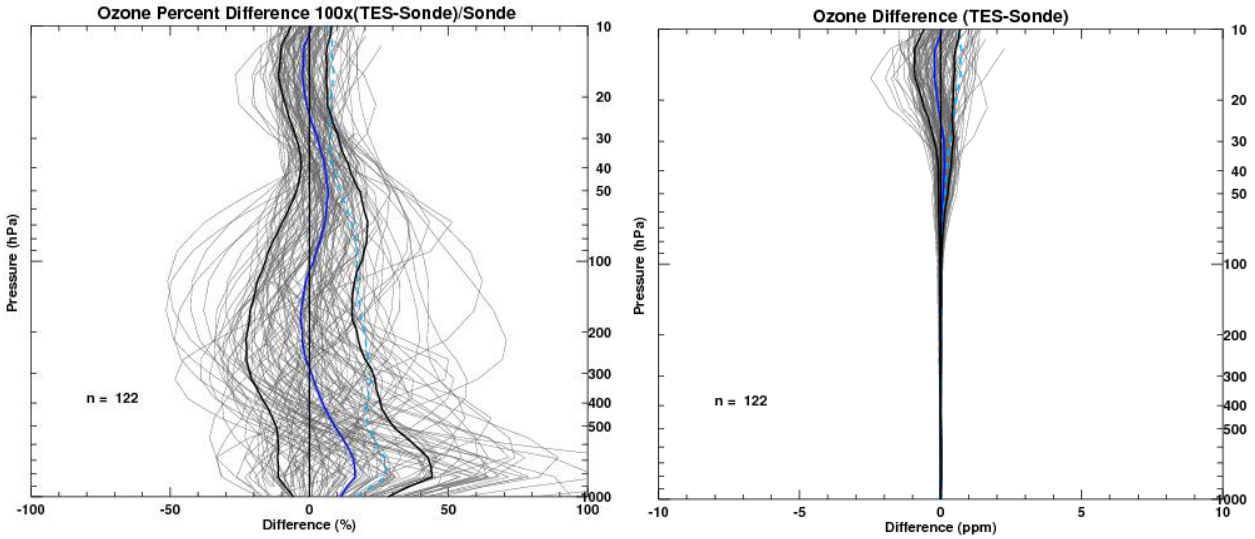


**(E: Southern low- and midlatitudes 15$^{o}$ S to 60$^{o}$ S)**

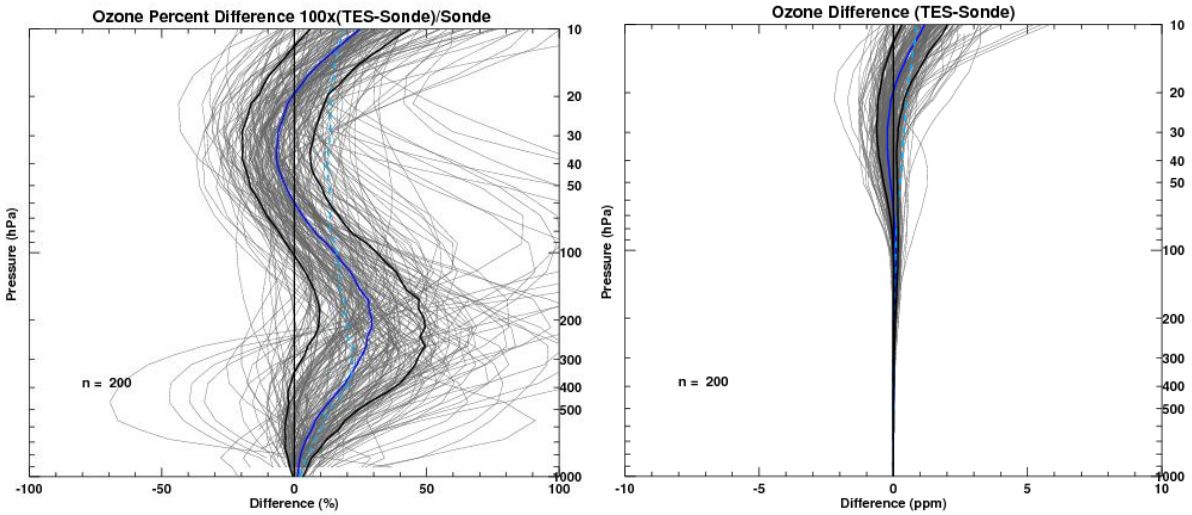


**(F: Antarctic 60$^{o}$ S to 90$^{o}$ S)**

**Figure 5-1** TES-sonde percent differences and absolute differences in six latitude zones. Individual profiles are shown in gray, mean and one standard deviation ranges are overlaid in dark blue and broken light-blue, respectively. Mean minus one standard deviation and mean plus one standard deviation ranges are overlaid in black. The number of coincident comparisons is "n." This Figure illustrates comparisons using TES V004. (A: Arctic, B: Northern Midlatitudes, C: Northern Subtropics, D: Tropics, E: Southern low- and midlatitudes, and F: Antarctic)

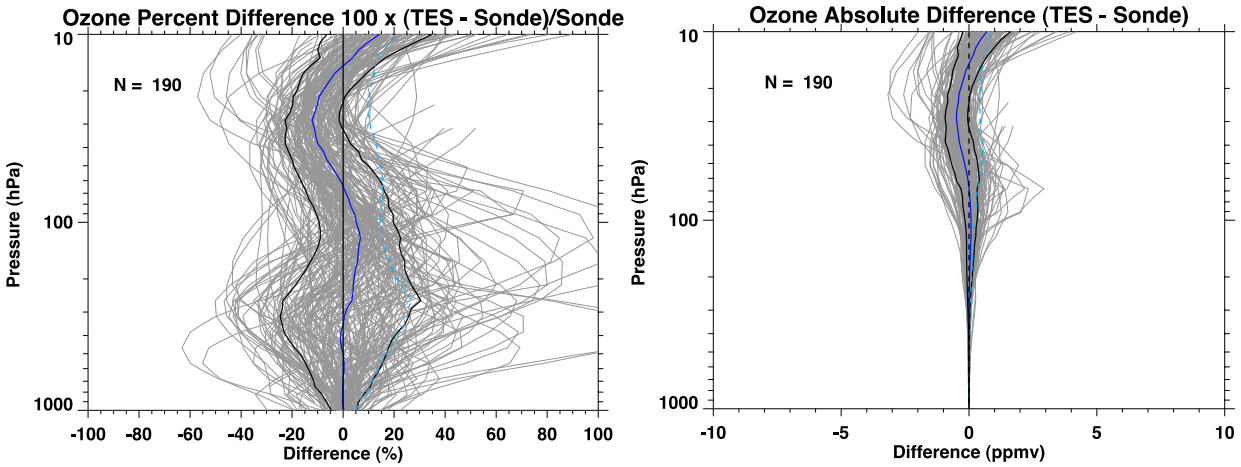


**(A: Arctic 56° N to 90° N)**

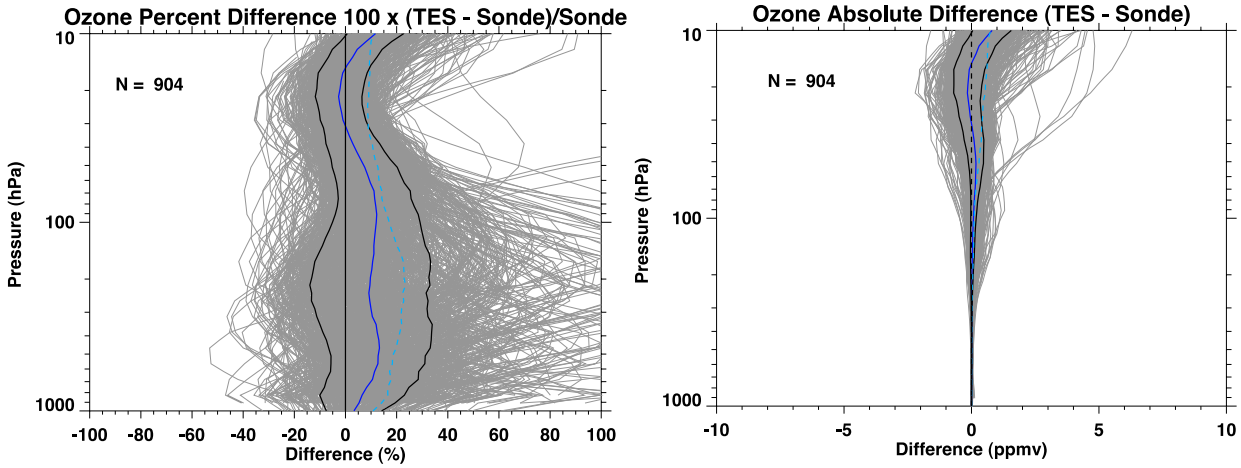


**(B: Northern Midlatitudes 35° N to 56° N)**

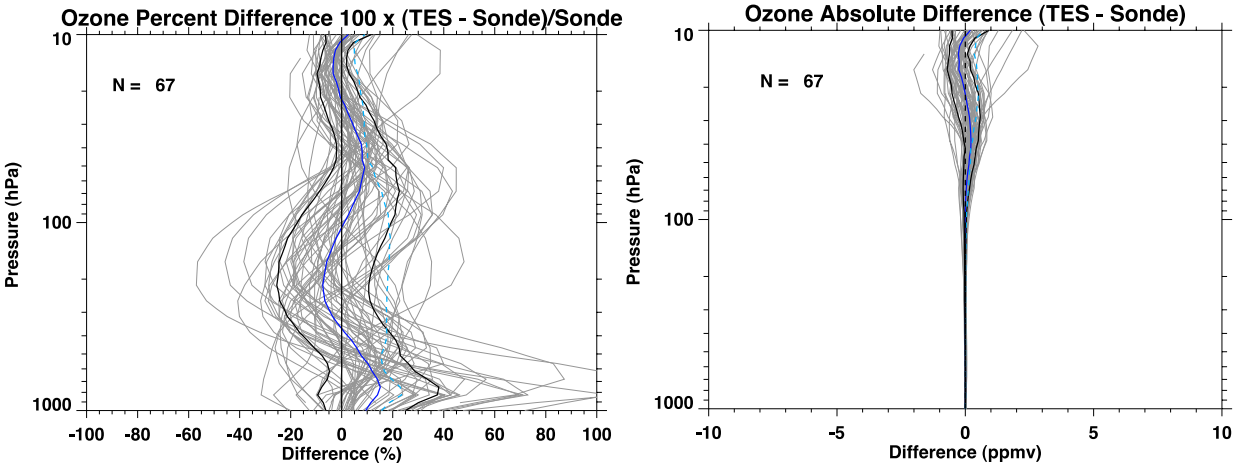


**(C: Northern Subtropics 15° N to 35° N)**

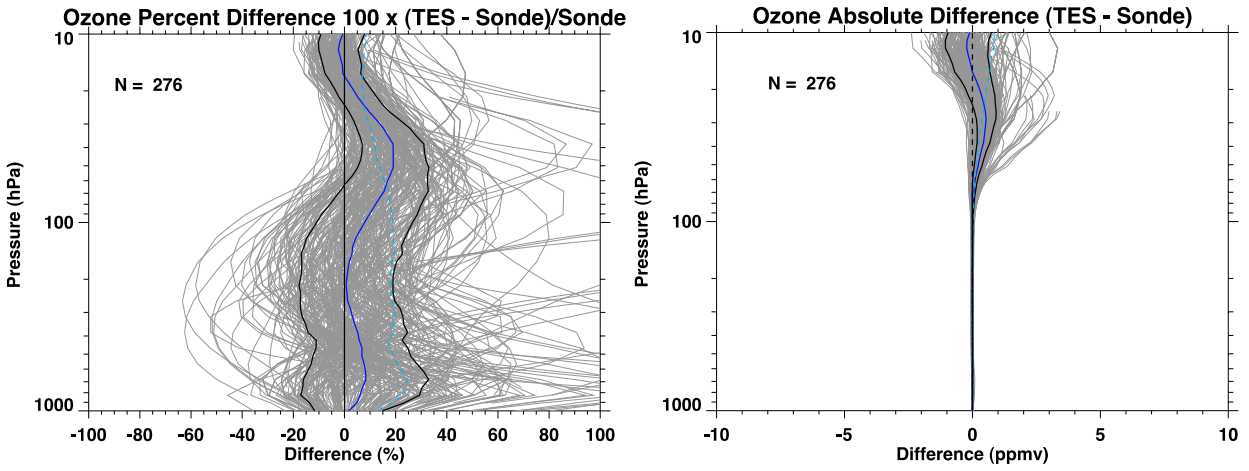


**(D: Tropics 15° S to 15° N)**

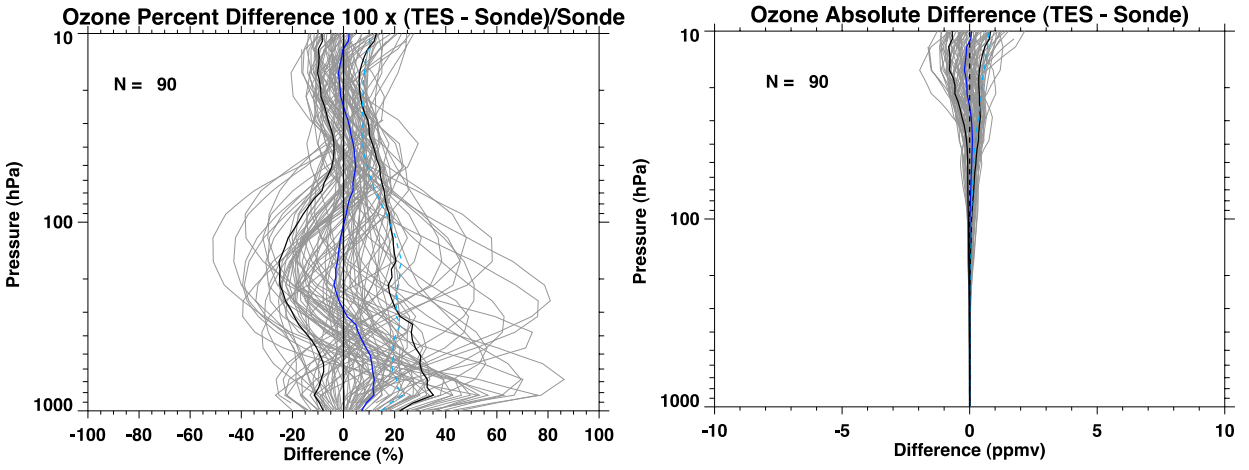


**(E: Southern low- and midlatitudes 15° S to 60° S)**

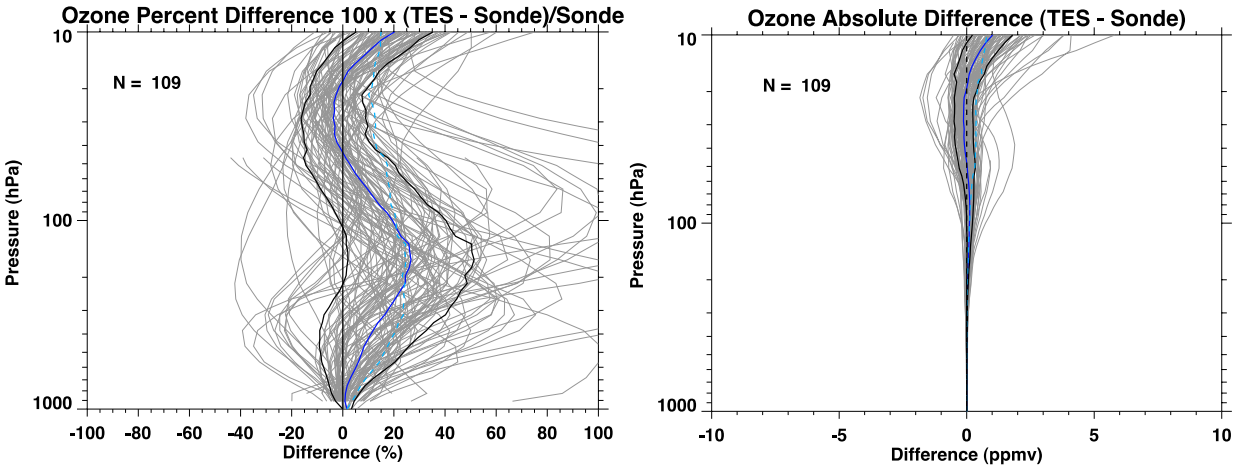


**(F: Antarctic 60° S to 90° S)**

**Figure 5-2** TES-sonde percent differences and absolute differences in six latitude zones. Individual profiles are shown in gray, mean and one standard deviation ranges are overlaid in

dark blue and broken light-blue, respectively. Mean minus one standard deviation and mean plus one standard deviation ranges are overlaid in black. The number of coincident comparisons is "n." This Figure illustrates comparisons using TES V005. (A: Arctic, B: Northern Midlatitudes, C: Northern Subtropics, D: Tropics, E: Southern low- and midlatitudes, and F: Antarctic)

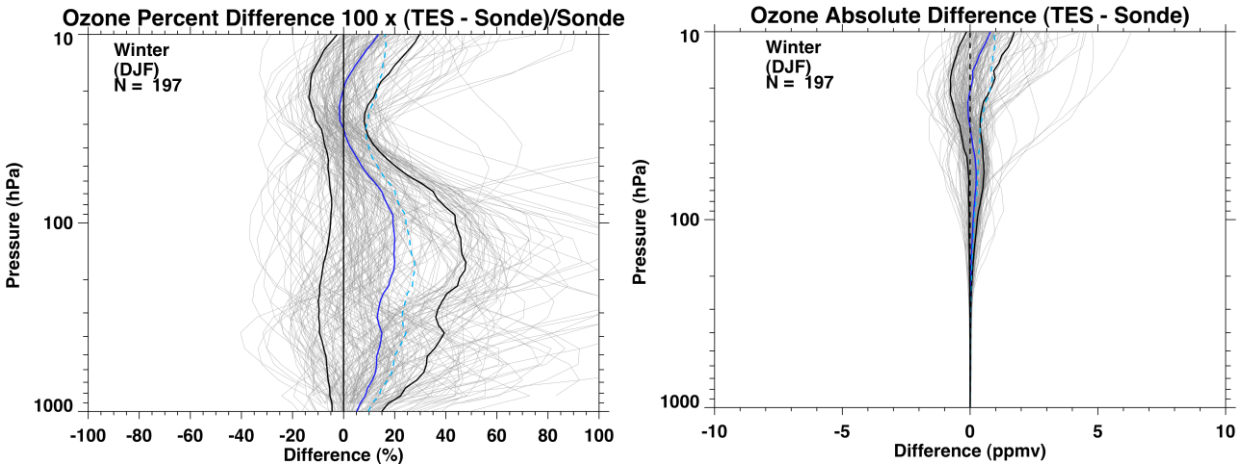


**Winter**

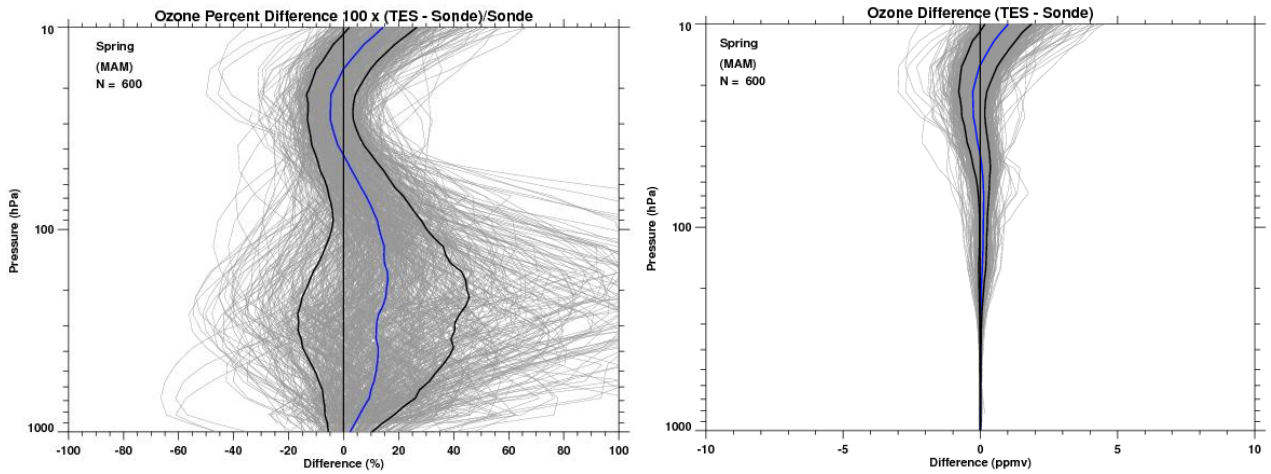


**Spring**

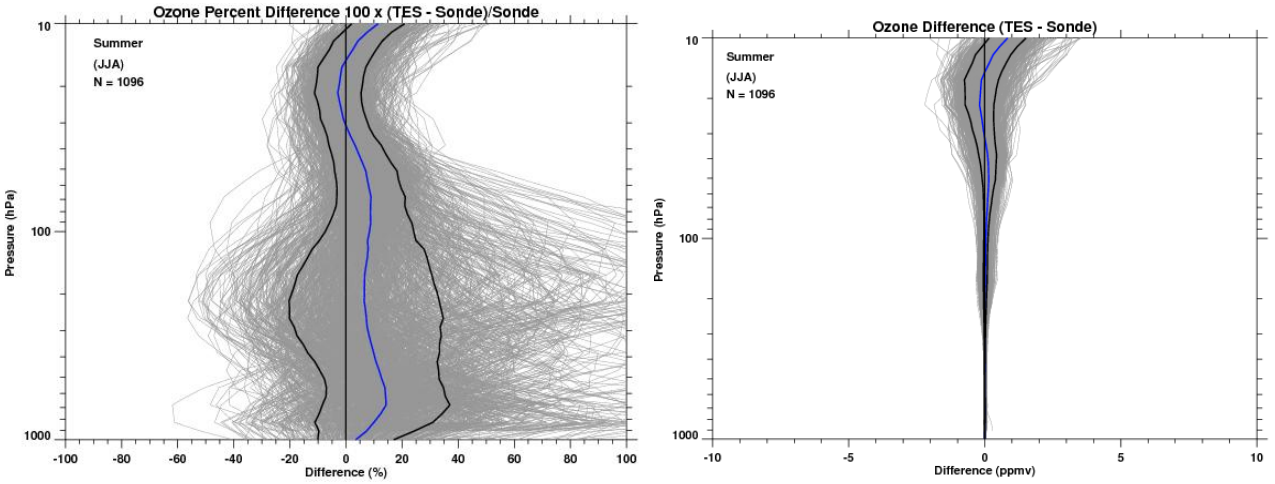


**Summer**

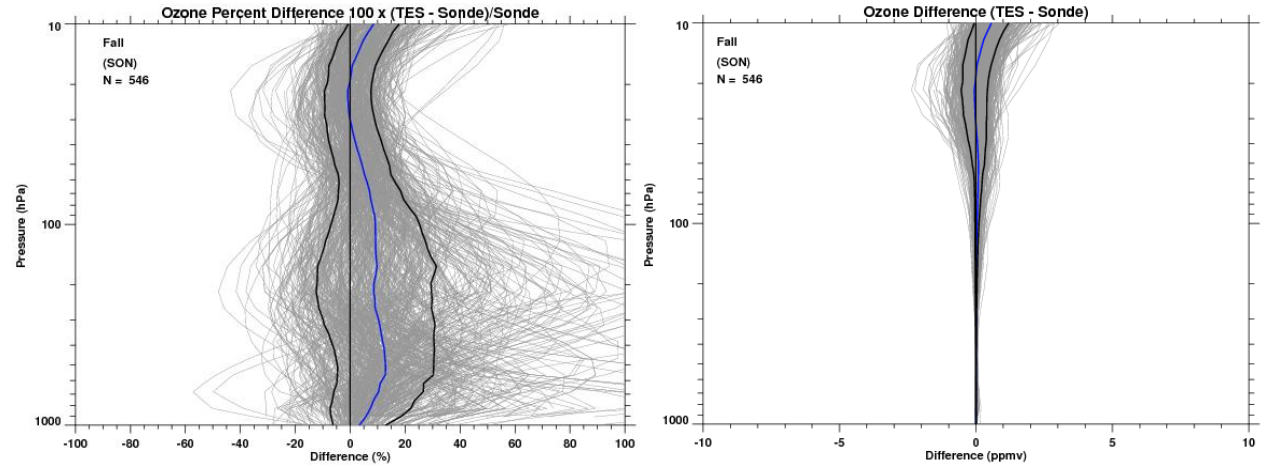


**Fall**

**Figure 5-3** TES-sonde ozone percent differences and absolute differences (for TES V004) for the four seasons (months abbreviated in parentheses) in the northern midlatitudes (35 to 56$^{o}$ N). Individual profiles are shown in gray, mean and one standard deviation ranges are overlaid in dark blue and broken light-blue, respectively. Mean minus one standard deviation and mean plus one standard deviation ranges are overlaid in black. The number of coincident comparisons is "n." This Figure illustrates comparisons using TES V004.

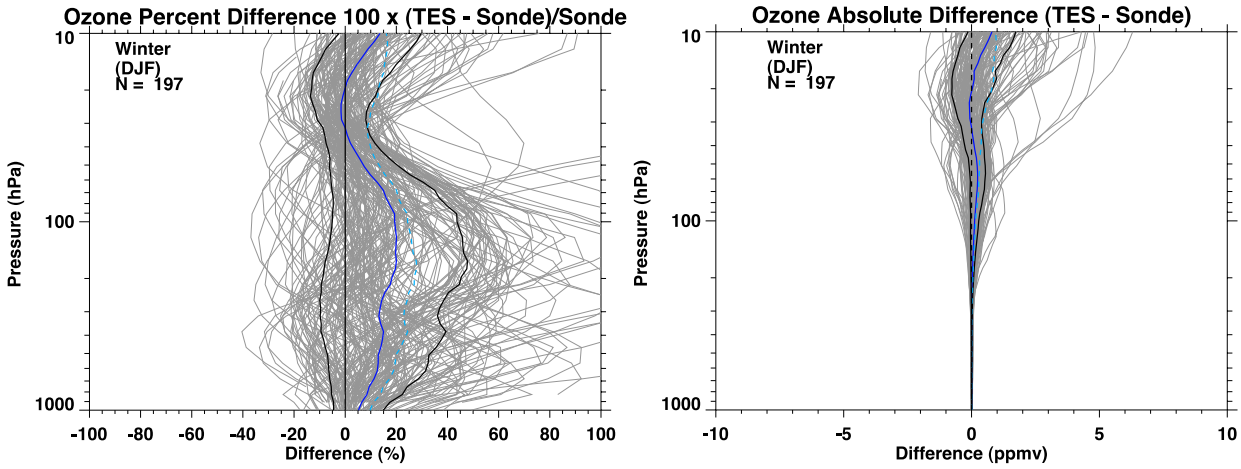


**Winter**

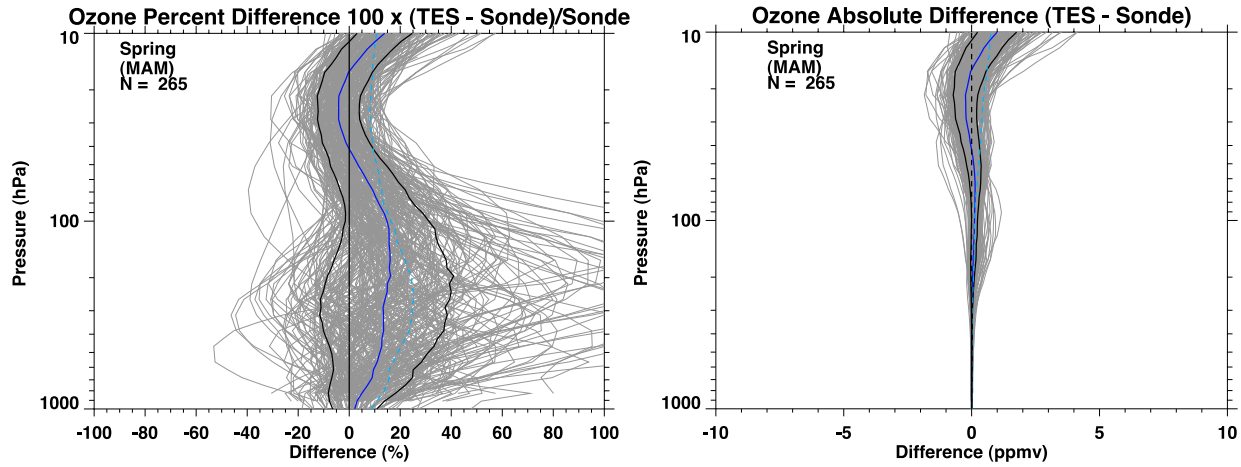


**Spring**

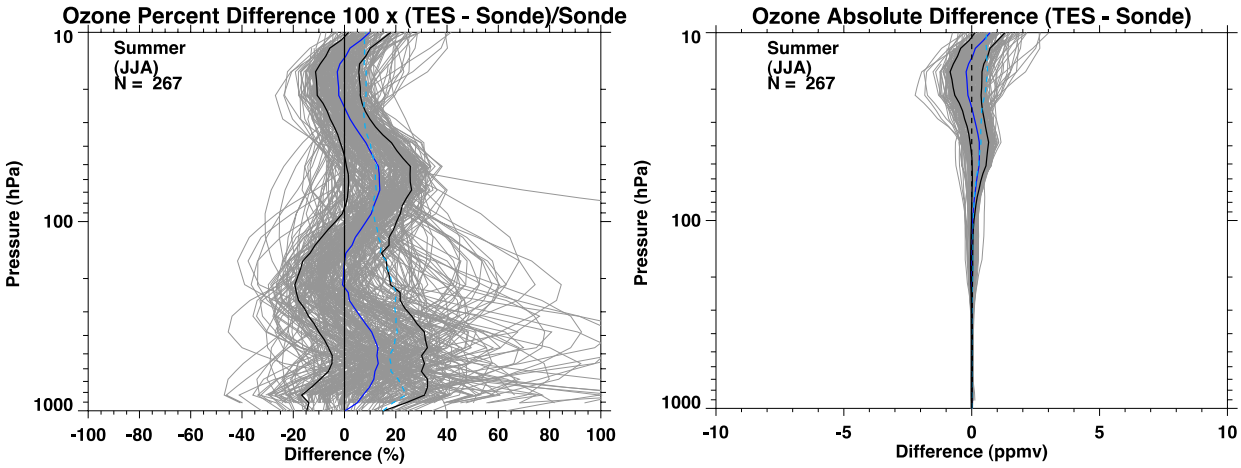


**Summer**

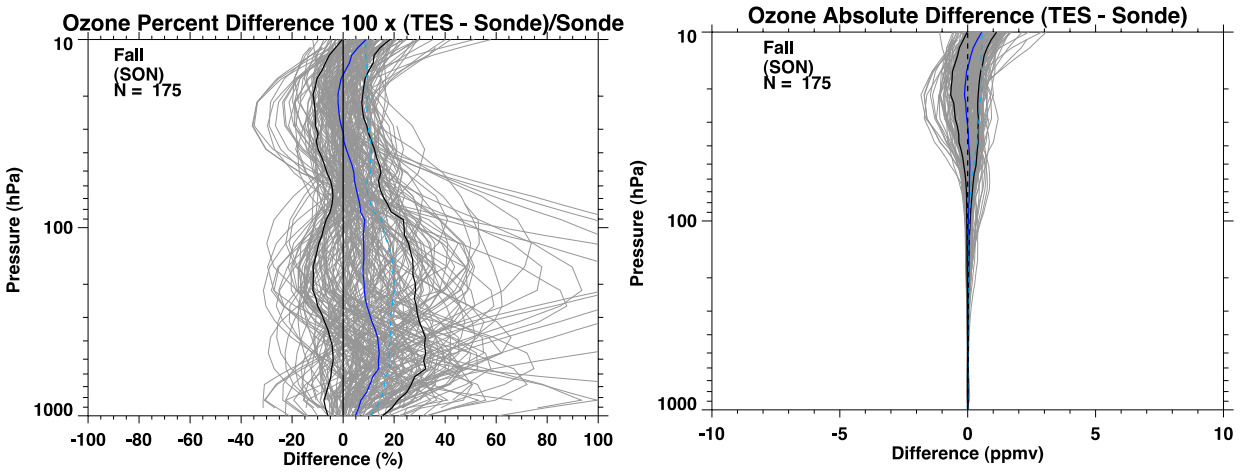


**Figure 5-4** TES-sonde ozone percent differences and absolute differences (for TES V005) for the four seasons (months abbreviated in parentheses) in the northern midlatitudes (35 to 56° N). Individual profiles are shown in gray, mean and one standard deviation ranges are overlaid in dark blue and broken light-blue, respectively. Mean minus one standard deviation and mean plus one standard deviation ranges are overlaid in black. The number of coincident comparisons is "n." This Figure illustrates comparisons using TES V005.

## 5.3 References

### 5.3.1 Primary TES Nadir Ozone References

[1] Boxe, C.S., J.R. Worden, K.W. Bowman, S.S. Kulawik, J.L. Neu, W.C. Ford, G.B. Osterman, R.L. Herman, A. Eldering, D.W. Tarasick, A.M. Thompson, D.C. Doughty, M.R. Hoffmann, S.J. Oltmans (2010), Validation of northern latitude Tropospheric Emission Spectrometer stare ozone profiles with ARC-IONS sondes during ARCTAS: sensitivity, bias and error analysis, *Atmospheric Chemistry and Physics*, doi:10.5194/acp-10-9901-2010, October 20, 2010.

[2] Nassar, R., J.A. Logan, H.M. Worden, I.A. Megretskaia, K.W. Bowman, G.B. Osterman, A.M. Thompson, D.W. Tarasick, S. Austin, H. Claude, M.K. Dubey, W.K. Hocking, B.J. Johnson, E. Joseph, J. Merrill, G.A. Morris, M. Newchurch, S.J. Oltmans, F. Posny, F.J. Schmidlin, H. Vömel, D.N. Whiteman, J.C. Witte (2008), Validation of Tropospheric Emission Spectrometer (TES) Nadir Ozone Profiles Using Ozonesonde Measurements, *J. Geophys. Res. 113*, D15S17, (doi:10.1029/2007JD008819), May 7, 2008.

### 5.3.2 TES References

[3] Herman, R. and G. Osterman (editors), Christopher Boxe, Kevin Bowman, Karen Cady-Pereira, Tony Clough, Annmarie Eldering, Brendan Fisher, Dejian Fu, Robert Herman, Daniel Jacob, Line Jourdain, Susan Kulawik, Michael Lampel, Qinbin Li, Jennifer Logan, Ming Luo, Inna Megretskaia, Ray Nassar, Gregory Osterman, Susan Paradise, Vivienne Payne, Hank Revercomb, Nigel Richards, Mark Shephard, Dave Tobin, Solene Turquety, Felicia Vilnrotter, Helen Worden, John Worden, Lin Zhang (2011), Earth Observing System (EOS) Tropospheric Emission Spectrometer (TES) Data Validation Report (Version F05_05, F05_06, F05_07 data), Version 4.0, JPL Internal Report D-33192, November 23, 2011.

### 5.3.3 General References

[4] Logan, J.A., An analysis of ozonesonde data for the troposphere: Recommendations for testing 3-D models, and development of a gridded climatology for tropospheric ozone, *J. Geophys. Res., 104,* 16115-16149, 1999.

# 6. Validation of TES Retrievals of Carbon Monoxide

## 6.1 Overview

TES CO and other species retrievals are currently being processed in version V005. All the original TES CO data validation activities, including comparisons with in-situ aircraft data, and with MOPITT V003 data and other satellite data, have been carried out for TES V003 or V002 data. The TES CO V004 data have no systematic changes from previous versions. In TES CO V005, two major changes were made: we adopted CO a priori from MOZART V04 model results (eight-year monthly averages) and the new constraint matrix used in retrievals. They are the same model a priori and constraint used in MOPITT CO V004 retrievals.

We briefly describe the TES instrument performance over six years on orbit, the positive effect of the optical bench warm-up conducted early Dec 2005 on filter 1A1 and the CO retrievals, and the recent (post April 2011) worsening throughputs in CO data due to instrument control system degradation. We give an overview of the characterization of TES CO retrievals, including the roles of a priori profiles and the averaging kernels. A brief overview of the global distributions of TES CO measurements is given for different seasons. For CO V005, we present comparisons of TES CO profiles with in situ measurements from several aircraft campaigns, including INTEX-B, AVE, and CR-AVE. Validation of TES CO V005 data using MOPITT V004 data are conducted for more Global Survey runs. These comparisons not only offer good qualitative checks for TES data, e.g., the characteristics of the CO global distribution or the shapes of their vertical profiles, but also offer quantitative validations of TES CO retrievals.

## 6.2 Instrument performance before and after optical bench warm-up

For constant emission source, e.g., on-board black body, the signal strength in TES 1A1 filter (1900-2300 $cm^{-1}$) is not constant over time and the variation of the signal strength is reflected in the CO retrievals. Figure 6-1 displays the normalized integrated spectral magnitude (ISM) (top panel), beam splitter temperature (middle panel), and degree of freedom for signal (DOFS) for latitudes of 30°N-30°S as a function of time (Rinsland et al., 2006). Data after the middle of 2006 stays about the same level. The ISM is a sensitive indicator of the signal levels of the TES detectors and is calculated by integrating a spectrum over wavenumber. It is the primary quantity used to quantify and detect trends in the TES instrument alignment and performance. An overall trend of declining ISM with time and the measured beamsplitter temperature is apparent, with increases in beamsplitter temperatures when the detectors are de-iced periodically. The warming of the TES optical bench on Nov 29-Dec 2, 2005 improved the TES beamsplitter alignment, with an integrated spectral magnitude increase for the 1A1 filter by a factor of 3.4 as compared to the pre-warm up value.

The TES CO retrieval ‘sensitivity’, or the parameters describing the retrieval vertical information in the troposphere, e.g., the Degree of Freedom for signal (DOF) and the retrieval errors, are much improved after the optical bench warm up in early December 2005 as a result of the better alignment of the instrument and increased signal to noise.

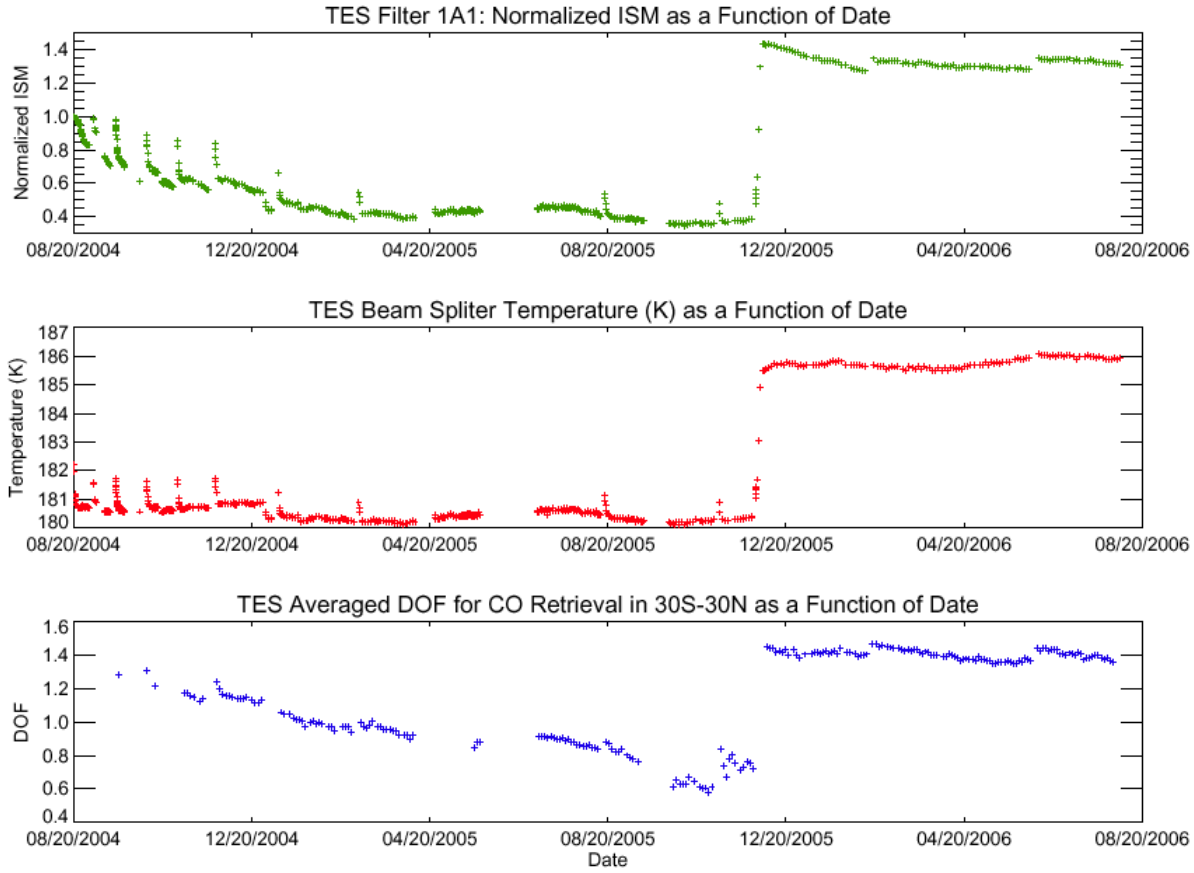


**Figure 6-1** Time series of measured normalized Integrated Spectral Magnitude (ISM) (top panel), beamsplitter temperature (middle panel), and average DOFS for 30°N-30°S latitude. The ISM is normalized to 1.0 at the beginning of the time series.

## 6.3 Problems in filter 1A1 signal used for CO retrieval since 2011

The aging of TES mechanically moving components, e.g., Interferometer Control System (ICS) has started to affect TES measured signals since early 2011. The majority of the problematic scans show 'over/underflows' or 'spikes' in the interferogram DNs (Data Number). TES Level 1A software detects and flags these scans and removes them from the L1B and L2 processing. Compared to 2004-2010 data we therefore see drop-offs in valid number of CO retrievals in the TES product since early 2011.

To illustrate the rate of CO data drop-offs over TES lifetime, Figure 6-2 shows the percent of bad interferogram scans (Fatal Error in L1A) per science/calibration run (e.g., a Global Survey or a Transect run). This percentage number seems jump between zero (all good) and 100% (all bad) depending on a given run number. Users should definitely expect to see a lot of missing CO retrievals in data files since 2011.

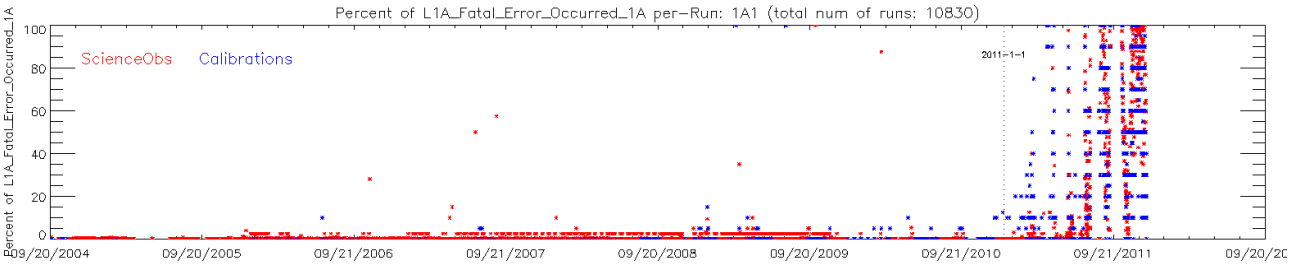


**Figure 6-2** Time series of percentage of 'L1A Fatal Error in 1A1' scans per-run. The time Jan 1, 2011 is marked in dotted-line.

## 6.4 Major changes from V004 to V005 in CO retrieval

Two major changes in TES CO V005 retrievals are made from previous version data: the a priori states and the constraints. The new MOZART-4 model data was provided to TES from the NCAR (National Center for Atmospheric Research) group. These new model results for CO VMR were averaged monthly in 10 degree latitude by 60 degree longitude boxes as the a priori state. We examined the new CO global seasonal distributions and confirmed that they have overcome some unrealistic features in the previous MOZART CO a priori state, e.g., higher CO concentrations in the upper troposphere than those in the boundary near the source regions in fall tropics. The constraint matrix for TES CO retrievals is also replaced by adopting the same algorithm provided by the MOPITT team for deriving their V004 data (Deeter et al., 2010). The new global constraint matrix is seen posting a slightly tighter constraint compared to the five band latitude constraints used for previous TES CO retrievals in the troposphere, except for the tropics; for example, the diagonals were set to 0.3 in lnVMR (about 30%).

The changes to the a priori states and the constraints will be reflected in the TES CO products. We examine the differences between TES V004 and V005 to see if they can be explained quantitatively by the different a priori and constraint. We also perform the comparisons of TES and MOPITT CO to evaluate their statistical differences by removing the known a priori effects as it has been done previously.

## 6.5 Global distributions of CO from TES measurements

Carbon monoxide is a by-product of incomplete combustion of fossil fuels and biomass, and is produced by oxidation of methane ($CH_4$) and other hydrocarbons. The global distributions of TES CO fields reflect this basic understanding, e.g., the enhanced CO regions and their seasonal variations are co-located with the known source regions. Figure 6-3 shows TES CO monthly mean distributions at 681.3 hPa for Jan, Apr, July, and Oct 2009. In general, the northern hemisphere (and the tropics) show much more CO than the southern hemisphere due to the known distribution of natural and industrial sources. CO values in the winter/spring are larger than summer/fall due to the longer lifetime in seasons with less photochemical activity.

In central Africa, the enhanced CO corresponding to biomass burning occurs in two time periods, in Dec/Jan/Feb for latitudes north of the equator and in Jul-Oct south of the equator, corresponding to the local dry seasons. In South America, the biomass burning induced maximum in CO concentration occurred during Aug/Sep/Oct near equator. Enhanced levels of CO over E. China can be related local pollution and can be seen throughout the year in the TES observations.

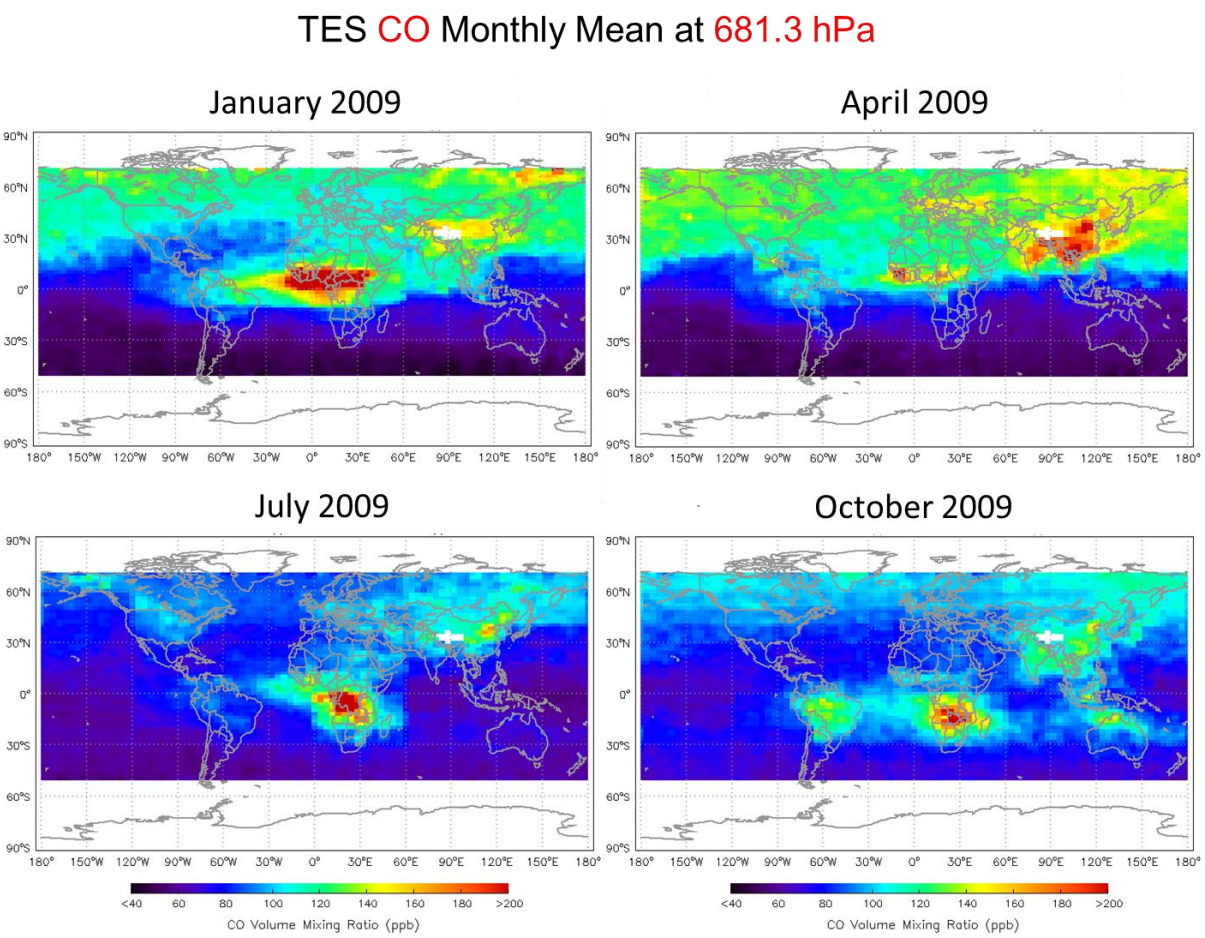


**Figure 6-3** TES CO Global Distributions at 681.3 hPa for the Four Typical Months, Jan, April, July, and Oct 2009.

## 6.6 CO validation: Comparisons to in situ Aircraft Measurement

During the past few years, several aircraft campaigns were conducted to study tropospheric chemistry and transport, and provide data for validation of the measurements made by the instruments on the Aura satellite. The TES team participated in the Aura Validation Experiment (AVE) campaigns: Oct-Nov 2004 based near Houston, Jan-Feb 2005 based in Portsmouth, NH (PAVE), and in Jan-Feb 2006 based in Costa Rica (CR-AVE). TES also participated in INTEX-B (International Chemical Transport Experiment), which had deployments in Houston, Honolulu and Anchorage in March-May 2006. The TES CO data from the time periods of these campaigns were compared with the in situ measurements for the aircraft flights when there are the best coincidences between TES measurement location and the aircraft CO profiles. Most validation results are reported in papers by M. Luo et al., 2007b and J. Lopez et al., 2008. We plan to repeat these comparisons for TES V005 CO data since major changes in retrieval a priori and constraints are made. These new comparisons will be made in the next a few months. Here we give a brief review of the aircraft data validation for previous version TES CO data.

In all aircraft campaigns, TES made a series of step and stare nadir observations with some footprints coinciding with the aircraft tracks and the spiral profiling locations. During the AVE and CR-AVE campaigns, CO was measured by the NASA Ames Research Center Argus instrument on the WB-57 aircraft. The CO profiles were also measured by Aircraft Laser Infrared Absorption Spectrometer (ALIAS) of JPL during CR-AVE. During the INTEX-B campaign the DACOM instrument by the NASA Langley Research Center was on board to measure CO.

For the TES and aircraft CO comparisons, all possible aircraft profiles, including profiles taken while taking-off and landing, and the vertical spirals, are extracted to match with TES profiles closest in times and locations. A few aircraft profiles and ~2-4 TES CO profiles per aircraft profile can be identified per campaign station, normally within a couple of hours and a couple to a few hundred kilometers. The next procedure is to apply TES retrieval operator to the in-situ profile, $x_{aircraft}$, to obtain the simulated aircraft profile as seen by TES, $x_{simul\text{-}aircraft}$,

$$x_{simul\text{-}aircraft} = Ax_{aircraft} + (I - A)x_a. \qquad \text{(Equation 6-1)}$$

where $x_a$ is the TES CO retrieval a priori profile from the MOZART model, and A is the averaging kernel. This profile as seen by TES is then compared to the TES retrieved CO profile.

In summary, the averaged comparisons are the best in the Houston region for the two campaigns in Oct 2004 and March 2006. The differences between Argus and TES CO profiles are within TES retrieval errors and equivalent to CO spatial/temporal variability detected in both TES and Argus measurements. The comparisons of TES and DACOM CO profiles near Hawaii and Anchorage in April-May 2006 are not as good. In these regions, the aircraft DACOM CO profiles are characterized by plumes or enhanced CO layers, consistent with known features in the tracer fields due to transpacific transport of polluted air parcels originating from East Asia. In TES V005 CO comparison, the effects of a priori should be removed and these conclusions should remain the same.

## 6.7 CO validation: comparisons to MOZAIC, ACE, MLS, and AIRS data sets

Some preliminary results are obtained in TES CO data validation using the CO data sets of MOZAIC (Measurements of Ozone and water vapor by In-service AIrbus aircraft, http://mozaic.aero.obs-mip.fr), ACE (Atmospheric Chemistry Experiment), MLS (Microwave Limb Sounder), and AIRS (Atmospheric Infrared Sounder). Detailed results are documented either in the previous version TES Validation Report (V003) or papers Rinsland et al., 2008, Warner et al., 2008.

## 6.8 CO Validation: Comparisons to MOPITT Data

Both TES and MOPITT (Measurements Of Pollution In The Troposphere) have updated CO data products to the new versions (V005 for TES and V004 for MOPITT) using updated a priori and constraints for CO retrievals from their previous version data. The a priori used by the two teams are from the same MOZART model simulation results. TES uses 10 degree latitude by 60 degree longitude monthly bins of the model data as the a priori. TES also uses the same algorithm as that of MOPITT to compute the constraint matrix used for all profile retrievals (Deeter et al., 2010), e.g., 0.3 diagonals in lnVMR (~30%) and 100 hPa vertical correlation

distances. In theory, different a priori or constraints will affect final CO products and to change their global distributions from precious versions, but when proper a priori, averaging kernels, and error estimates are considered in applications, the different version data should be consistent. Here we make comparisons between new versions of TES and MOPITT CO data using the technique that was applied in a previous study (Luo et al., 2007a). We did three TES Global Surveys, Sept 20-21, 2004, the original GS for the publication, a TES GS taken June 5-6, 2009, and a TES GS taken June 6-7, 2010 after the new instrument calibration scheme was adopted.

The retrieval results of TES 16-orbit global survey measurements in Sept 20-21, 2004 (Run ID 2147) have been examined extensively by the TES science team. In CO comparisons, MOPITT data are down-sampled to near the TES geolocations. Figure 6-4 shows TES and down-selected MOPITT CO VMR at 681 hPa and interpolated horizontally to illustrate the distribution more clearly. The two CO distribution fields are very similar partially due to the usage to the same a priori. This is an improvement from Luo et al. (2007a) using older versions of TES and MOPITT CO data.

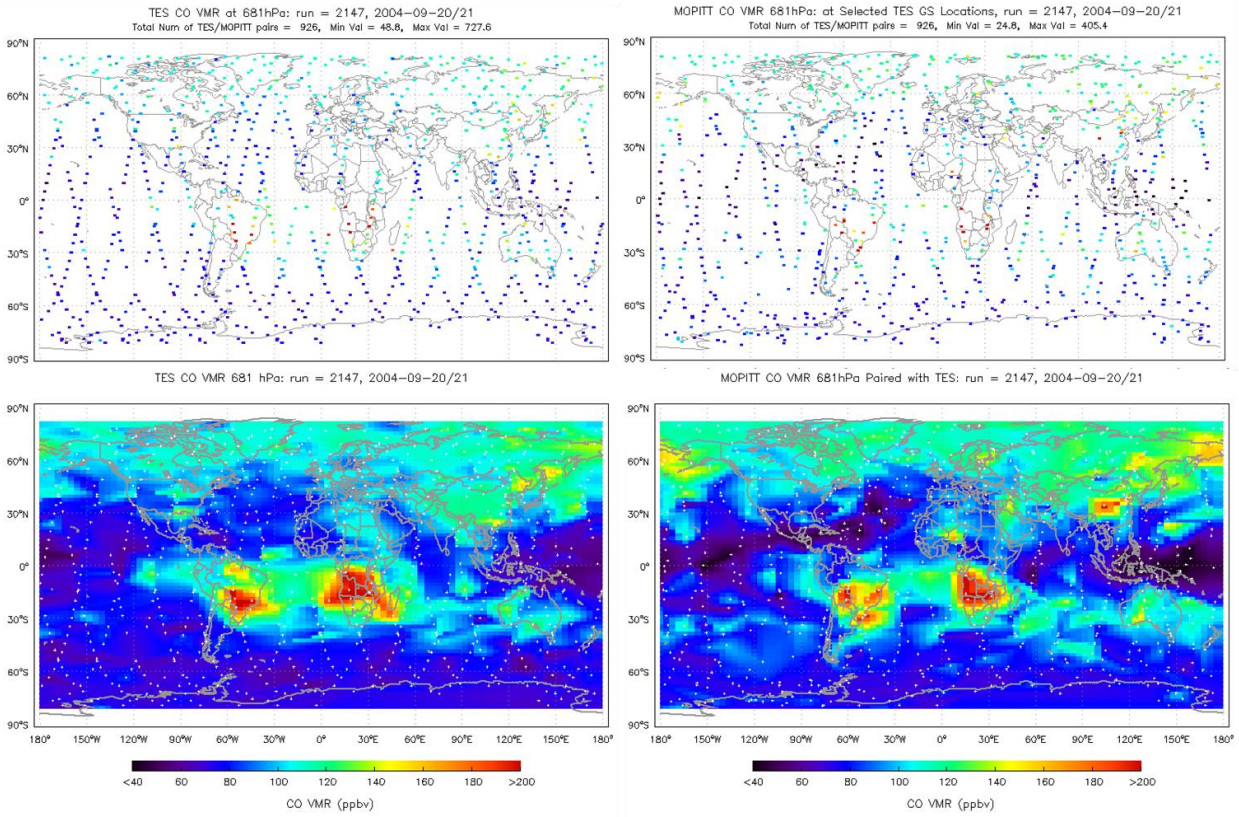


**Figure 6-4** TES (left column) and down-sampled MOPITT (right column) CO VMRs at 681 hPa. The corresponding date is one TES Global Survey, Sept 20-21, 2004. Top panels are TES and MOPITT CO VMRs at or near TES geolocations. Bottom panels are horizontally interpolated CO VMR maps with footprints in white dots.

Quantitative comparisons between TES and MOPITT CO at low, mid and upper troposphere and total column for this day are carried out. Three steps are performed in the comparison, direct comparison, adjusting TES CO profiles to MOPITT a priori profile, and applying TES averaging kernels to MOPITT retrieved profiles. The final comparison is to compare TES retrieved CO profiles adjusted to MOPITT a priori and the MOPITT retrieved CO profiles adjusted to MOPITT averaging kernel. The agreement between the two CO fields becomes better in all tropospheric levels and the total column, especially in the lower and upper troposphere where both instruments do not have much sensitivity in their measurements. Figure 6-5 shows the direct and final comparisons of the CO VMRs at 681 hPa between TES and MOPITT. The final comparisons show TES CO is slightly lower than that of MOPITT by <5% in global averages.

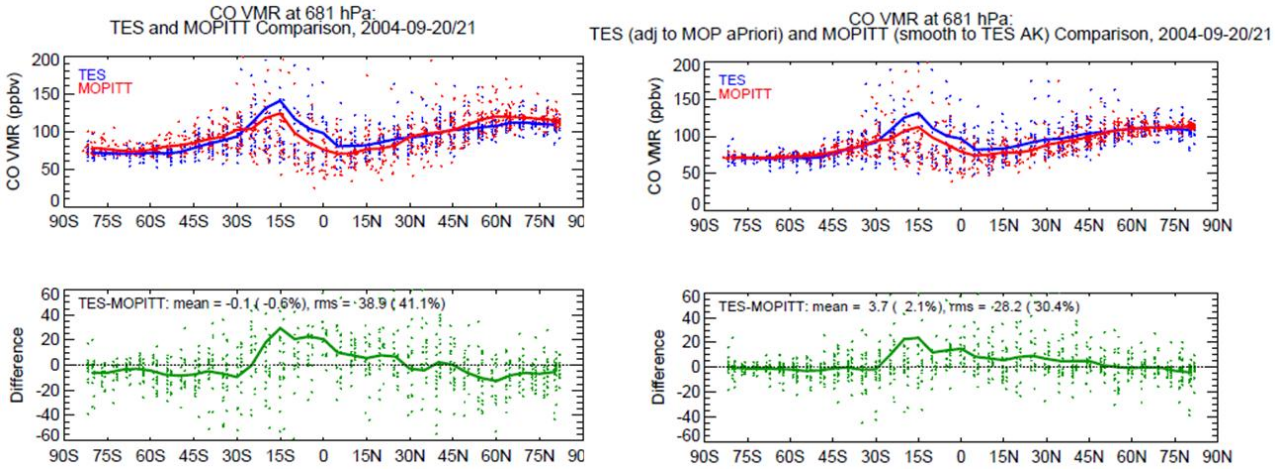


**Figure 6-5** Comparisons of CO VMR at 681 hPa reported by TES and MOPITT. The left two panels are the 'direct' comparisons. The right two panels are the comparisons after the TES CO being adjusted to MOPITT a priori profile and MOPITT CO profiles being adjusted by applying TES averaging kernels (Luo et al., 2007a).

To summarize the comparison results for Sept 20-21, 2004 and other two TES GS periods, three tables are used below.

**Table 6-1 TES-MOPITT CO comparisons for Sept 20-21, 2004**

| | 681 hPa | | 215 hPa | | Total Column | |
|---|---|---|---|---|---|---|
| | Mean Diff (%) | RMS of Diff (%) | Mean Diff (%) | RMS of Diff (%) | Mean Diff (%) | RMS of Diff (%) |
| Direct Compare | -0.6% | 41% | -0.5% | 29% | -0.9% | 20% |
| TES adj to MOP aPriori vs MOP | -0.5% | 36% | -0.2% | 29% | | |
| TES adj to MOP aPriori vs MOP adj to TES AK | 2.1% | 30% | 0.5% | 19% | | |
| RMS of MOP in 500km/24hrs of TES location | MOP at 700hPa<br>10-20% (land)<br>2-3% (ocean) | | MOP at 200hPa<br>5-30% (land)<br>1-2% (ocean) | | | |
| TES Retrieval Err | 10-20% | | 10-15% (20-30% S Pole) | | ~10%(20-30% S Pole) | |
| MOP Retrieval Err | 25-30% | | 25-30% | | 5-10% | |

**Table 6-2 TES-MOPITT CO comparisons for June 5-6, 2009**

| | 681 hPa | | 215 hPa | | Total Column | |
|---|---|---|---|---|---|---|
| | Mean Diff (%) | RMS of Diff (%) | Mean Diff (%) | RMS of Diff (%) | Mean Diff (%) | RMS of Diff (%) |
| Direct Compare | -5.1% | 30% | -7.1% | 30% | -6.4% | 15% |
| TES adj to MOP aPriori vs MOP | -3.1% | 28% | -8% | 30% | | |
| TES adj to MOP aPriori vs MOP adj to TES AK | -1.4% | 17% | -6.3% | 18% | | |
| RMS of MOP in 500km/24hrs of TES location | 10-15% | | 5-20% | | | |
| TES Retrieval Err | 10-20% | | 10-15% | | 5-15% | |
| MOP Retrieval Err | 25-30% | | 20-30% | | 5-10% | |

**Table 6-3 TES-MOPITT CO comparisons for Jun 6-7, 2010**

| | 681 hPa | | 215 hPa | | Total Column | |
|---|---|---|---|---|---|---|
| | Mean Diff (%) | RMS of Diff (%) | Mean Diff (%) | RMS of Diff (%) | Mean Diff (%) | RMS of Diff (%) |
| Direct Compare | -1% | 31% | -12% | 29% | -6% | 16% |
| TES adj to MOP aPriori vs MOP | -0.5% | 28% | -13% | 29% | | |
| TES adj to MOP aPriori vs MOP adj to TES AK | -0.3% | 17% | -7.7% | 19% | | |
| RMS of MOP in 500km/24hrs of TES location | 10-25% | | 10-30% | | | |
| TES Retrieval Err | 10-20% | | 10-15% | | ~10% | |
| MOP Retrieval Err | 25-30% | | 20-30% | | 5-10% | |

In all comparisons, the RMS (root-mean-square) of the TES-MOPITT differences are seen reducing from direct comparisons to the comparisons with slight differences in a priori and averaging kernels considered as described in Luo et al. (2007a). For TES GS run2147, Sept 20-21, 2004 in Table 6-1, the comparison conclusions are similar to that of Luo et al. (2007a) made for TES and MOPITT earlier version data. Here we add the calculation of the variability (RMS) of MOPITT CO within 500km/24hrs of TES location and time. This number indicates that the comparison RMS can partially be explained by miss-matches between the two instruments in space and time. We also listed estimated retrieval errors by the two instrument teams that also contribute to the explanations of the final RMS in the differences. However, we notice a few percent of TES CO lower mean bias compared to that of MOPITT in the upper troposphere (215 hPa) in Table 6-2 and Table 6-3 (marked red) for the two GSs in 2009 and 2010.

## 6.9 CO validation: summary

Carbon Monoxide: Comparisons have been carried out between TES carbon monoxide retrievals and those from a variety of satellite and aircraft instruments. Global patterns of carbon monoxide as measured by TES are in good qualitative agreement with those seen by MOPITT on the NASA Terra satellite. Comparisons of profiles of CO between TES and MOPITT show better agreement when a priori information is accounted for correctly. TES carbon monoxide agrees to within the estimated uncertainty of the aircraft instruments, including both errors and the variability of CO itself. In the upper troposphere, TES CO are found to bias lower compared to that of MOPITT by a few percent.

## 6.10 References

### 6.10.1 TES Carbon Monoxide References

[1] Lopez, J.P., M. Luo, L.E. Christensen, M. Loewenstein, H. Jost, C.R. Webster, and G. Osterman (2008), TES carbon monoxide validation during two AVE campaigns using the Argus and ALIAS instruments on NASA's WB-57F, *Journal of Geophysical Research, 113*, D16S47, (doi:10.1029/2007JD008811) August 2, 2008.

[2] Luo, M., C.P. Rinsland, C.D. Rodgers, J.A. Logan, H. Worden, S. Kulawik, A. Eldering, A. Goldman, M.W. Shephard, M. Gunson, and M. Lampel (2007a), Comparison of carbon monoxide measurements by TES and MOPITT: the influence of a priori data and instrument characteristics on nadir atmospheric species retrievals, *J. Geophys. Res., 112*, D09303, (doi:101029/2006JD007663) May 3, 2007a.

[3] Luo, M., C. Rinsland, B. Fisher, G. Sachse, G. Diskin, J. Logan, H. Worden, S. Kulawik, G. Osterman, A. Eldering, R. Herman and M. Shephard (2007b), TES carbon monoxide validation with DACOM aircraft measurements during INTEX-B 2006, *J. Geophys. Res., 112*, D24S48, (doi:10.1029/2007JD008803) December 20, 2007b.

[4] Rinsland, C.P., M. Luo, J.A. Logan, R. Beer, H.M. Worden, J.R. Worden, K. Bowman, S.S. Kulawik, D. Rider, G. Osterman, M. Gunson, A. Goldman, M. Shephard, S.A. Clough, C. Rodgers, M. Lampel, and L. Chiou (2006), Nadir Measurements of carbon monoxide distributions by the Tropospheric Emission Spectrometer onboard the Aura Spacecraft: Overview of analysis approach and examples of initial results, *Geophys. Res. Lett., 33*, (L2280610.1029/2006GL027000) November 22, 2006.

[5] Rinsland, C.P., M Luo, M.W. Shephard, C. Clerbaux, C.D. Boone, P.F. Bernath, L. Chiou, and P.F. Coheur (2008), Tropospheric Emission Spectrometer (TES) and Atmospheric Chemistry Experiment (ACE) measurements of tropospheric chemistry in tropical southeast Asia during a moderate El Niño in 2006, *J Quant Spectrosc Radiat Transfer, 109/10*, 10.1016/j.jqsrt.2007.12.020, 1931-1942, May 16, 2008.

[6] Warner, J., C. Barnet, M. Luo, G. Sachse (2008), Improved Tropospheric Carbon Monoxide Profiles Using Collocated AIRS and TES Satellite Measurements, submitted to *Geophys. Res. Lett.*, 2008.

[7] Deeter, M.N., D.P. Edwards, J.C. Gille, L.K. Emmons, G. Francis, S.-P. Ho, D. Mao, D. Masters, H. Worden, James R. Drummond, and Paul C. Novelli (2010), The MOPITT version 4 CO product: Algorithm enhancements, validation, and long-term stability, *J. Geophys. Res.*, 115, D07306, doi:10.1029/2009JD013005, April 15, 2010.

# 7. Validation of TES nadir Temperature Retrievals with Radiosondes

## 7.1 Executive Summary

TES V005 nadir temperature (TATM) retrievals have been compared with nearly coincident radiosonde (hereafter sonde) measurements from the NOAA ESRL global sonde database. For TES V005 TATM minus Tradiosonde (with averaging kernel applied), the bias is +0.2 to +0.5 K in the lower troposphere, -0.5 K in the upper troposphere. This is an improvement over previous versions of TES TATM. The rms is less than 1 K in the stratosphere and upper troposphere, but increases to 1.7 K in the lower troposphere. In clear sky conditions (average cloud effective optical depth less than 0.1), the bias improves in the lower troposphere but increases to +0.5 K at 500 hPa pressure level.

## 7.2 Previous versions of TES TATM retrievals

Validation of version V004 TATM was presented in the previous TES validation report (Herman et al., 2011). The bias of TES V004 TATM versus radiosondes was calculated to be:

bias over ocean < 0.6 K (531 TES-sonde matches),

bias over land < 0.5 K (1118 matches).

This was an improvement over the 1 to 2 K upper tropospheric cold bias in TES V003 TATM.

The rms was best determined from the NOAA ESRL database because exact sonde launch times were known, which allowed a closer match in time to the TES retrieval. The TES TATM rms in V004 was 1 K in the stratosphere and upper troposphere, and 1.5 K in the lower troposphere (at 500 to 900 hPa), compared to 2-4 K in V003. This included a 0.5 to 1 K uncertainty simply due to the spatial and temporal variability of atmospheric temperature (e.g., Tobin et al., 2006).

## 7.3 Details of TES V005 TATM retrieval

For V005 TATM, there are two retrieval steps. First, for latitudes between 40° S and 40° N, there is a simultaneous retrieval of TATM, $O_3$, and $CO_2$. Second, there is a sequential retrieval of TATM. For both V004 and V005, this sequential retrieval uses the 2B1 filter. The microwindows selected for temperature retrieval are within the $CO_2$ $\nu_2$ band, spanning 671.32 to 901.48 $cm^{-1}$ (14.896 μm to 11.093 μm wavelength). In previous versions V002 and V003, TATM, $H_2O$, and $O_3$ were retrieved simultaneously (Bowman et al., 2002, 2006; Worden et al., 2004). Constraints are altitude-dependent Tikhonov constraints (Kulawik et al., 2006). For V005, there is now surface temperature (TSUR) initial guess refinement for daytime land retrievals when the initial guess is too low. The surface emissivity has two additions; freshwater emissivity over a freshwater scene and ice emissivity when TSUR < 265 K over water.

The TES V004 and V005 L2 retrieval processes use a $CO_2$ climatology that incorporates improved seasonal and geographic variations in $CO_2$, as well as scaling to account for the annual increase in global $CO_2$ levels. This is highly relevant to temperature retrievals from the $CO_2$ $\nu_2$ band because inaccurate assumptions about atmospheric $CO_2$ concentrations may lead to significant errors in atmospheric temperature retrievals, up to 0.5 K (see Figure 14 of Divakarla et al., 2006). The climatology is based on model results for the year 2004 from a chemical

transport model (CTM) used in conjunction with a variety of other models to provide $CO_2$ surface fluxes [David Baker, pers. comm.]. The CTM used to create the time-varying three-dimensional $CO_2$ fields (longitude, latitude and pressure) is the Model of Atmospheric Transport and Chemistry (MATCH) (Nevison et al., 2008). Key surface $CO_2$ fluxes are derived from models including biospheric fluxes from the Carnegie Ames Stanford Approach (CASA) land biosphere model, oceanic fluxes from the WHOI model and a realistic, annually-varying fossil fuel source scheme (Nevison et al., 2008). The $CO_2$ fields generated by the model compare well to GLOBALVIEW atmospheric $CO_2$ data. Model results were provided to the TES team for the year 2004. Monthly mean profiles were calculated for two longitude bins and 10-degree latitude bins. This binned monthly mean climatology for 2004 was then scaled upward yearly (by 1.0055) to match the annual increase in $CO_2$.

### 7.4 A priori constraint vector

For each individual sequence and scan, the initial guess in the TES retrieval algorithm is set equal to an a priori profile (constraint vector). The TES V005 a priori constraint vectors come from NASA's Goddard Earth Observing System (GEOS) data assimilation system GEOS-5 (Rienecker et al., 2008). These data are produced by the Global Modeling and Assimilation Office (GMAO) at the NASA Goddard Space Flight Center (GSFC), on a 0.625° longitude by 0.5° latitude grid. GEOS-5 data are then interpolated to the locations and pressure levels of TES retrievals. The a priori covariance matrices used for retrieval regularization are described in Bowman et al. (2006). GEOS-5 assimilates a wide range of operational satellite data and in situ sonde measurements. Sonde profiles are strong constraints on the thermal structure and winds throughout the troposphere, with an emphasis on continental regions where the observing network is denser. Space-based observations include the High Resolution Infrared Sounders (HIRS) and Advanced Microwave Sounders (AMSU) instruments on NOAA's operational sounders, which directly constrain temperature and moisture. GEOS-5 includes a direct assimilation of radiances from AMSU and HIRS in a three-dimensional variational assimilation, as well as radiances from the Advanced Infrared Sounder (AIRS) and AMSU instruments on NASA's EOS Aqua platform (Zhu and Gelaro, 2008). The previous GEOS-4 assimilated observations of temperature and water vapor using a one-dimensional variational approach (Bloom et al., 2005), where a retrieval was made using a six-hour forecast as a priori state; the retrieved variables were assimilated.

### 7.5 Current Validation Status of V005 nadir temperature

This section summarizes the latest validation comparisons for V005 TES nadir TATM retrievals. TES retrievals have been filtered by the master quality flag. The TES observation operator has been applied to the sonde profiles, and differences are shown as TATM minus Tradiosonde (with averaging kernel). Levels where TES has no sensitivity to temperature (i.e. where the sum of the row of the averaging kernel equals zero) are not included in the calculation of the mean difference.

TES V005 TATM was compared with a global sonde database from the National Oceanic and Atmospheric Administration (NOAA) Earth System Research Laboratory (ESRL) Global Systems Division, formerly Forecast Systems Laboratory [M. Govett, pers. comm.]. The advantage of this database is that it includes the exact sonde release time (for sonde dates

through the end of 2007), which improves the temporal coincidence between TES and sonde, and the temperature rms. The NOAA ESRL database combines the IGRA global data with North American Global Telecommunications Service (GTS) sonde observations. Both undergo extensive checks for errors and hydrostatic consistency.

TES global surveys from 2004-2007 are matched with sonde profiles from the NOAA ESRL database within 100 km and -0.5 hr to +1.5 hr. The tightly constrained time match is possible because the exact sonde release time is known. Times are offset so that, on average, the sonde has ascended to the middle troposphere by the time of the Aura overpass and TES retrieval.

Figure 7-1 shows comparisons of TES V005 TATM with NOAA ESRL sondes. Outliers have been removed by using an iterative 3-sigma rejection algorithm. The solid red line is the temperature bias (TES minus sonde with averaging kernel) and the dashed red line is the temperature rms. The blue line is the TES observation error (measurement error plus systematic error). For TES V005 TATM minus Tradiosonde (with averaging kernel applied), the bias is +0.2 to +0.5 K in the lower troposphere, -0.5 K in the upper troposphere. This is an improvement over previous versions of TES TATM. The rms is less than 1 K in the stratosphere and upper troposphere, but increases to 1.7 K in the lower troposphere. In clear sky conditions (average cloud effective optical depth less than 0.1), the bias improves in the lower troposphere but increases to +0.5 K at 500 hPa pressure level.

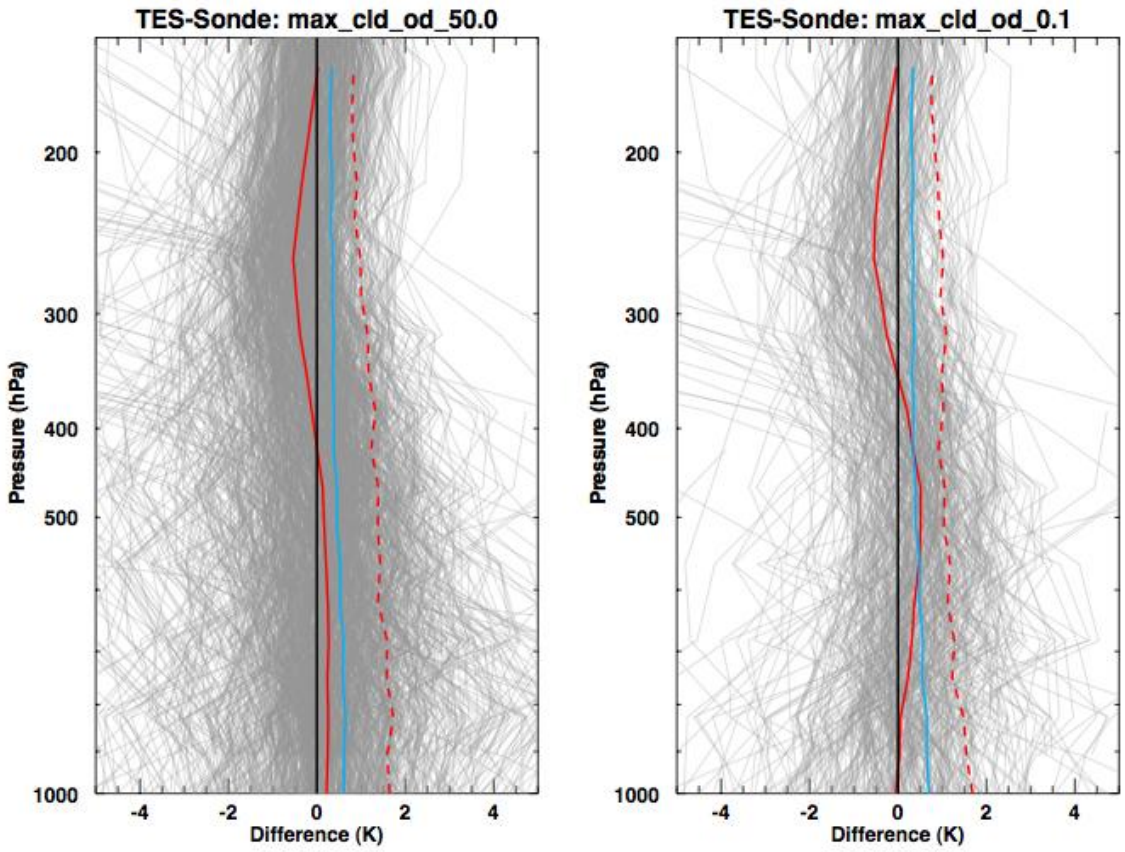


**Figure 7-1** Temperature differences between TES V005 TATM and NOAA ESRL radiosondes with observation operator applied: (left) all 971 comparisons, (right) comparisions filtered by

average cloud effective optical depth < 0.1. Shown are individual temperature differences (thin grey lines), bias (solid red line), rms (dashed red line), and the TES observation error (solid blue line). Figure prepared using Karen Cady- Pereira's idl code and an output save file from the TES sonde comparison tool.

## 7.6 TES Temperature Retrieval Stability 2006-2011

A recent DFM by J. Hegarty et al. (2012) presented an analysis of TES TATM retrieval stability over the lifetime of the TES instrument. An excerpt of that DFM is included below (Hegarty et al., 2012).

### 7.6.1 Background on retrieval stability

The TES retrievals have been validated with radiosondes, ozonsondes, aircraft measurements, and other satellite measurements (e.g. Osterman et al., 2007, 2008; Nasser et al., 2008; Richards et al., 2008; see http://tes.jpl.nasa.gov/documents/publications/ for a comprehensive list of studies). In addition, the radiance measurements within 30° of the equator were shown to be stable over a four year period from 2005 - 2009 (Connor et al., 2011). However, the TES instrument exceeded its five-year expected lifetime in 2009 and has since experienced several age-related mechanical problems that have required some mitigating changes to its operations. The question arises as to whether these changes and any other age-related degradation of the instrument may have altered the retrieval quality or its characteristics in any meaningful way. We present here a long-term evaluation of TES retrieval stability using TATM retrievals from January 2006 – July 2011. TATM was chosen for the evaluation because it is the first parameter retrieved and its quality impacts the subsequent retrieval of all the other parameters.

### 7.6.2 Analysis and Results

The TES V005 TATM retrieval stability evaluation used global survey (GS) data in two geographical boxes referred to as the Tropical Pacific Box (10° S – 10° N, 160° W – 120° W) and the North Atlantic Box (30° N – 60° N, 60° W – 20° W). Though both boxes were centered over oceans, the North Atlantic Box intersected the North American and European land masses and both contained some island points. To avoid the complicating factor introduced by highly variable land surface emissivity all the land points within the boxes were screened from the evaluation data set using the TES surface type flag. Additionally points were screened for quality using the TES retrieval quality flag and for optically thick clouds using an average cloud effective optical depth threshold of 0.5.

To evaluate the retrieval stability the monthly mean and standard deviation of the TATM residual between TES and the Global Modeling and Data Assimilation Office (GMAO) GEOS-5 model (Rienecker et al., 2008), which provides the first guess and a priori for the TATM retrieval, were calculated. These statistics were produced for the surface and at four standard TES pressure levels; 825 hPa, 464 hPa, 261 hPa, and 100 hPa. The statistics for both geographical boxes, shown in Figure 7-2, indicate only minor month-to-month variability and no substantial trends over the entire five-and-a-half year period. The TES TATM retrieval in the Tropical Pacific Box had an average bias of -0.8 K at the surface and -1.0 K near the tropopause

(100 hPa). In the North Atlantic Box the TES surface and tropopause (261 hPa) TATM were also biased by -0.6 K and -0.8 K, respectively. There were no substantial biases at other levels.

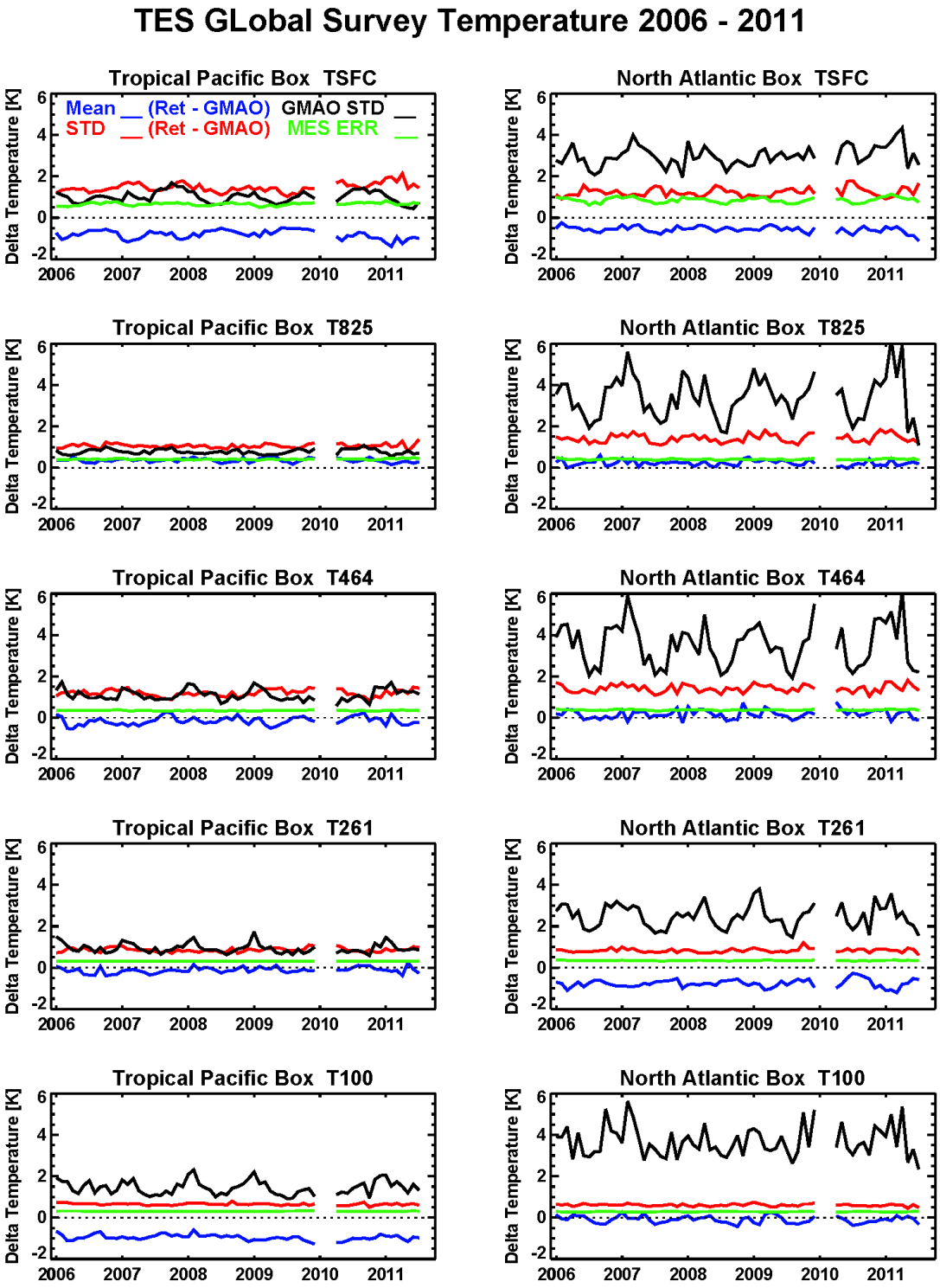


**Figure 7-2** Mean (blue) and standard deviation (red) of TES TATM minus GMAO GEOS-5 temperature residuals with GMAO standard deviation (GMAO STD, black) and TES

measurement error estimate (TES ERR, green) for the surface (TSUR), 825, 464, 261, and 100 hPa pressure levels. Figure courtesy of J. Hegarty, AER (Hegarty et al., 2012).

The standard deviation of the residual was generally smaller than the standard deviation of the GMAO GEOS-5 but larger than the TES estimated measurement error (Figure 7-2). The exception was for the surface temperature (TSUR) in the Tropical Pacific Box which had a slight increase in standard deviation early in 2011 to a maximum value of 2.13 K in April. The TSUR bias also decreased to its lowest value of -1.4 K during February of 2011 and was -1.25 during April 2011. However, both statistics relaxed back to values more in line with those of the entire period during the months of May - July of 2011.

Overall, based on this analysis it appears that the TES retrieval quality has remained stable from 2006 - 2011.

## 7.7 References

### 7.7.1 TES Temperature References

[1] Hegarty, J., S.S. Kulawik, V.H. Payne, K.E. Cady-Pereira, TES Temperature Retrieval Stability 2006-2011, TES Internal DFM, 2012.

### 7.7.2 TES References

[2] Bowman, K. W., J. Worden, T. Steck, H. M. Worden, S. Clough, and C. Rodgers (2002), Capturing time and vertical variability of tropospheric ozone: A study using TES nadir retrievals, *J. Geophys. Res., 107, No. D23,* 4723, (doi:10.1029/2002JD002150) December 14, 2002.

[3] Bowman, K. W., C. D. Rodgers, S. S. Kulawik, J. Worden, E. Sarkissian, G. Osterman, T. Steck, M. Luo, A. Eldering, M. W. Shephard, H. Worden, M. Lampel, S. A. Clough, P. Brown, C. Rinsland, M. Gunson, R. Beer (2006), Tropospheric emission spectrometer: Retrieval method and error analysis, *IEEE Trans. Geosci. Remote Sens., 44(5),* 1297-1307, May 2006.

[4] Connor, T.C., M.W. Shephard, V.H. Payne, K.E. Cady-Pereira, S.S. Kulawik, M. Luo, G. Osterman, M. Lampel (2011), Long-term stability of TES satellite radiance measurements, *Atmospheric Measurement Techniques, 4,* doi:10.5194/amt-4-1481-2011, 1481–1490, July 25, 2011.

[5] Herman, R. and Osterman G. (editors), Christopher Boxe, Kevin Bowman, Karen Cady-Pereira, Tony Clough, Annmarie Eldering, Brendan Fisher, Dejian Fu, Robert Herman, Daniel Jacob, Line Jourdain, Susan Kulawik, Michael Lampel, Qinbin Li, Jennifer Logan, Ming Luo, Inna Megretskaia, Ray Nassar, Gregory Osterman, Susan Paradise, Vivienne Payne, Hank Revercomb, Nigel Richards, Mark Shephard, Dave Tobin, Solene Turquety, Felicia Vilnrotter, Helen Worden, John Worden, Lin Zhang (2011), Earth Observing System (EOS) Tropospheric Emission Spectrometer (TES) Data Validation Report (Version F05_05, F05_06, F05_07 data), Version 4.0, JPL Internal Report D-33192, November 23, 2011.

[6] Kulawik, S. S., G. B. Osterman, D. B. A. Jones, and K. W. Bowman (2006), Calculation of Altitude-Dependent Tikhonov Constraints for TES Nadir Retrievals, *IEEE Transactions on Geoscience and Remote Sensing, 44 (No.5),* Special Issue on Aura, 1334-1342, May 2006.

[7] Nassar, R., J.A. Logan, H.M. Worden, I.A. Megretskaia, K.W. Bowman, G.B. Osterman, A.M. Thompson, D.W. Tarasick, S. Austin, H. Claude, M.K. Dubey, W.K. Hocking, B.J. Johnson, E. Joseph, J. Merrill, G.A. Morris, M. Newchurch, S.J. Oltmans, F. Posny, F.J. Schmidlin, H. Vömel, D.N. Whiteman, J.C. Witte (2008), Validation of Tropospheric Emission Spectrometer (TES) Nadir Ozone Profiles Using Ozonesonde Measurements, *J. Geophys. Res. 113*, D15S17, (doi:10.1029/2007JD008819), May 7, 2008.

[8] Osterman, G., S.S. Kulawik, H.M. Worden, N.A.D. Richards, B.M. Fisher, A. Eldering, M.W. Shephard, L. Froidevaux, G. Labow, M. Luo, R.L. Herman, K.W. Bowman, A.M. Thompson (2008), Validation of Tropospheric Emission Spectrometer (TES) Measurements of the Total, Stratospheric and Tropospheric Column Abundance of Ozone, *J. Geophys. Res., 113*, D15S16, (doi:10.1029/2007JD008801) May 7, 2008.

[9] Osterman, G. B. (editor), K. Bowman, K. Cady-Pereira, T. Clough, A. Eldering, B. Fisher, R. Herman, D. Jacob, L. Jourdain, S. Kulawik, M. Lampel, Q. Li, J. Logan, M. Luo, I. Megretskaia, R. Nassar, G. Osterman, S. Paradise, V. Payne, H. Revercomb., N. Richards, M. Shephard, D. Tobin, S. Turquety, F. Vilnrotter, H. Worden, J. Worden, and L. Zhang (2007), Earth Observing System (EOS) Tropospheric Emission Spectrometer (TES) Data Validation Report (Version F04_04 data), Version 3.0, JPL Internal Report D-33192, November 5, 2007, available at: http://eosweb.larc.nasa.gov/PRODOCS/tes/validation/

[10] Richards, N.A.D., G.B. Osterman, E.V. Browell, J.W. Hair, M. Avery and Q.Li, Validation of Tropospheric Emission Spectrometer ozone profiles with aircraft observations during the Intercontinental Chemical Transport Experiment–B, *J. Geophys. Res., 113*, D16S29, (doi:10.1029/2007JD008815) May 23, 2008.

[11] Worden, J., S. S. Kulawik, M. W. Shephard, S. A. Clough, H. Worden, K. Bowman, and A. Goldman (2004), Predicted errors of tropospheric emission spectrometer nadir retrievals from spectral window selection, *J. Geophys. Res., 109*, D09308, May 15, 2004.

### 7.7.3 General References

[12] Bloom, S., A. da Silva, D. Dee, M. Bosilovich, J.-D. Chern, S. Pawson, S. Schubert, M. Sienkiewicz, I. Stajner, W.-W. Tan, M.-L. Wu (2005). Documentation and Validation of the Goddard Earth Observing System (GEOS) Data Assimilation System - Version 4. *Technical Report Series on Global Modeling and Data Assimilation 104606, Vol. 26*, 187 pages, April 2005. Available from (paste entire link including pdf into browser):

http://ntrs.nasa.gov/archive/nasa/casi.ntrs.nasa.gov/20050175690_2005173043.pdf.

[13] Divakarla, M. G., C. D. Barnet, M. D. Goldberg, L. M. McMillin, E. Maddy, W. Wolf, L. Zhou, and X. Liu (2006), Validation of Atmospheric Infrared Sounder temperature

and water vapor retrievals with matched radiosonde measurements and forecasts, *J. Geophys. Res.*, *111*, D09S15, (doi: 10.1029/2005JD006116) April 6, 2006.

[14] Nevison, C. D., N. M. Mahowald, S. C. Doney, I. D. Lima, G. R. van der Werf, J. T. Randerson, D. F. Baker, P. Kasibhatla, and G. A. McKinley (2008), Contribution of ocean, fossil fuel, land biosphere and biomass burning carbon fluxes to seasonal and interannual variability in atmospheric $CO_2$, *J. Geophys. Res.*, *113*, G01010, (doi:10.1029/2007JG000408) February 12, 2008.

[15] Rienecker, M. M., M. J. Suarez (editor), R. Todling, J. Bacmeister, L. Takacs, H.-C. Liu, W. Gu, M. Sienkiewicz, R. D. Koster, R. Gelaro, I. Stajner and J.E. Nielson (2008), The GEOS-5 Data Assimilation System- Documentation of Versions 5.0.1, 5.1.0, and 5.2.0 *NASA Technical Report Series on Global Modeling and Data Assimilation 104606, Vol.27.*, December 2008.

[16] Tobin, D. C., H. E. Revercomb, R. O. Knuteson, B. M. Lesht, L. L. Strow, S. E. Hannon, W. F. Felt, L. A. Moy, E. J. Fetzer, and T. S. Cress (2006), Atmospheric Radiation Measurement site atmospheric state best estimates for Atmospheric Infrared Sounder temperature and water vapor retrieval validation, *J. Geophys. Res.*, *111*, doi: 10.1029/2005JD006103.

[17] Zhu, Y., and R. Gelaro (2008), Observation Sensitivity Calculations Using the Adjoint of the Gridpoint Statistical Interpolation (GSI) Analysis System, *Monthly Weather Review, Volume 136, Issue 1*, pp. 335-351, (DOI:10.1175/MWR3525.1) January 2008 - available from http://gmao.gsfc.nasa.gov/pubs/ref/archive/ref_2008.php.

# 8. Sea Surface Temperature

TES retrievals of sea surface temperature rely on validation of previous data versions, as described in detail in the TES Validation Report V003 (Osterman et al., 2007). V003 sea surface temperature (SST) was compared with Reynolds Optimally Interpolated (ROI) weekly SST for the time period Jan 2005 through July 2008. In clear sky conditions, TES SST versus ROI has a bias of -0.04 K (daytime) and -0.20 K (nighttime). The day/night difference is within the uncertainty of the predicted value based on ocean skin versus ocean bulk SST [D. Kerola, pers. comm.].

## 8.1 References

### 8.1.1 TES References

[1] Osterman, G., (editor), K. Bowman, K. Cady-Pereira, T. Clough, A. Eldering, B. Fisher, R. Herman, D. Jacob, L. Jourdain, S. Kulawik, M. Lampel, Q. Li, J. Logan, M. Luo, I. Megretskaia, R. Nassar, G. Osterman, S. Paradise, V. Payne, H. Revercomb., N. Richards, M. Shephard, D. Tobin, S. Turquety, F. Vilnrotter, H. Worden, J. Worden, and L. Zhang (2007), Earth Observing System (EOS) Tropospheric Emission Spectrometer (TES) Data Validation Report (Version F04_04 data), Version 3.0, JPL Internal Report D-33192, November 5, 2007

# 9. Water Vapor

The main objectives for obtaining retrieved water vapor from TES are to measure the isotopic ratio of HDO/H2O (see Section 10) and to obtain the most likely state of the atmosphere within the field-of-view. This applies whether water vapor is a tracer of air mass, of chemical interest, or whether it is an interferent. A number of comparisons have been made between TES V005 water vapor and other data sources, including radiosondes and aircraft. More than most species retrieved by TES, tropospheric water vapor is highly variable over short distances. Therefore, the key to water validation is to perform statistics on large datasets to determine possible biases. The most mature of all these analyses is the comparison to radiosondes and that work is presented in this document.

TES uses an optimal estimation non-linear least squares retrieval (Bowman et al., 2006). The latest version V005 uses a wide band retrieval (1100 to 1330 $cm^{-1}$) to jointly estimate the mixing ratios of four species: HDO, $H_2O$, $CH_4$, and $N_2O$ (Worden et al., 2012). This new retrieval dramatically improves the vertical resolution in the lower troposphere for water vapor. This is indicated by the sharpness of individual TES averaging kernel rows, as shown in Figure 9-1 below (Worden et al., 2012).

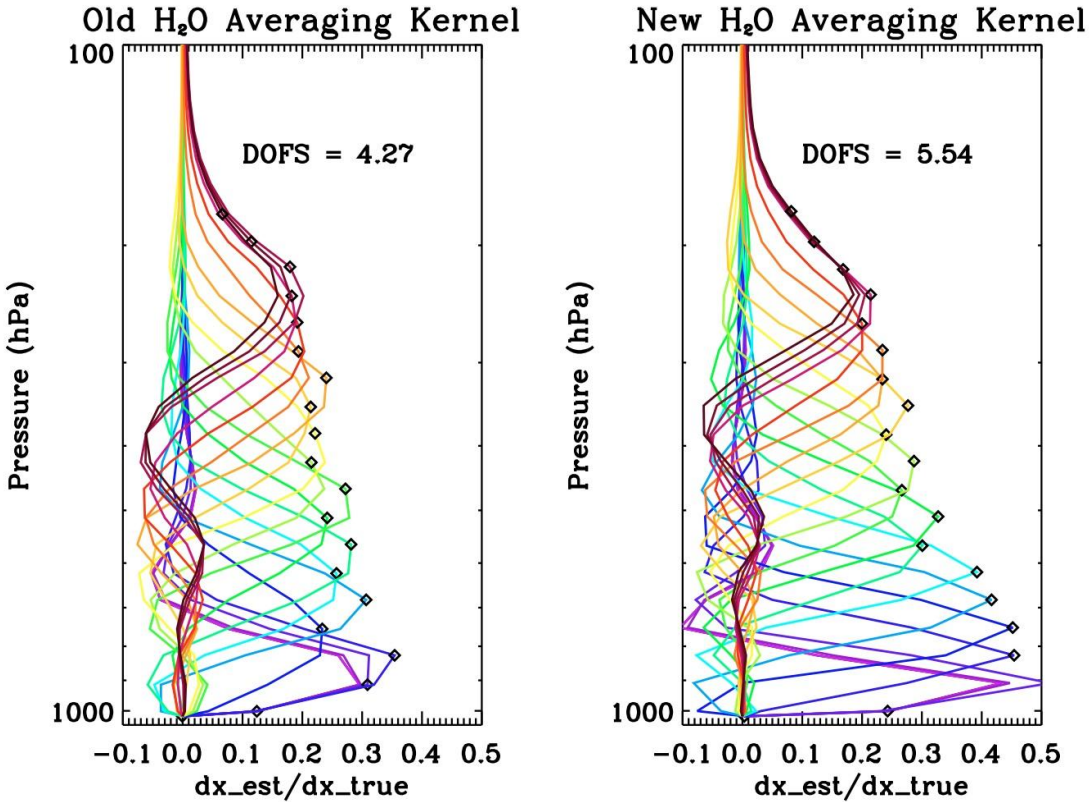


**Figure 9-1** Averaging kernels for a TES water vapor retrieval over a tropical ocean scene (Worden et al., 2012): (left) V004 averaging kernel with limited sensitivity at 800 hPa pressure. (right) V005 averaging kernel with enhanced sensitivity at 800 hPa, and at higher [pressures

down into the planetary boundary layer (PBL). Diamonds and color coding indicate the pressure level of each averaging kernel.

V005 TES water vapor retrievals have greater sensitivity in the lower troposphere than V004. A good indicator of the sensitivity of TES to water vapor at each pressure level is the diagonal of the averaging kernel. Figure 9-2 shows the diagonal of the averaging kernel for a V004 Transect-mode special observation of water vapor, and Figure 9-3 shows the same for V005.

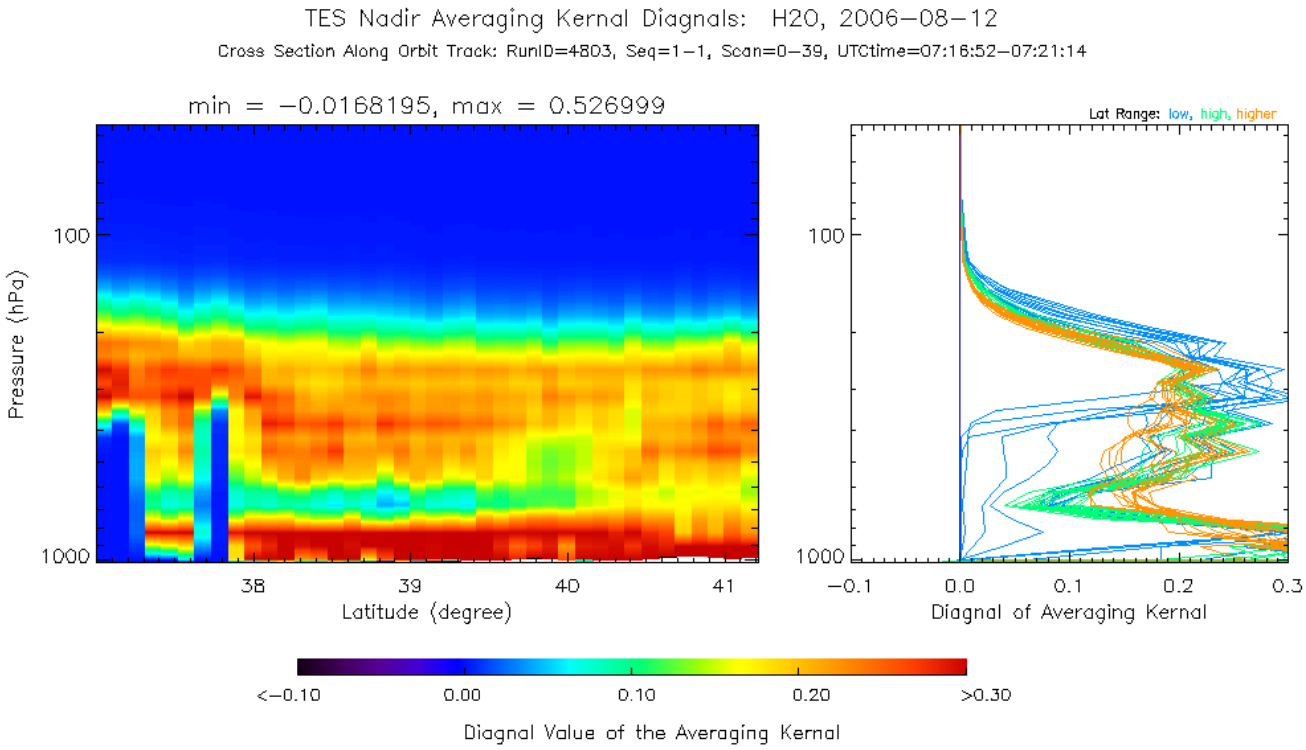


**Figure 9-2** Plots of the TES V004 averaging kernel diagonal for water vapor, 12 Aug 2006 Transect-mode special observation (run id 4803). Figure courtesy of Ming Luo.

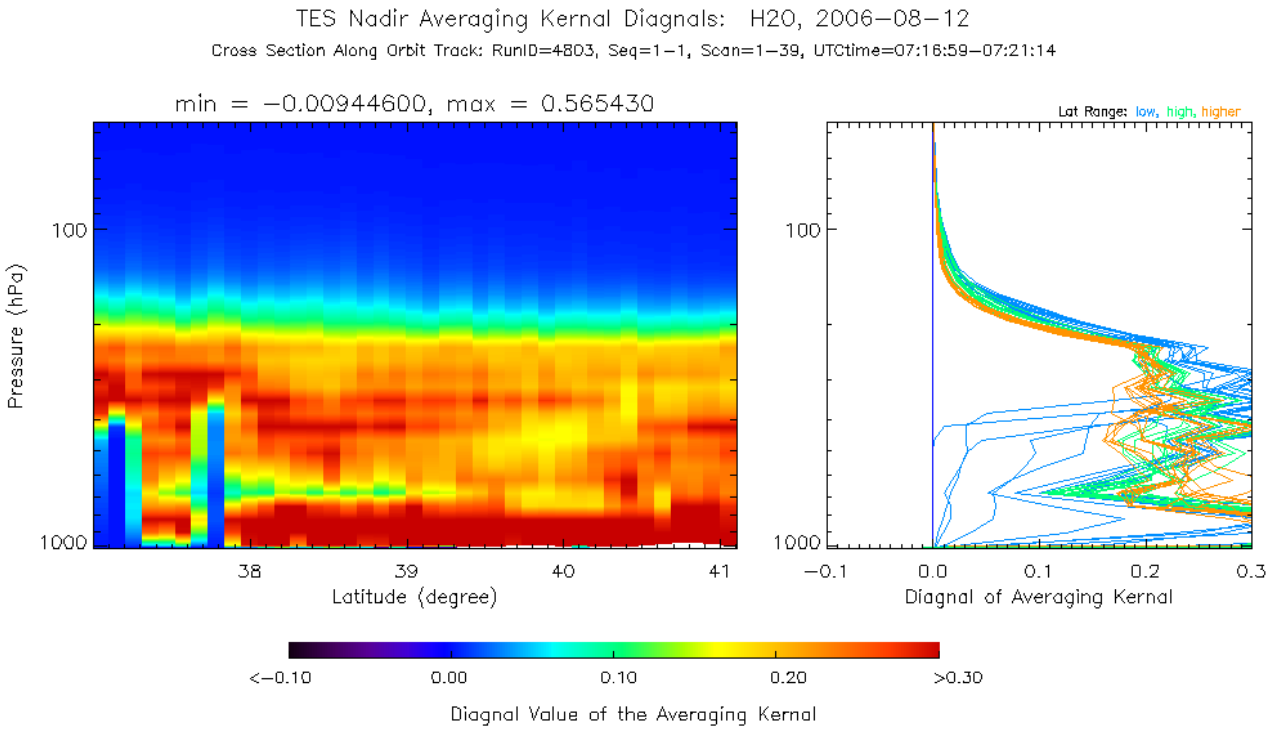


**Figure 9-3** Plots of the TES V005 averaging kernel diagonal for water vapor, 12 Aug 2006 Transect-mode special observation (run id 4803). Note the greater sensitivity (higher values) in the lower troposphere compared to Figure 9-2. Figure courtesy of Ming Luo.

## 9.1 Previous versions of TES Water Vapor Retrievals

Version V004 introduced sequential retrieval of temperature, ozone and water vapor. Sequential retrieval reduced the potential impact of systematic errors not adequately accounted for in the retrieval. For V004, the sequential steps were: (i) atmospheric temperature (TATM) retrieved using microwindows in the $CO_2$ $\nu 2$ region, (ii) joint retrieval of water vapor and ozone, (iii) joint retrieval of water vapor and HDO. Water was typically reported from the $H_2O$/HDO step. Shephard et al. (2008) showed that V004 significantly reduced biases relative to the a priori GEOS-5 compared to earlier versions of the TES retrievals. Shephard et al. (2008) also performed a radiance closure experiment on TES V003 water vapor from the Water Vapor Validation Experiments (WAVES) campaign at Beltsville, Maryland. This experiment indicated that the estimated systematic errors from the forward model, TES V003 measurements, in-situ observations, and the retrieved temperature profile and clouds were likely not large enough to account for systematic differences in tropospheric water vapor.

In V003, TES water vapor was reported from the $H_2O$/HDO joint retrieval step, which came after the $O_3/H_2O/T$ joint retrieval step. Version V003 introduced the four following improvements that influenced the TES water vapor retrievals: (i) improved TES temperature retrievals due to inclusion of the $CO_2$ $\nu 2$ spectral region with improved $CO_2$ forward model calculations (Shephard et al., 2008), (ii) the migration of TES initial guess and a priori from GEOS-4 to GEOS-5, (iii) a lowered minimum value for the a priori cloud optical depth in order

to better handle clouds with lower optical depths, and (iv) the addition of more surface microwindows to help characterize the surface.

## 9.2 A priori constraint vector

The initial guess in the TES retrieval algorithm is set equal to an a priori profile (constraint vector). The TES V005 a priori constraint vectors come from NASA's Goddard Earth Observing System (GEOS) data assimilation system GEOS-5 (Rienecker et al., 2008). These analyses are produced by the Global Modeling and Assimilation Office (GMAO) at the NASA Goddard Space Flight Center (GSFC). GEOS-5 profiles are produced on a 0.625° longitude by 0.5° latitude grid. These profiles are interpolated to the locations and pressure levels of TES retrievals. The a priori covariance matrices used for retrieval regularization are described in Bowman et al. (2006). GEOS-5 assimilates a wide range of operational satellite data and in situ radiosonde measurements. Radiosonde profiles are strong constraints on the thermal structure and winds throughout the troposphere, with an emphasis on continental regions where the observing network is denser. Space-based observations include the High Resolution Infrared Sounders (HIRS) and Advanced Microwave Sounders (AMSU) instruments on NOAA's operational sounders, which directly constrain temperature and moisture. GEOS-5 includes a direct assimilation of radiances from AMSU and HIRS in a three-dimensional variational assimilation, as well as radiances from the Advanced Infrared Sounder (AIRS) and AMSU instruments on NASA's EOS Aqua platform (Zhu and Gelaro, 2008). The previous GEOS-4 assimilated observations of temperature and water vapor using a one-dimensional variational approach (Bloom et al., 2005), where a retrieval was made using a six-hour forecast as a priori state; the retrieved variables were assimilated.

## 9.3 Comparison of TES Water Vapor with Radiosondes

For purposes of evaluating the quality of TES water vapor retrievals, the most readily available correlative data are provided by radiosondes launched in coordination with the Aura overpass. In 2006, Sippican (Mark II) radiosondes were launched from the DOE Atmospheric Radiation Measurement Southern Great Plains site (ARM SGP) in Oklahoma in coordination with TES special observations [F. Schmidlin, pers. comm.]. Figure 9-4 shows that TES V005 water vapor retrievals have some skill in identifying the top of the boundary layer.

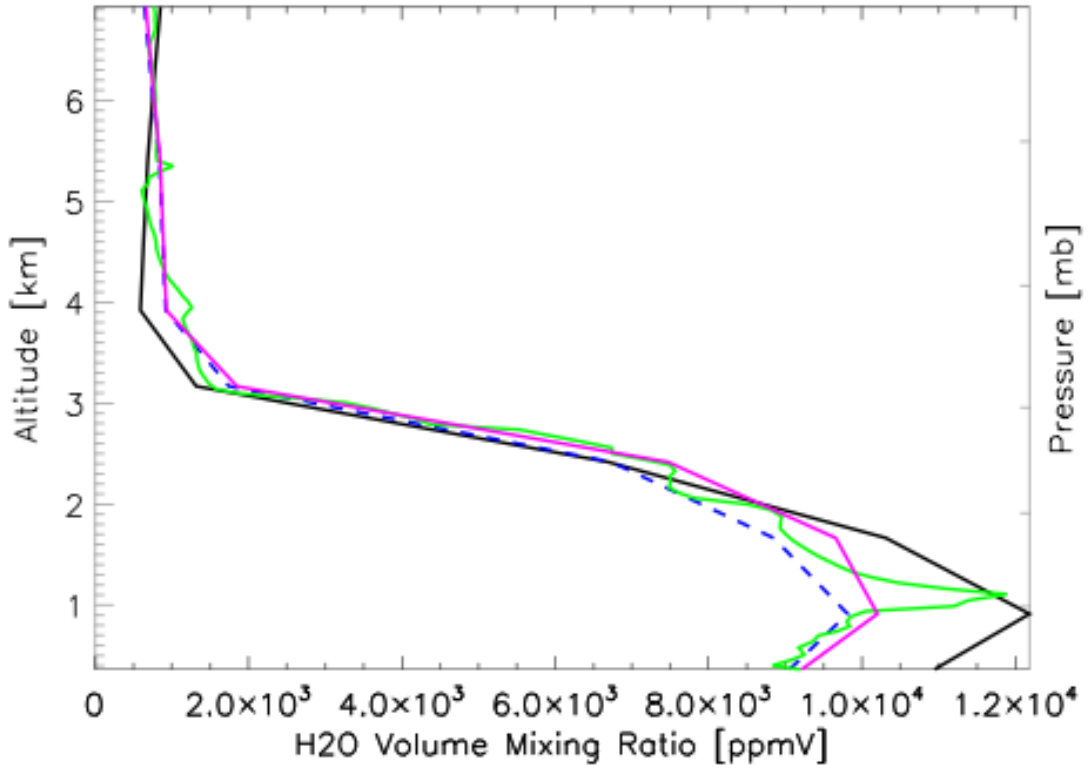


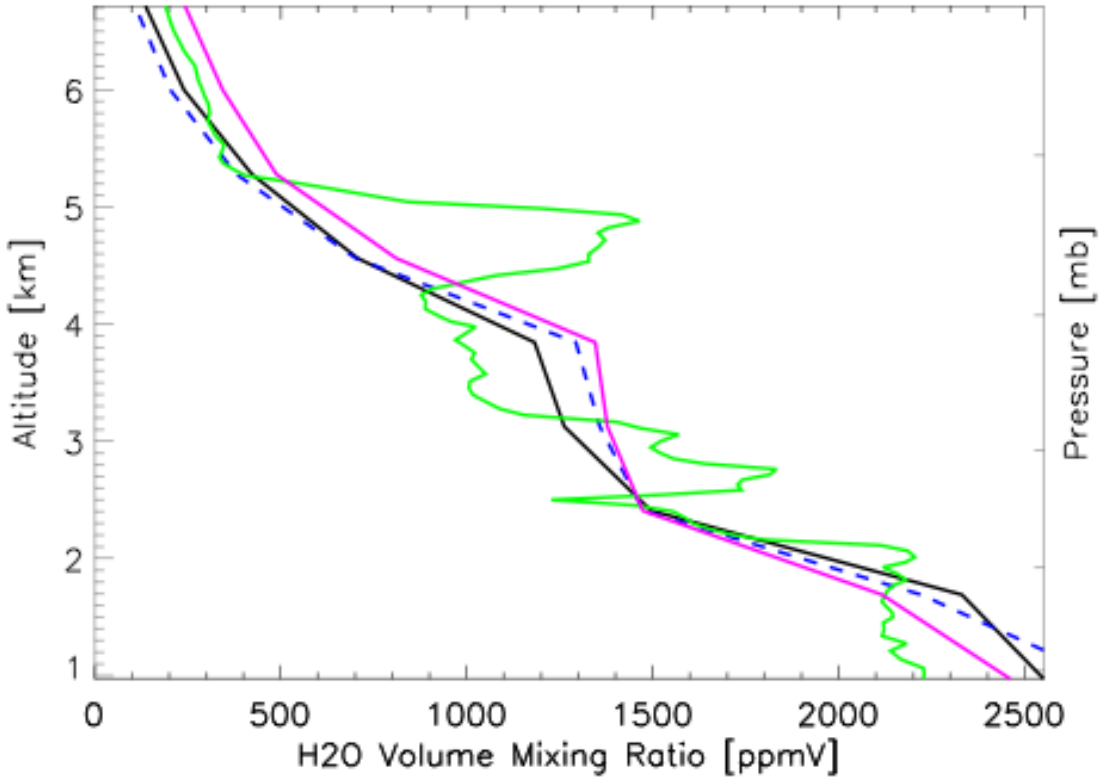

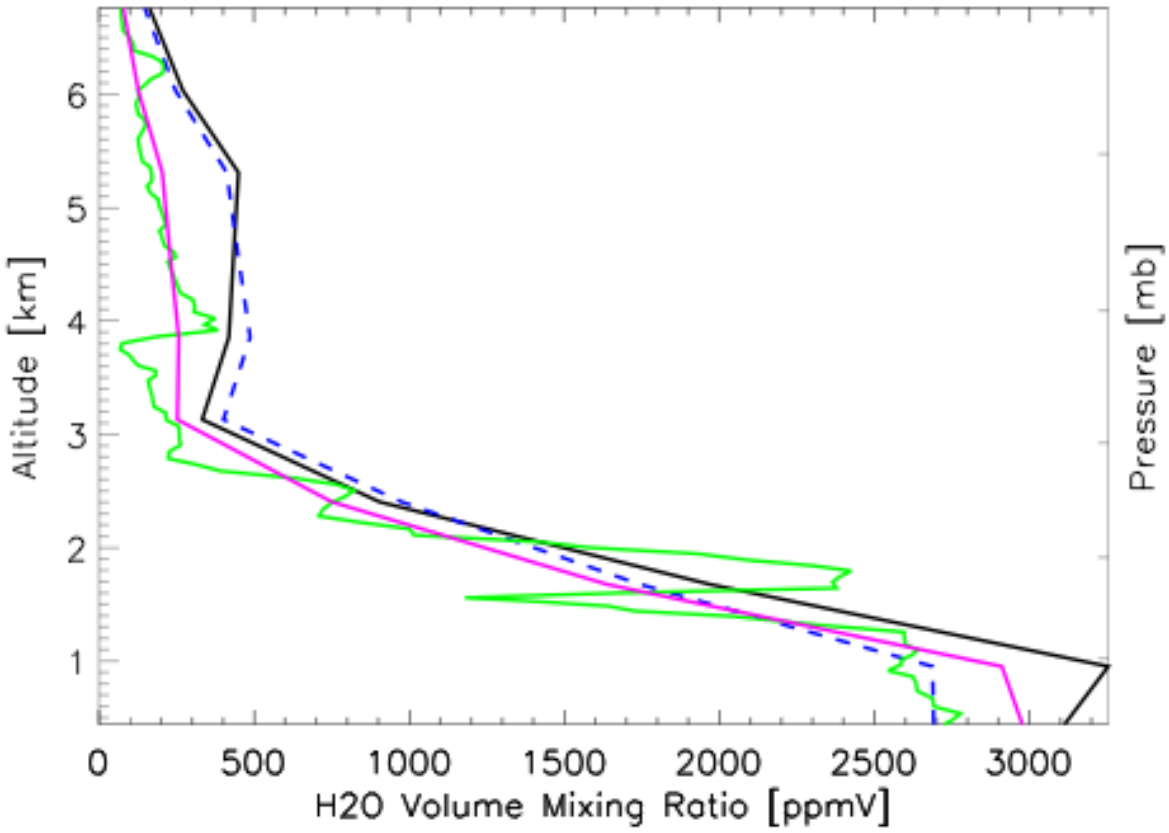


**Figure 9-4** Comparison of TES V005 water vapor with Sippican (Mark II) radiosondes launched from the ARM SGP site: radiosonde water volume mixing ratio (green), radiosonde with TES averaging kernel (magenta), TES retrieval (black), and GMAO GEOS-5 (blue dashed line).

On 13 April 2011, a radiosonde launch was coordinated with a TES Transect-mode special observation as part of the NASA Mid-Latitude Airborne Cirrus Properties Experiment (MACPEX) [D. Hurst, pers. comm.]. The in situ measurements of the boundary layer meteorology are shown in Figure 9-5, while the comparison with TES V005 retrieval is shown in Figure 9-6.

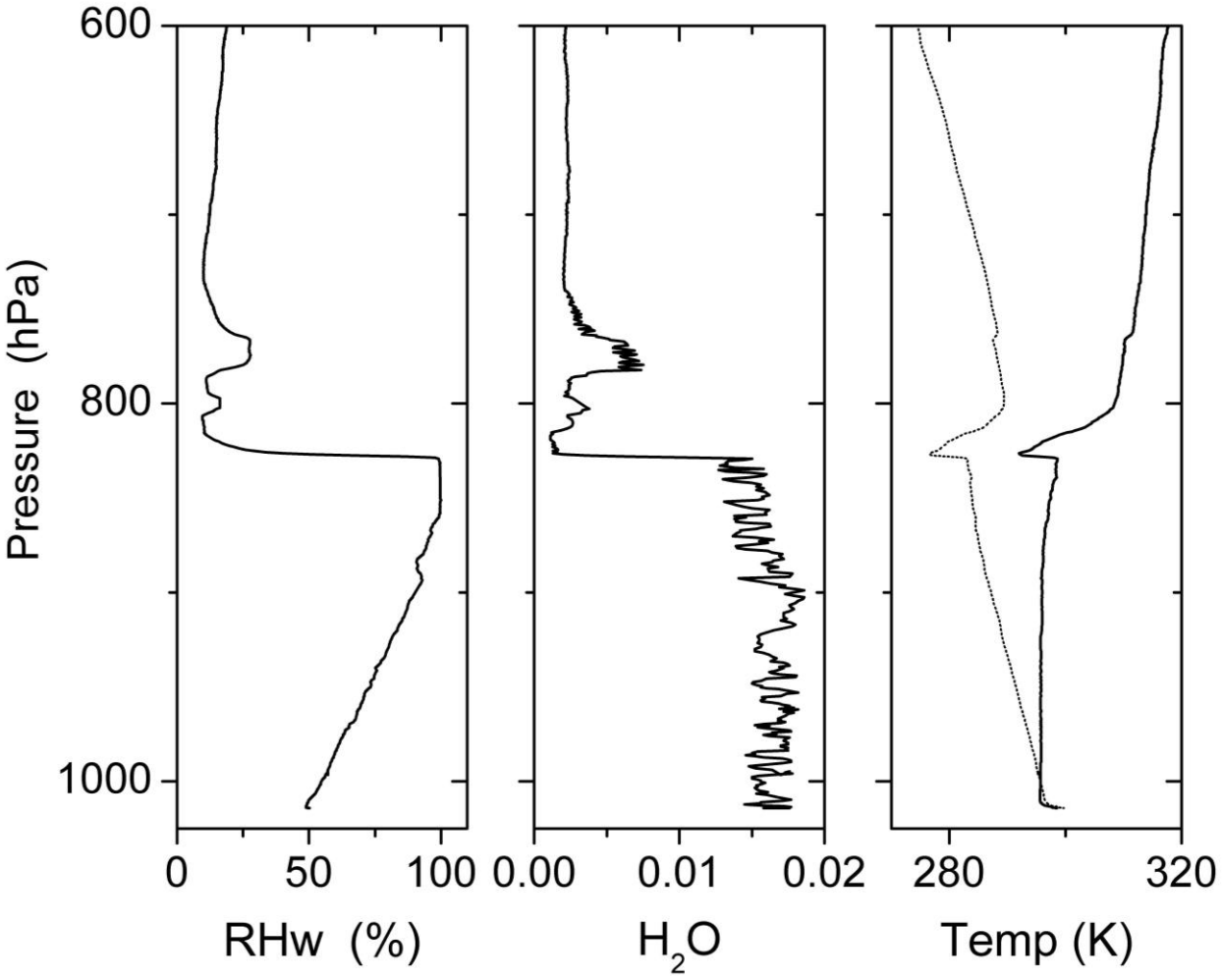


**Figure 9-5** Boundary layer meteorology over Houston, Texas, 13 April 2011. (left panel) Relative humidity from a Humirel sensor on an iMet radiosonde, (panel 2) water vapor from a Frost-Point Hygrometer (FPH), and (panel 3) temperature and potential temperature. All of the in-situ measurements indicate the top of the boundary layer is at 829 hPa.

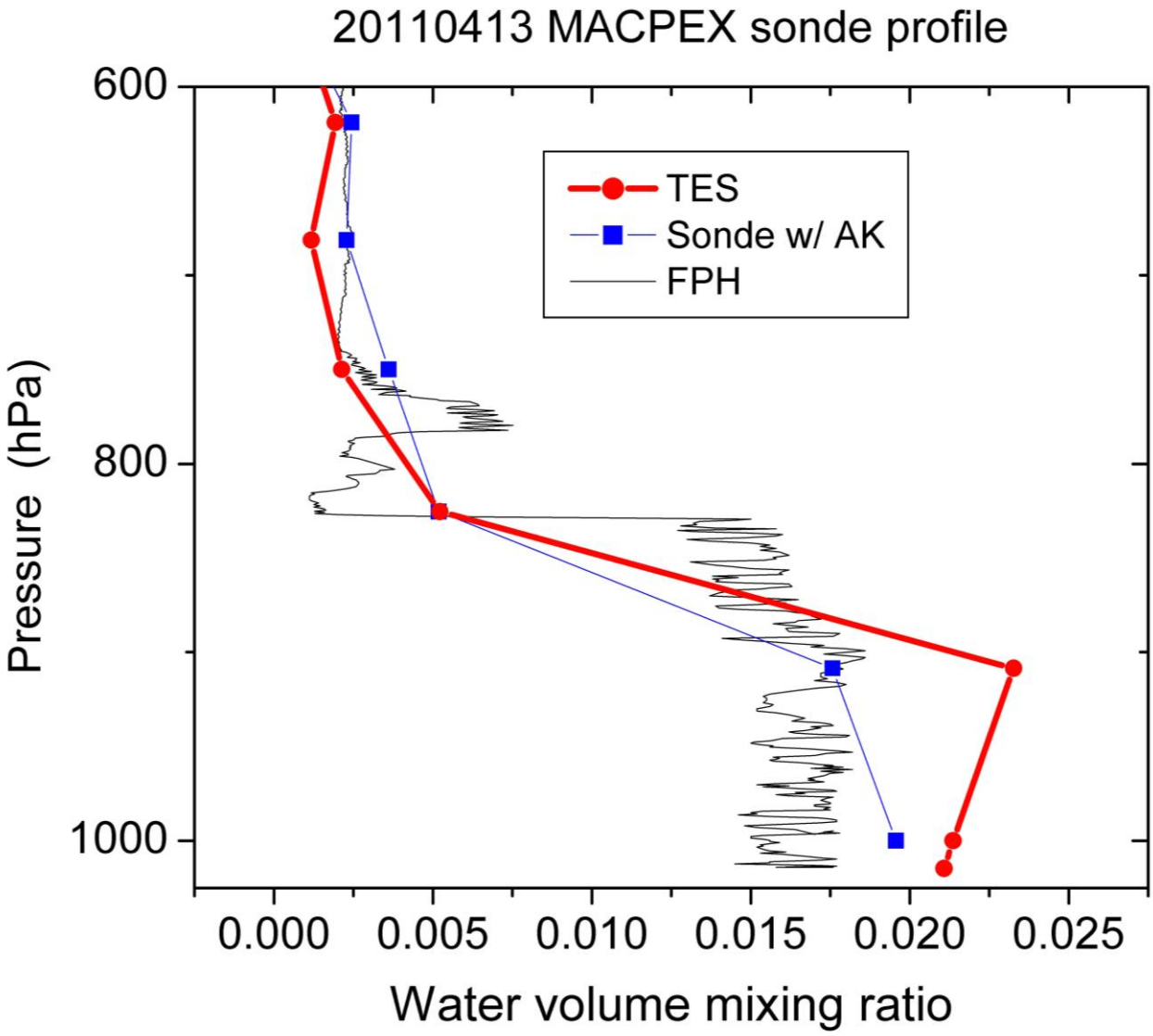


**Figure 9-6** Boundary layer meteorology over Houston, Texas, 13 April 2011. Comparison of TES V005 water vapor retrieval (red) with an iMet radiosonde profile (black), and the radiosonde water with averaging kernel applied (blue).

## 9.4 Statistical Evaluation of TES Water Vapor Bias and RMS with respect to Radiosondes

Radiosonde data come from a global database from the National Oceanic and Atmospheric Administration (NOAA) Earth System Research Laboratory (ESRL) Global Systems Division [M. Govett, pers. comm.]. The NOAA ESRL database combines the IGRA global data with North American Global Telecommunications Service (GTS) radiosonde observations. This database features the exact radiosonde launch time, which improves the temporal coincidence between TES and radiosonde significantly. The disadvantage of radiosondes is the spatial

mismatch between the satellite retrieval footprint (8 km by 5 km for TES) and the radiosonde data (a vertical profile of in-situ measurement with no horizontal information). Coincidence constraints are TES-radiosonde matches within 100 km and -0.5 hours to +1.5 hours. The tightly constrained time match is possible because the exact launch time of the radiosonde is known. Times are offset so that, on average, the radiosonde has ascended to the middle troposphere by the time of the Aura overpass and TES retrieval. The TES observation operator (averaging kernel) has been applied to the radiosonde profiles, and standard water data quality flags applied to the TES retrieval (Osterman et al., TES Data User's Guide D-38042, 2009). Outliers have been removed by using an iterative three-sigma rejection algorithm. Figure 9-7 shows the comparison between TES V005 water vapor and radiosondes for the cases of all cloud optical depth 0 to 50 (left panel) and "clear sky" average cloud effective optical depth less than 0.1 (right panel). Not much difference is seen in the bias, but the rms is improved slightly in the clear sky case. The bias ranges from +10% to -12% in the lower troposphere, with a positive bias up to +15% in the middle troposphere at 400 hPa.

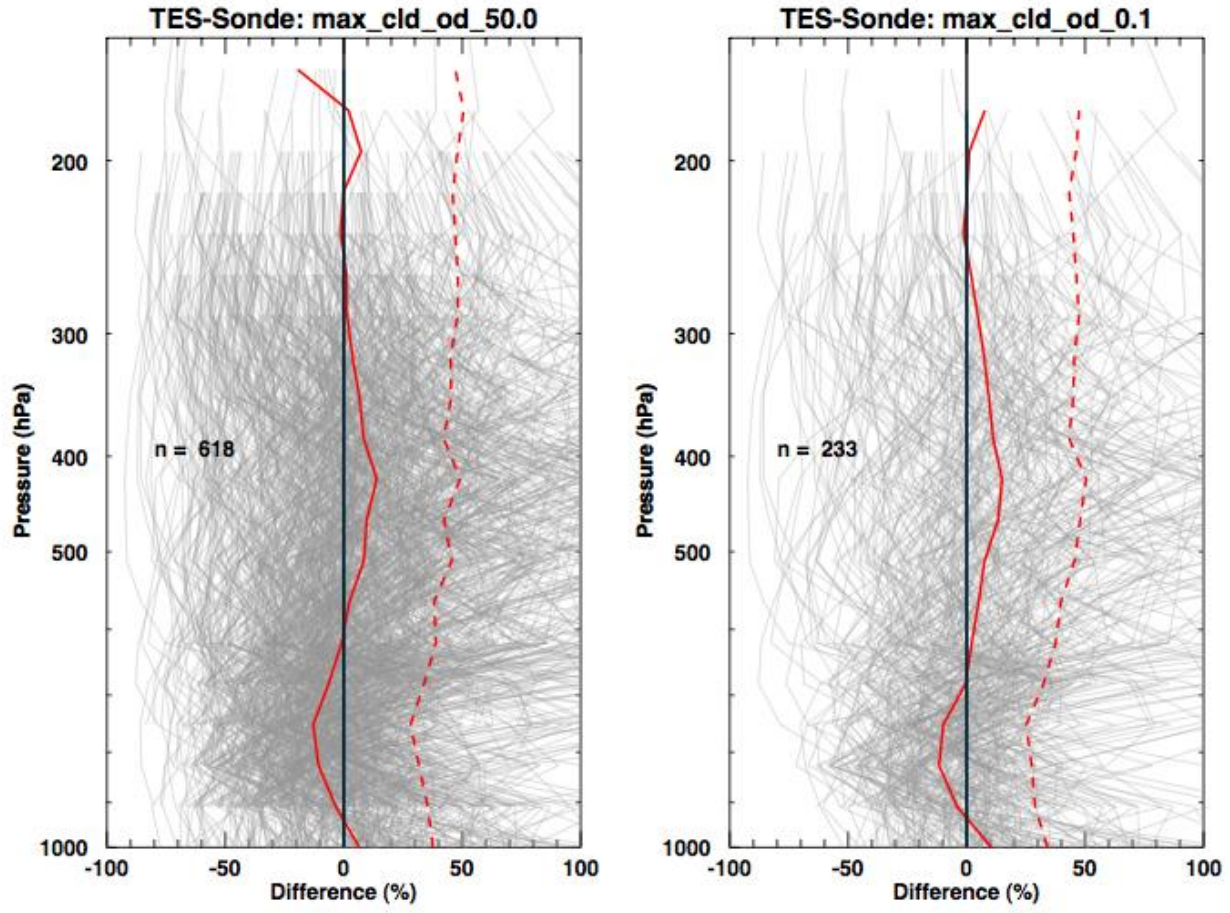


**Figure 9-7** Water vapor percent differences between TES V005 retrievals and radiosondes (with averaging kernel applied) in the NOAA ESRL database. TES geolocation coincidence within 100 km distance and -0.5 to +1.5 hours of radiosonde launch time. In each panel, n individual matches are shown (thin grey lines) with rms (dashed red lines) and bias (solid red lines). Differences are calculated as (TES-radiosonde)/TES. Figure prepared using Karen Cady-Pereira's idl code and an output save file from the TES sonde comparison tool.

## 9.5 Executive Summary

TES uses an optimal estimation non-linear least squares retrieval (Bowman et al., 2006). The latest version V005 uses a wide band retrieval (1100 to 1330 $cm^{-1}$) to jointly estimate the mixing ratios of four species: HDO, $H_2O$, $CH_4$, and $N_2O$ (Worden et al., 2012). This new retrieval dramatically improves the vertical resolution in the lower troposphere for water vapor. Comparisons have been made between TES V005 water vapor profiles and radiosonde profiles, demonstrating greater sensitivity to boundary layer water vapor than previous versions. Comparisons were also made with the NOAA ESRL global radiosonde database for close coincidences of <100 km and -0.5 hours to +1.5 hours. TES V005 water vapor has a small bias of +10% to -12% in the lower troposphere, with a positive bias up to +15% in the middle troposphere at 400 hPa. The rms differences tend to increase from 30% near the surface to 50% in the middle troposphere.

## 9.6 References

### 9.6.1 TES $H_2O$ References

[1] Worden, J., S. Kulawik, C. Frankenberg, V. Payne, K. Bowman, K. Cady-Peirara, K. Wecht, J.-E. Lee, D. Noone (2012), Profiles of $CH_4$, HDO, $H_2O$, and $N_2O$ with improved lower tropospheric vertical resolution from Aura TES radiances, *Atmospheric Measurement Techniques, 5, 397–411, 2012*, doi:10.5194/amt-5-397-2012, February 20, 2012.

### 9.6.2 TES References

[2] Bowman K. W., C. D. Rodgers, S. S. Kulawik, J. Worden, E. Sarkissian, G. Osterman, T. Steck, M. Lou, A. Eldering, M. Shephard, H. Worden, M. Lampel, S. A. Clough, P. D. Brown, C. P. Rinsland, M. Gunson, and R. Beer (2006), Tropospheric emission spectrometer: Retrieval method and error analysis, *IEEE Transactions on Geoscience and Remote Sensing*, *44(5)*, 1297-1307, May 2006.

[3] Osterman, G., (editor), K. Bowman, A. Eldering, B. Fisher, R. Herman, D. Jacob, L. Jourdain, S. Kulawik, M. Luo, R. Monarrez, G. Osterman, S. Paradise, V. Payne, S. Poosti, N. Richards, D. Rider, D. Shepard, M. Shephard, F. Vilnrotter, H. Worden, J. Worden, H. Yun and L. Zhang, Earth Observing System (EOS) Tropospheric Emission Spectrometer (TES) Level 2 (L2) Data User's Guide (Up to & including Version 4 data), Version 4.0, JPL Internal Report D-38042, May 20, 2009.

[4] Shephard, M. W., R.L. Herman, B.M. Fisher, K.E. Cady-Pereira, S. A. Clough, V. H. Payne, D.N. Whiteman, J. P. Comer, H. Vömel, L.M. Miloshevich, Ricardo Forno, M. Adam, G. B. Osterman, A. Eldering, J. R. Worden, L. R. Brown, H. M. Worden, S. S. Kulawik, D. M. Rider, A. Goldman, R. Beer, K. W. Bowman, C. D. Rodgers, M. Luo, C. P. Rinsland, M. Lampel, M. R. Gunson (2008), Comparison of Tropospheric Emission Spectrometer nadir water vapor retrievals with in situ measurements, *J. Geophys. Res., 113*, D15S24, (doi:10.1029/2007JD008822) May 16, 2008.

### 9.6.3 General References

[5] Bloom, S., A. da Silva, D. Dee, M. Bosilovich, J.-D. Chern, S. Pawson, S. Schubert, M. Sienkiewicz, I. Stajner, W.-W. Tan, M.-L. Wu (2005). Documentation and Validation of the Goddard Earth Observing System (GEOS) Data Assimilation System - Version 4. *Technical Report Series on Global Modeling and Data Assimilation 104606, Vol. 26,* 187 pages, April 2005. Available from (paste entire link including pdf into browser):

http://ntrs.nasa.gov/archive/nasa/casi.ntrs.nasa.gov/20050175690_2005173043.pdf

[6] Rienecker, M. M., M. J. Suarez (editor), R. Todling, J. Bacmeister, L. Takacs, H.-C. Liu, W. Gu, M. Sienkiewicz, R. D. Koster, R. Gelaro, I. Stajner and J.E. Nielson (2008), The GEOS-5 Data Assimilation System- Documentation of Versions 5.0.1, 5.1.0, and 5.2.0 *NASA Technical Report Series on Global Modeling and Data Assimilation 104606, Vol.27.*, December 2008.

[7] Zhu, Y., and R. Gelaro (2008), Observation Sensitivity Calculations Using the Adjoint of the Gridpoint Statistical Interpolation (GSI) Analysis System, *Monthly Weather Review, Volume 136, Issue 1*, pp. 335-351, (DOI:10.1175/MWR3525.1) January 2008 - available from http://gmao.gsfc.nasa.gov/pubs/ref/archive/ref_2008.php.

# 10. HDO/$H_2O$

For validation of V4 HDO, we refer the reader to Worden et al. (2011).

## 10.1 Comparison of V5.1 to V5 and V4 HDO.

V5.1 estimates of HDO/$H_2O$ show considerable more sensitivity to the isotopic composition of water vapor with typically 2 DOFS of freedom in the tropics and ~1 DOF at high latitudes. This increased sensitivity allows the TES estimates to resolve lower tropospheric and mid-tropospheric variability of the HDO/$H_2O$ vapor ratio (see Worden et al., 2012) with the expense of increased uncertainty over tropical oceans.

We find that the HDO/$H_2O$ estimates are consistent with the previous TES release within the altitude range where the sensitivity overlaps (Figure 10-1). However, the new version is biased higher by approximately 7.5 per mil. Consequently, the estimated bias correction factor for V5.1 should be 5.55% (Worden et al., 2011).

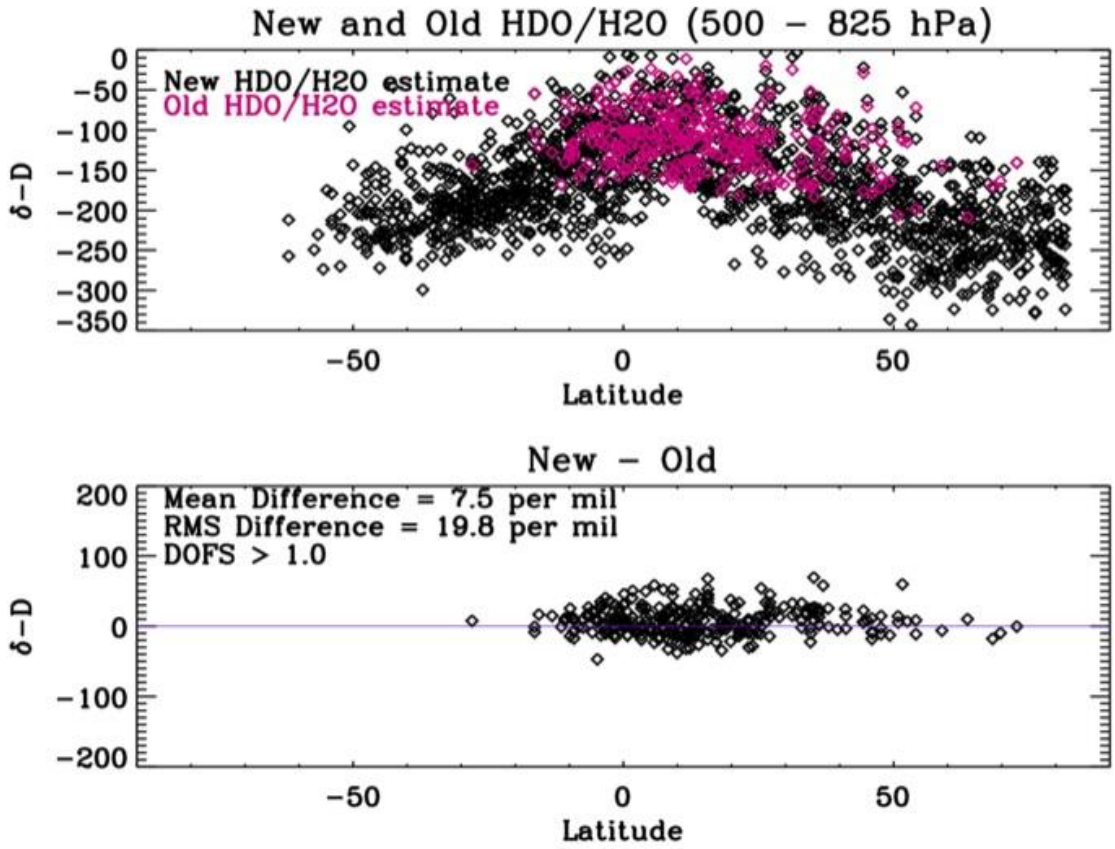


**Figure 10-1** (top) Comparison of the new (V005) and old (V004) HDO/$H_2O$ estimates. A DOFS threshold of 1.0 is used for the data in the top panel for both releases. (bottom) Difference between old and new HDO/$H_2O$ estimates for the overlapping data shown in the top panel. $\delta\text{-}D = 1000(\mathrm{HDO/H_2O}/3.11\times10^{-4} - 1.)$.

## 10.2 References

### 10.2.1 TES HDO/$H_2O$ References

[1] Worden, J., D. Noone, J. Galewsky, A. Bailey, K. Bowman, D. Brown, J. Hurley, S. Kulawik, J. Lee, M. Strong (2011), Estimate of bias in Aura TES HDO/$H_2O$ profiles from comparison of TES and in situ HDO/$H_2O$ measurements at the Mauna Loa observatory, *Atmospheric Chemistry and Physics, 11,* 4491–4503, 2011, doi:10.5194/acp-11-4491-2011, May 12, 2011.

### 10.2.2 TES References

[2] Worden, J., S. Kulawik, C. Frankenberg, V. Payne, K. Bowman, K. Cady-Peirara, K. Wecht, J.-E. Lee, D. Noone (2012), Profiles of $CH_4$, HDO, $H_2O$, and $N_2O$ with improved lower tropospheric vertical resolution from Aura TES radiances, *Atmospheric Measurement Techniques, 5, 397–411, 2012*, doi:10.5194/amt-5-397-2012, February 20, 2012.

# 11. Methane

## 11.1 Overview of current validation status of TES V005 methane

TES V005 methane ($CH_4$) has been compared with aircraft vertical profiles over the Pacific from the HIAPER Pole-to-Pole Observation (HIPPO) program. Further details of the V005 $CH_4$ algorithm can be found in Worden et al. (2012), while a detailed description of validation against HIPPO data can be found in Wecht et al. (2012). TES methane retrievals contain around 2 degrees of freedom for signal (DOFS) - between less than 1 in polar regions and 2.5 in the tropics, depending on season and location. Since the number of DOFS is small compared to the 67 vertical levels of the Level 2 data product, attempts to interpret TES $CH_4$ (or differences between TES $CH_4$ and some other data sources such as model fields or in situ data) on any one of the 67 levels is ill-advised. Methane is relatively well-mixed in the troposphere, especially in the vertical, so TES $CH_4$ may be represented by "representative tropospheric volume mixing ratios" (RTVMRs), associated with effective pressures that describe the locations in the atmosphere where most of the retrieval information originates. For TES retrievals with DOFS ≤ 1.6, the TES vertical profile is mapped to a single RTVMR, $y_R$. For TES retrievals with DOFS > 1.6, the TES vertical profile is mapped to an upper and lower tropospheric RTVMR, termed $y_U$ and $y_L$ respectively. Further discussion of the RTVMR quantity can be found in Payne et al. (2009) and in the TES Level 2 Data User's Guide (Osterman et al., 2009).

## 11.2 Differences between the V005 and V004 retrievals

V005 represents a major change to the $CH_4$ algorithm and results. Previous versions (V004 or lower) of the TES $CH_4$ retrieval algorithm used a "spectral-window" approach to minimize uncertainty from interfering species at the expense of reduced vertical resolution and sensitivity. For V005, joint estimates of $H_2O$, HDO, $CH_4$ and nitrous oxide ($N_2O$) are made using radiances from almost the entire spectral region between 1100 $cm^{-1}$ and 1330 $cm^{-1}$. The retrieval constraints have also been modified in order to better use this information. This change in approach results in a greater number of degrees of freedom for signal (see Figure 11-1) and enhanced sensitivity in the lower troposphere for the V005 retrievals compared to the V004 (see Figure 11-2). The V005 algorithm is described in greater detail in Worden et al. (2012).

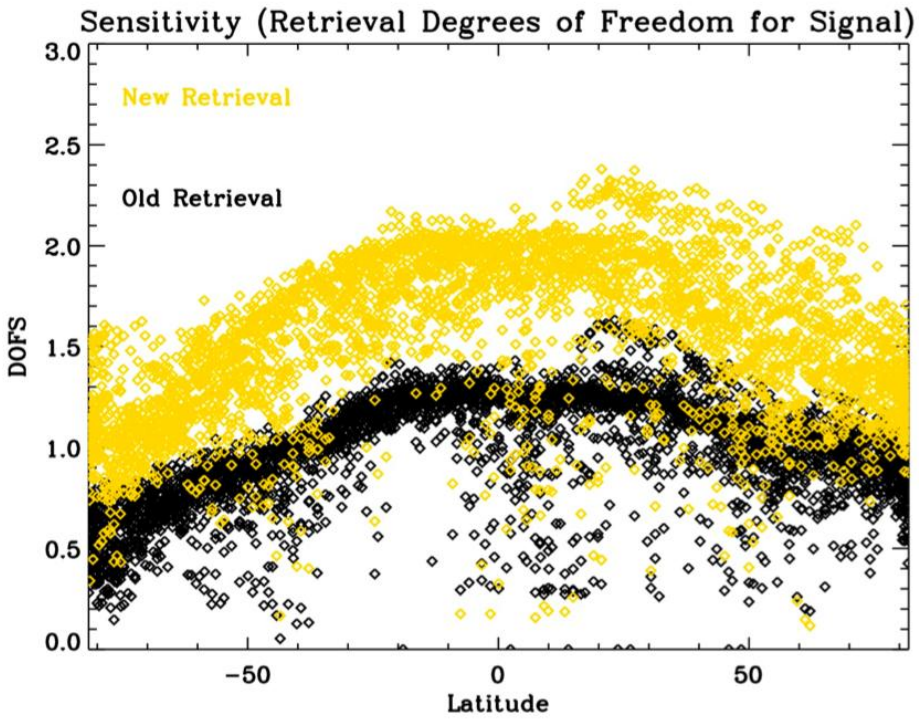


**Figure 11-1** Degrees of freedom for signal for V005 (yellow) and V004 (black) CH4 retrievals as a function of latitude. Figure reproduced from Worden et al. (2012).

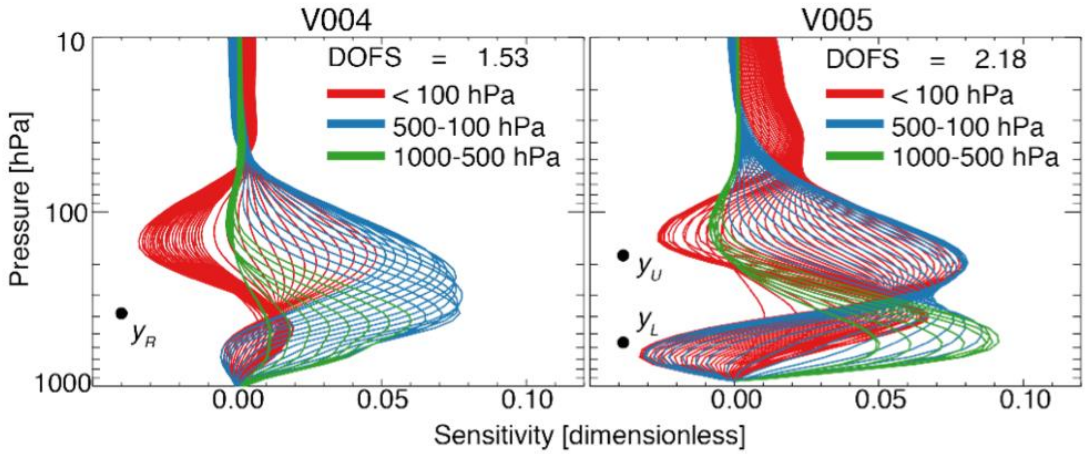


**Figure 11-2** Typical averaging kernel matrices for TES methane retrievals over the tropical ocean: V004 (left) and V005 (right). Black circles indicate the pressure levels used for comparison to the HIPPO aircraft observations. Figure reproduced from Wecht et al. (2012).

### 11.3 $CH_4$ profile correction using $N_2O$ estimate

The joint retrieval with $N_2O$ offers an opportunity for reducing errors in V005 $CH_4$ estimates. Although $N_2O$ varies much less than $CH_4$ in the troposphere, the magnitude of the sensitivity of the radiance to variations in $N_2O$ and $CH_4$ are nearly the same in the spectral region used in the V005 retrievals. Consequently, errors that affect estimates of $N_2O$ will have a similar radiative effect to errors that affect estimates of $CH_4$. For this correction approach using $N_2O$, we therefore assume that the tropospheric $N_2O$ profile is well represented by the a priori profile, and that deviations in the retrieved $N_2O$ from the prior are a result of systematic error. For these estimates we use a priori $N_2O$ profiles from the Whole Atmosphere Community Climate Model (WACCM) (e.g., Tilmes et al., 2007). Interference error from temperature, clouds, and emissivity should affect both $CH_4$ and $N_2O$ very similarly, and correction of $CH_4$ by $N_2O$ should therefore reduce the $CH_4$ errors. This correction takes the following form:

$$\boldsymbol{x}_{adj} = \boldsymbol{x}_c - \boldsymbol{x}_n + \boldsymbol{x}^a_n \qquad \text{(Equation 11-1)}$$

where $x_c$ is the estimate for log($CH_4$), $x_n$ is the (log) estimate for $N_2O$, and the adj superscript means "adjusted" or corrected.

### 11.4 TES/HIPPO comparisons

TES V005 $CH_4$ is compared to vertical $CH_4$ profiles measured aboard NSF's Gulfstream V (GV) during the first two HIPPO missions in January and October-November 2009 (HIPPO I and HIPPO II respectively). The GV transected the Pacific Ocean from 85N to 67S, performing in-progress vertical profiles every 220 km or 20 minutes (Wofsy et al., 2011). During HIPPO, $CH_4$ was measured with a Quantum Cascade Laser Spectrometer (QCLS) at 1 Hz frequency with accuracy of 1.0 ppb and precision of 0.5 ppb (Kort et al., 2011). Each HIPPO vertical profile extends from near-surface to 330-180 hPa. TES measurements are generally most sensitive to methane between 600 and 200 hPa. For direct comparison to TES, HIPPO profiles are mapped to the 67 levels of the TES pressure grid and extrapolated above the GV ceiling using the TES a priori, scaled to match HIPPO observations at the uppermost measurement altitude. The TES observation operator is then applied to the HIPPO profile and RTVMRs are calculated.

For each HIPPO vertical profile (covering 220 km in 20 minutes), we calculate a mean location and time. We then find all TES observations coincident with the HIPPO profile in a 750 km and 24 h coincidence window. Where a single TES observation is coincident with multiple HIPPO profiles, we match it to the nearest profile in space and time. We calculate $y_R$, $y_L$ and $y_U$ from the TES and HIPPO profiles. From the statistics of the TES-HIPPO differences, $\Delta y_R$, $\Delta y_L$ and $\Delta y_U$, we calculate a mean TES bias (mean value of $\Delta y$) and residual standard deviation (standard deviation of $\Delta y$). Shrinking the size of the coincidence window has very little effect on the validation statistics.

The residual standard deviation contains contributions from random instrument error in the TES retrievals and error induced by extrapolating above the observed HIPPO profiles. We use $CH_4$ observations from HIPPO, the Airborne Southern Hemisphere Ozone Experiment (ASHOE), the Stratospheric Tracers of Atmospheric Transport (STRAT), and the Photochemistry of Ozone Loss in the Arctic Region in Summer (POLARIS) (Elkins et al., 1996, Hurst et al., 1999) to infer negligible error in extrapolation up to the local tropopause or 200 hPa, whichever is higher, and an error standard deviation of 6 % above. We then estimate TES instrument error by assuming instrument and extrapolation errors add in quadrature.

Figure 11-3 shows a positive mean bias in TES $CH_4$ between 1.0 % and 3.7 % and TES instrument error of 1.4 % - 1.6 % depending on the unit of validation. Latitudinal variability observed by HIPPO is captured well by TES. Validation results are summarized in Table 11-1. Mean biases and random instrument errors are obtained from TES-HIPPO difference statistics ($\Delta y$). Mean biases for $y_L$ are significantly different for low latitudes (20°S-20°N) and high latitudes (> 20°). Other error statistics do not vary significantly with latitude. Further discussion of TES V005 $CH_4$ validation with HIPPO I and II profiles can be found in Wecht et al. (2012).

**Table 11-1 Mean biases and random instrument errors for representative tropospheric volume mixing ratios (RTVMRs) from the TES V005 retrievals**

| Observations | Mean bias (ppb) | Instrument error (ppb) | # TES obs |
|---|---|---|---|
| $y_R$ **(DOFS < 1.6)** | 28.7 | 24.7 | 109 |
| $y_U$ | 42.3 | 26.5 | 280 |
| $y_L$ **(20°S-20°N)** | 16.9 | 28.9 | 136 |
| $y_L$ **(> 20°)** | 28.8 | 28.7 | 144 |

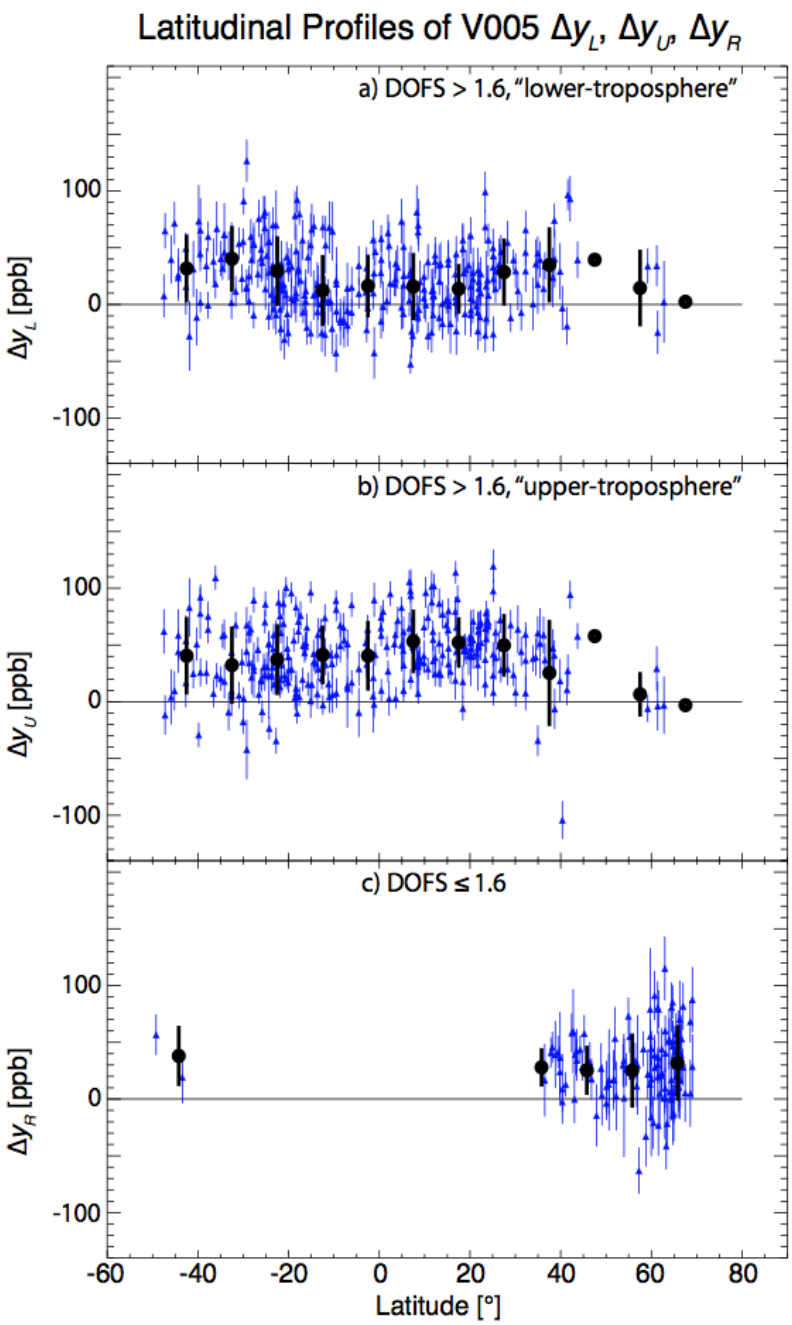


**Figure 11-3** Latitudinal profiles of the differences Δy between TES V005 and HIPPO CH4 concentrations during HIPPO I & II in January and October-November 2009. The top two panels show results for the lower and upper tropospheric TES data (ΔyL and ΔyU, respectively) in scenes where the degrees of freedom for signal (DOFS) exceeds 1.6. The bottom panel shows results for the RTVMR (ΔyR) in scenes where the DOFS is lower than 1.6. Blue vertical bars are the theoretical error standard deviations reported in the TES retrievals. Black circles and vertical bars are the means and standard deviations binned by 10◦ latitude. Figure reproduced from Wecht et al. (2012).

## 11.5 Comments or limits on utility of the data

Atmospheric $CH_4$ is known to be vertically well-mixed in the free troposphere. Worden et al. (2012) and Wecht et al. (2012) have shown that the TES V005 $CH_4$ profiles exhibit an unrealistic profile shape and a high bias that increases with height in the troposphere. (The upper tropospheric high bias was also shown for previous versions of TES $CH_4$ that were only sensitive in the upper troposphere.) Possible reasons for the bias are discussed in Worden et al. (2012).

Applying the $N_2O$ correction discussed above mitigates, but does not remove these errors in the $CH_4$ profile. An additional quality check can be applied whereby the user can test on the standard deviation of the TES V005 CH4 profile for pressures greater than 200 mbar. Selection of profiles where the DOFS>1 and the standard deviation of the profile below 200 mbar is less than 0.015 has been shown to increase precision compared to HIPPO data. However, this additional quality check does exclude a large fraction of the data (one third to one half).

In addition, since TES $CH_4$ retrievals contain only around 2 DOFS, they contain limited information on the vertical distribution of methane. Therefore, it is not recommended to view the data in terms of individual pressure levels. The RTVMR representation has been shown to be valuable in the analysis of the TES methane dataset. Further details on calculating RTVMRs may be found in the TES Level 2 Data Users Guide (Osterman et al., 2009) and in Payne et al. (2009).

## 11.6 Executive Summary

The validation of the TES $CH_4$ product described here is sufficient to characterize the latitudinal dependence of the mean bias and the instrument error. Work so far suggests that TES $CH_4$ contains useful information when viewed using the "representative tropospheric volume mixing ratio" (RTVMR) approach. TES shows a positive mean bias of 1.0 % - 3.7 % with random instrument error of 1.4 % - 1.6 % with respect to measurements made during the first two HIPPO missions. TES successfully captures the latitudinal gradient observed during HIPPO I and II.

## 11.7 References

### 11.7.1 TES $CH_4$ References

[1] Payne, V.H., S.A. Clough, M.W. Shephard, R. Nassar and J.A. Logan (2009), Information-centered representation of retrievals with limited degrees of freedom for signal: Application to methane from the Tropospheric Emission Spectrometer, *J. Geophys. Res., 114*, (doi:10:1029/2008JD010155) May 27, 2009.

[2] Wecht, K.J., D.J. Jacob, S.C. Wofsy, E.A. Kort, J.R. Worden, S.S. Kulawik, D.K. Henze, M. Kopacz, and V. H. Payne (2012), Validation of TES methane with HIPPO aircraft observations: implications for inverse modeling of methane sources, *Atmos. Chem. Phys., 12*, 1823–1832, 2012.

[3] Worden, J., S. Kulawik, C. Frankenberg, V. Payne, K. Bowman, K. Cady-Pereira, K. Wecht, J.-E. Lee, and D. Noone (2012), Profiles of $CH_4$, HDO, $H_2O$, and $N_2O$ with

improved lower tropospheric vertical resolution from Aura TES radiances, *Atmos. Meas. Tech., 5*, 397–411, 2012.

### 11.7.2 TES References

[4] Osterman, G., (editor), K. Bowman, A. Eldering, B. Fisher, R. Herman, D. Jacob, L. Jourdain, S. Kulawik, M. Luo, R. Monarrez, G. Osterman, S. Paradise, V. Payne, S. Poosti, N. Richards, D. Rider, D. Shepard, M. Shephard, F. Vilnrotter, H. Worden, J. Worden, H. Yun and L. Zhang (2009), Earth Observing System (EOS) Tropospheric Emission Spectrometer (TES) Level 2 (L2) Data User's Guide (Up to & including Version 4 data), Version 4.0, JPL Internal Report D-38042, May 20, 2009.

### 11.7.3 General References

[5] Elkins, J.W., D.W. Fahey, J.M. Gilligan, G.S. Dutton, T.J. Baring, C.M. Volk, R.E. Dunn, R.C. Myers, S.A. Montzka, P.R. Wamsley, A.H. Hayden, J.H. Butler, T.M. Thompson, T.H. Swanson, E.J. Dlugokencky, P. C. Novelli, D.F. Hurst, J.M. Lobert, S.J. Ciciora, R.J. McLaughlin, T.L. Thompson, R.H. Winkler, P.J. Fraser, L.P. Steele and M.P. Lucarelli (1996), Airborne gas chromatograph for in situ measurements of long- lived species in the upper troposphere and lower stratosphere, *Geophys. Res. Lett., 23*, 347–350, 1996.

[6] Hurst, D.F., G.S. Dutton, P.A. Romashkin, P.R. Wamsley, F.L. Moore, J.W. Elkins, E.J. Hintsa, E. M. Weinstock, R.L. Herman, E. J. Moyer, D. C. Scott, R. D. May, and C.R. Webster (1999), Closure of the total hydrogen budget of the northern extratropical lower stratosphere, *J. Geophys. Res.-Atmos., 104*, 8191–8200, 1999.

[7] Kort, E.A., P.K. Patra, K. Ishijima, B.C. Daube, R. Jiménez, J. Elkins, D. Hurst, F.L. Moore, C. Sweeney and S. C. Wofsy (2011), Tropospheric distribution and variability of $N_2O$: Evidence for strong tropical emissions, *Geophysical Research Letters, Vol. 38*, L15806, doi:10.1029/2011GL047612, August 6, 2011.

[8] Tilmes, S., D.E. Kinnison, R.R. Garcia, R. Muller, F. Sassi, D.R. Marsh and B.A. Boville (2007), Evaluation of heterogeneous processes in the polar lower stratosphere in the Whole Atmosphere Community Climate Model, *J. Geophys. Res., 112*, D24301, doi:10.1029/2006JD008334, 2007.

[9] Wofsy, S.C., the HIPPO Science Team and Cooperating Modellers and Satellite Teams (2011), HIAPER Pole-to-Pole Observations (HIPPO): Fine grained, global scale measurements for determining rates for transport, surface emissions, and removal of climatically important atmospheric gases and aerosols, *Phil. Trans. of the Royal Society A, vol. 369 (no. 1943)*, 2073-2086, May 28, 2011.

# 12. Cloud Products

TES retrievals of cloud products rely on validation of previous data versions, as described in detail in the TES Validation Report V004 (Herman et al., 2011).

## 12.1 References

### 12.1.1 TES References

[1] Robert Herman and Gregory Osterman (editors), Christopher Boxe, Kevin Bowman, Karen Cady-Pereira, Tony Clough, Annmarie Eldering, Brendan Fisher, Dejian Fu, Robert Herman, Daniel Jacob, Line Jourdain, Susan Kulawik, Michael Lampel, Qinbin Li, Jennifer Logan, Ming Luo, Inna Megretskaia, Ray Nassar, Gregory Osterman, Susan Paradise, Vivienne Payne, Hank Revercomb, Nigel Richards, Mark Shephard, Dave Tobin, Solene Turquety, Felicia Vilnrotter, Helen Worden, John Worden, Lin Zhang (2011), Earth Observing System (EOS) Tropospheric Emission Spectrometer (TES) Data Validation Report (Version F05_05, F05_06, F05_07 data), Version 4.0, JPL Internal Report D-33192, November 23, 2011.

# 13. Carbon Dioxide Validation

## 13.1 Overview of current validation status of TES V005 $CO_2$

TES $CO_2$ is retrieved between 40S and 45N, with average cloud optical depth < 0.5, among other tests, for good quality. On average, TES $CO_2$ has an average of 0.65 degree of freedom for signal (DOFS) – with the most DOFS for daytime land cases (which can be on the order of 1 DOFS) and the least for nighttime or winter land cases (which can be on the order of 0.3 DOFS). Ocean targets (day or night) have intermediate DOFS with about 0.8 DOFS. The averaging kernel indicates sensitivity between the surface to above 100 mb, with the most sensitivity between about 700 and 300 mb, peaking at about 650 mb. Although a profile is retrieved and has been validated, there is very little independent information at the different profile levels and it is critical to utilize the provided averaging kernel when using TES data. TES V005 $CO_2$ has been compared with aircraft vertical profiles over the Pacific from the HIAPER Pole-to-Pole Observation (HIPPO) program (Wofsy et al., 2011) and over land at the SGP Arm site (Riley et al., 2009). Further details of this validation can be found in Kulawik et al. (2012). This validation was done with the prototype code which is nearly identical to the production code (PGE), but has some minor differences due to differences in the altitude grid calculation. The HIPPO analysis can be done with the processed PGE data, but the SGP analysis requires a full time series of TES at the SGP site and will need to await a more complete V005 dataset. Analysis of the PGE comparisons to HIPPO show about a 1.2 ppm error and an overall -0.7 ppm bias, as compared to the prototype which has about a 1.1 ppm error and an overall bias of +0.5 ppm. There are some outliers in the monthly mean values from both the prototype and the PGE and we are working on additional quality flags to screen these out. A fuller set of TES data needs to be examined before the V005 bias is officially set as different sites and times have relative biases on the order of 0.5 ppm. The single target error for TES $CO_2$ in the mid-Troposphere is on the order of 8 ppm, however averaging over 20 degrees longitude, 10 degrees latitude, and 1 month results in errors on the order of 1 ppm over both ocean and land targets. Through comparisons to validation data, we have found that the errors are underpredicted by a factor of about 1.5, and that the averaging kernel needs be corrected to account for the TES multi-step retrieval. The details of this correction are found in Kulawik et al. (2012) which involves a pressure-dependent scale factor. Although the TES $CO_2$ product is modest both in sensitivity and coverage, Nassar et al. (2011) found that TES added information to the surface flask measurements and was useful for estimating fluxes, both separately, and jointly with flask measurements. We have also recently found (manuscript in preparation) that TES assimilation into GEOS-Chem improves the amplitude of the mid-tropospheric $CO_2$ seasonal cycle as compared with aircraft profiles measured at the SGP-Arm site.

## 13.2 Differences between the V005 and V004 retrievals

This is the first version of this product, although TES prototype $CO_2$ has been shown and published in, e.g. Nassar et al. (2011) and Kulawik et al. (2010). The improvement over the previous prototype results is most seen over land, with improved correlations and reduced errors so that the predicted and actual errors are now reasonably consistent over land as well as ocean. Both land and ocean results are usable for V005.

### 13.3 Comparisons to HIPPO-1, HIPPO-2 and HIPPO-3

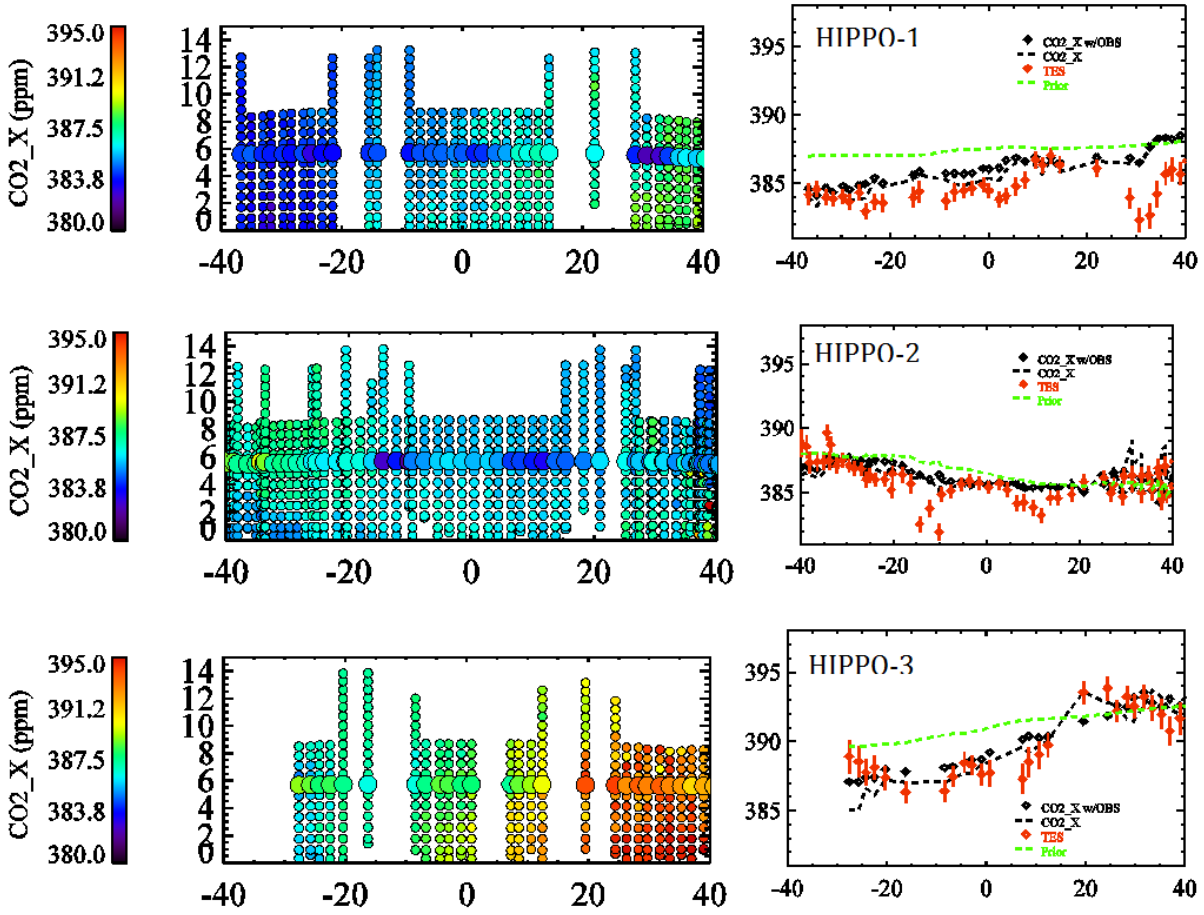


**Figure 13-1** Comparison of monthly averaged TES V005 observations at 511 hPa to HIPPO-identified profiles of CO2_X, which is $CO_2$ from two (harmonized) sensors averaged to 10s. Left shows a curtain plot of the HIPPO (small dots, no averaging kernel (AK) applied) and TES values (large dots), and right shows TES (red) compared to HIPPO at the altitude of maximum TES sensitivity with and without the averaging kernel applied (dots and dashed line, respectively). The green dotted line shows the TES prior.

As discussed in Kulawik et al. (2012), the HIPPO datasets are unique for validation in that they provide $CO_2$ profiles between the surface up through 9 - 13 km, far higher than most regular measurements which go up to 5 km. Other validation datasets, while still extremely valuable, are less suitable for validation, e.g. CONTRAIL, while very useful in that it crosses over a wide range of latitudes is less useful in that most measurements are between 9-11 km.

For comparisons, the TES $CO_2$ values are averaged +-10 degrees longitude +-4 degrees latitude and +-14 days. TES, while capturing most patterns, has issues in HIPPO-2 at +-15 degrees, and HIPPO-1 north of 30N. These seem to be regions where the systematic errors are not random and so do not average out and we are working on quality flags to screen out these cases.

## 13.4 References

### 13.4.1 TES $CO_2$ References

[1] Kulawik, S.S., D.B.A. Jones, R. Nassar, F.W. Irion, J.R. Worden, K.W. Bowman, T. Machida, H. Matsueda, Y. Sawa, S.C. Biraud, M.L. Fischer, A.R. Jacobson (2010), Characterization of Tropospheric Emission Spectrometer (TES) $CO_2$ for carbon cycle science, *Atmos. Chem. Phys., 10, (12),* 5601-5623, 2010.

[2] Kulawik, S.S., J.R. Worden, S.C. Wofsy, S.C. Biraud, R. Nassar, D.B.A. Jones, E.T. Olsen, G.B. Osterman, (2012), Comparison of improved Aura Tropospheric Emission Spectrometer (TES) $CO_2$ with HIPPO and SGP aircraft profile measurements, *Atmospheric Chemistry and Physics Discussions, 12,* 6283 – 6329, February 29, 2012.

[3] Nassar, R., D.B.A. Jones, S.S. Kulawik, J.R. Worden, K.W. Bowman, R.J. Andres, P. Suntharalingam, J.M. Chen, C.A.M. Brenninkmeijer, T.J. Schuck, T.J. Conway, D.E. Worthy (2011), Inverse modeling of $CO_2$ sources and sinks using satellite observations of $CO_2$ from TES and surface flask measurements, *Atmos. Chem. Phys., **11**, (12),* 6029-6047, June 24, 2011.

### 13.4.2 General References

[4] Riley, W.J., S.C. Biraud, M.S. Torn, M.L. Fischer,D. P. Billesbach, J.A. Berry (2009), Regional $CO_2$ and latent heat surface fluxes in the Southern Great Plains: Measurements, modeling, and scaling, *Journal of Geophysical Research-Biogeosciences, 114,* G04009, DOI: 10.1029/2009JG001003, 2009.

[5] Wofsy, S.C., the HIPPO Science Team and Cooperating Modellers and Satellite Teams (2011), HIAPER Pole-to-Pole Observations (HIPPO): Fine grained, global scale measurements for determining rates for transport, surface emissions, and removal of climatically important atmospheric gases and aerosols, *Phil. Trans. of the Royal Society A, vol. 369 (no. 1943),* 2073-2086, May 28, 2011.

# 14. Ammonia

## 14.1 $NH_3$ from TES

Ammonia is a highly reactive gas emitted principally by animal waste and fertilizer application, and to a lesser extent by industrial activity, mining and automobiles. Ammonia contributes significantly to several well-known environmental problems; excess deposition in terrestrial ecosystems can lead to soil acidification and loss of plant diversity; in coastal ecosystems, it can cause eutrophication, algal blooms, and loss of fish and shellfish. In the atmosphere $NH_3$ can combine with sulfates and nitric acid to form ammonium nitrate and ammonium sulfate, which constitute a substantial fraction of fine particulate matter (PM2.5). These particles are statistically associated with health impacts and contribute to radiative forcing by the atmosphere, while also impacting visibility. Nevertheless the knowledge of the magnitude and seasonal/spatial variability of the emissions is severely limited, mainly because this variability is very high (Carmichael et al., 2003; Walker et al., 2004). This high variability has several consequences: first, it requires intensive in situ monitoring; second, this monitoring is not globally available, it reduces the capability of models to predict ammonia concentrations; finally, while satellite measurements of $NH_3$ can provide the extensive coverage in time and space required for constraining model emissions, the variability makes it difficult to obtain in situ data that is co-incident enough to provide good validation data.

Sampling differences further complicate comparisons. Most $NH_3$ in situ measurements are point samples on the surface, either instantaneous or averaged over a week or longer. TES provides basically one value (see next section) over the 5.5x8.5 km TES footprint, and this value reflects the $NH_3$ concentration over the entire layer in which TES is sensitive to $NH_3$, usually the first few km above the surface. Thus direct quantitative comparisons are not feasible; instead we focus on consistency in trends in time and space.

Special Observations (SOs) provide sufficient sampling density to obtain meaningful correlations with in situ measurements. In this report we have focused on three regions for which there were SOs: North Carolina from February through November of 2009, eastern China from April 2007 through April 2010, and Central Valley in May 2010. For the first two regions we aggregated data in time and space. Since this required averaging results over many runs that have not yet been processed through V5.0, the $NH_3$ results from the AER prototype retrieval using V4.0 data were used. However, the subset of retrievals already processed through V5.0 is very consistent with the prototype retrievals. The $NH_3$ retrievals from the transects carried out over Bakersfield in the Central Valley are JPL operational products using the V5.0 algorithm.

## 14.2 Ammonia Observations

### 14.2.1 Retrieval Metric

Even though there is limited amount of information available from a $NH_3$ retrieval, typically ~1 DOFS, the retrieval sensitivity varies from profile-to-profile depending on the atmospheric state. To capture this sensitivity $NH_3$ must be retrieved at more levels than there is information. Therefore, at any single profile level the retrieved $NH_3$ VMR can contain a significant amount of the a priori profile. If the desired application is the creation of $NH_3$ maps or single level point comparisons from retrievals with limited amount of vertical information (e.g. 1 DOFS) then a

different metric is needed to reduce the influence of the a priori. To address this issue, Beer et al. (2008) utilized an averaging kernel weighted volume mixing ratio (AKVMR) for TES ammonia and methanol retrievals. Payne et al. (2009) developed a representative tropospheric volume mixing ratio (RTVMR) metric for TES methane profiles, which takes into account the measurement sensitivity to map the retrieved profile into four points (surface, peak sensitivity, tropopause, TOA) then selects the value near the peak sensitivity of the methane averaging kernel as the representative value. The mapping suitable for methane does not work for ammonia due to its near surface peak concentrations. For the point comparisons to be presented here, we developed a Representative Volume Mixing Ratio (RVMR) metric for TES $NH_3$, which differs from the methane RTVMR in that it maps the $NH_3$ VMR values from all the retrieval levels into a subset that is more representative of the information provided by the measurement (Shephard et al., 2011). Typically for $NH_3$ retrievals the RVMR represents a TES sensitivity weighted boundary layer averaged value with the influence of the a priori reduced as much as possible. The level to which the influence is reduced depends on the available retrieval information content for the observation: if there is one piece of information from a given retrieval then a single RVMR value can be generated with almost all of the a priori removed, making comparison with in-situ surface measurements simpler.

### 14.2.2 Variability in $NH_3$ over North Carolina

Livestock raising is a major economic activity in North Carolina. Since waste from livestock is the principal source of $NH_3$ the EPA maintains a monitoring network (CAMNET) in North Carolina. TES transects were taken over the CAMNET network region from February through December of 2009. The TES daytime and nighttime overpasses were near 13:30 and 1:30 local time respectively. The purpose of this combined ground/space observation effort was to evaluate the TES retrieval algorithm and to examine the relationships between the surface measurements, which are two week averages collected at a point, with the TES retrievals, which measure an instantaneous value over a column with a 5.5x8.5 km footprint. Comparing these two datasets with very different temporal and spatial sampling rates is challenging. The first step was to check the degree of correlation between the datasets.

The TES RVMR values were paired with the closest EPA monitoring station; correlation coefficients between the TES and CAMNET values were calculated separately for the day and night TES measurements, yielding a value of 0.41 during the day and 0.01 at night. This prompted an analysis of CMAQ model output and a different set of in situ measurements with much higher temporal sampling (Pinder et al., 2011), each sampled as TES (instantaneously) and CAMNET (two week means); both the test with model output and the surface measurements had effectively no correlation between the value at 1:30 am and the two week mean. This result showed that the day and nighttime data should be analyzed separately and that no comparisons could be made between TES nighttime measurements and the CAMNET two week means. Pinder et al. (2011) focused on the daytime data and found good agreement in seasonal trends, i.e., TES and CAMNET averages over the study region showed the same seasonal variability (Figure 14-1, left panel). The scale of the spatial variability is so small in this region (less than 1 km) that simple maps are not a useful tool. Instead, Pinder et al. (2011), reasoned that $NH_3$ concentrations should be correlated with the strength of nearby sources. Both the TES and CAMNET observations were binned by the number of livestock farms within 10 km (Figure 14-1, right panel) and showed the same dependence on livestock concentration.

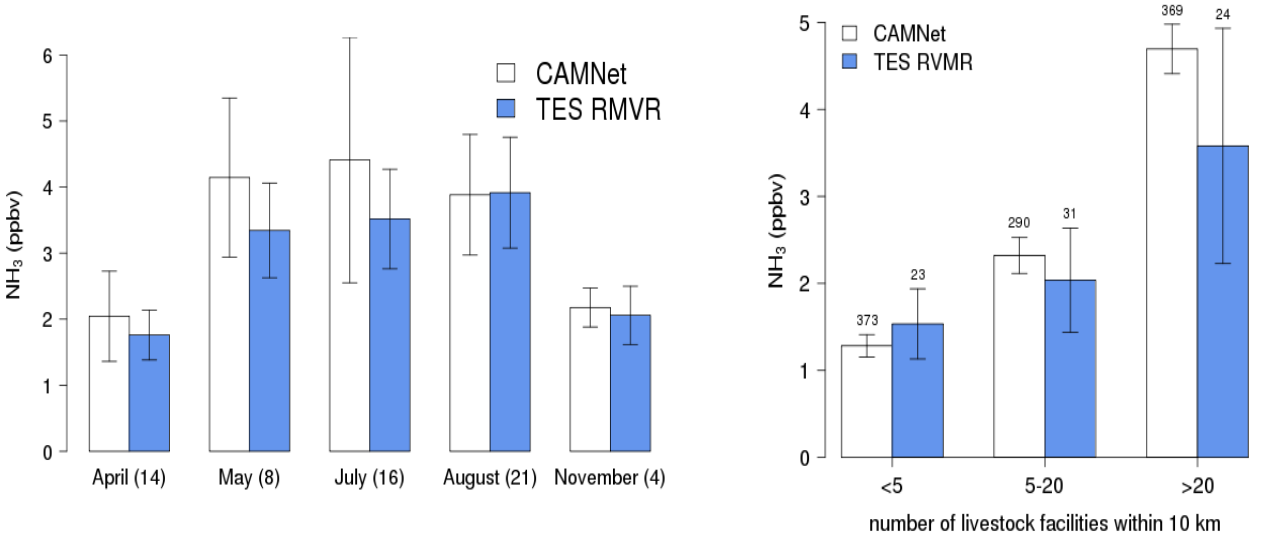


**Figure 14-1** Average daytime TES RVMR and CAMNet $NH_3$ observations by month of year for all months with more than three TES observations. The number of overlapping pairs for each month is shown in parenthesis. (right) Average daytime TES RVMR and CAMNet $NH_3$ binned by number of animal facilities within 10 km. Error bars denote the 95th percentile confidence interval for the mean.

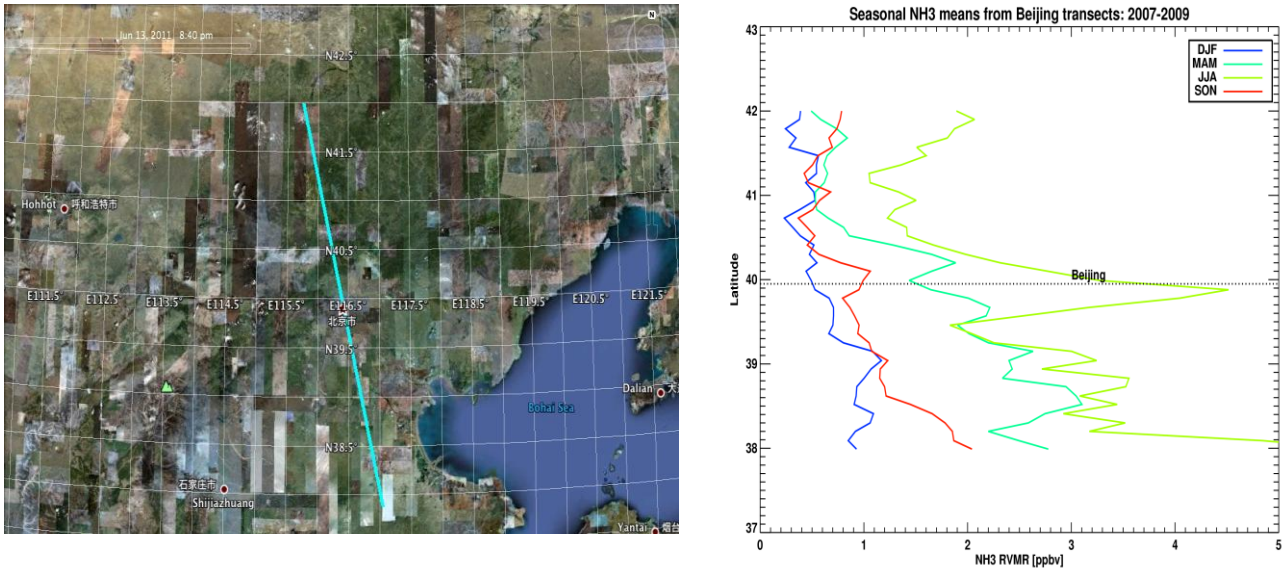


**Figure 14-2** Track of TES transects over eastern China (left); seasonal means of TES $NH_3$ along the transects (right).

### 14.2.3 TES transects over eastern China

TES measurements were taken over eastern China from April of 2007 through April of 2010. These were daytime transects with a track directly over Beijing (Figure 14-2, left) sampling both the urban area and the mainly agricultural regions to the north and south. Seasonal means at each scan location were calculated and plotted as a function of latitude (Figure 14-2, right). The

change in $NH_3$ concentrations between winter and summer is very marked all along the transect. There is a strong peak over Beijing in the summer, possibly arising from increased $NH_3$ production from neighboring rural areas due to warmer temperatures, added to the automobile and industrial emissions. Spring also brings increased $NH_3$ south of 41N, peaking at the southern end of the transect, where there is more intense agricultural activity.

The marked temporal variability in the signal over Beijing obtained from TES is well correlated with that observed from in situ measurements made by Meng et al. (2011) in northwestern Beijing over a similar period (Figure 14-3), with low winter and high summer values.

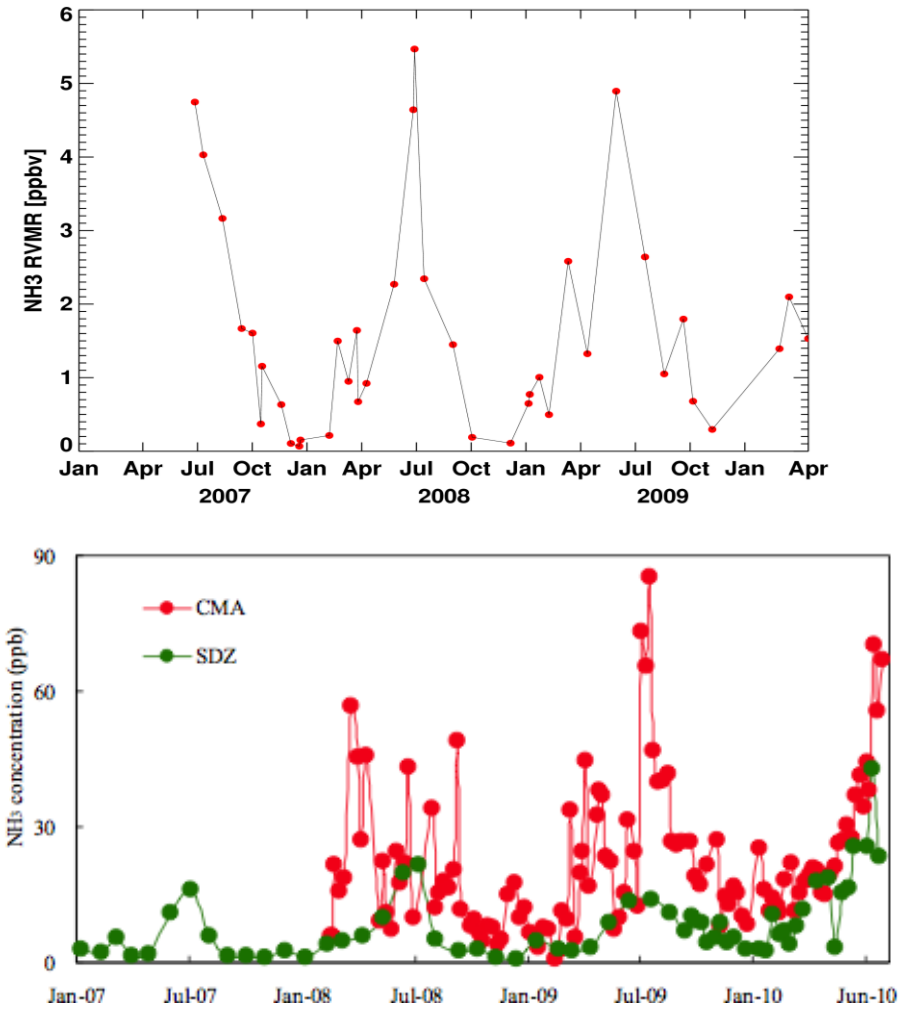


**Figure 14-3** Time series of $NH_3$ over Beijing from June 2007 through April 2010; TES RVMR (top); surface measurements (from Meng et al. (2011) (bottom)).

### 14.2.4 Bakersfield transects during CalNex

The San Joaquin Valley in California is a major agricultural center, producing a large fraction of America's fruit and vegetables; dairy farming is also important. This combination of activities leads to large production of ammonia (Clarisse et al., 2010), with concurrent impacts on air

quality, both in the valley and in surrounding regions, and on the ecosystems of the Sierra Nevada on its eastern side. These high $NH_3$emissions, along with warm and dry weather, make the San Joaquin Valley an ideal location for validation of $NH_3$ retrievals. As part of the California Nexus (CalNex) campaign in 2010 TES transects were carried out over the Central Valley, with a track right over Bakersfield (Figure 14-4, left), from late March through June. Monthly averages at each scan point (Figure 14-4, right) showed a strong spatial gradient, with the highest values north of Bakersfield, in the area around Tipton where there is intensive dairy farming. Of course this only demonstrates that TES can capture spatial variability in $NH_3$. A more quantitative evaluation of this capability was afforded by the $NH_3$ measurements collected on May 12, 2010 by the NOAA WP-3D aircraft, which flew along segments of the TES track (Figure 14-5, left) 300 m above the ground at 17:30 local time, measuring $NH_3$ measurements every 1 s. The aircraft $NH_3$ and the TES $NH_3$ obtained at 13:15 local time, (Figure 14-5, right) change in a consistent manner along the flight tracks: low values south of 34.7N, a small peak around 35N, a maximum at 36.1N for the aircraft and between 36.2N and 36.3N for TES. The offset between the aircraft and TES peak is possibly due to the difference in sampling time, but a more likely explanation is the distance between sampling points, which is around 11 km near the location of these peaks, sufficient distance for NH3 to vary significantly.

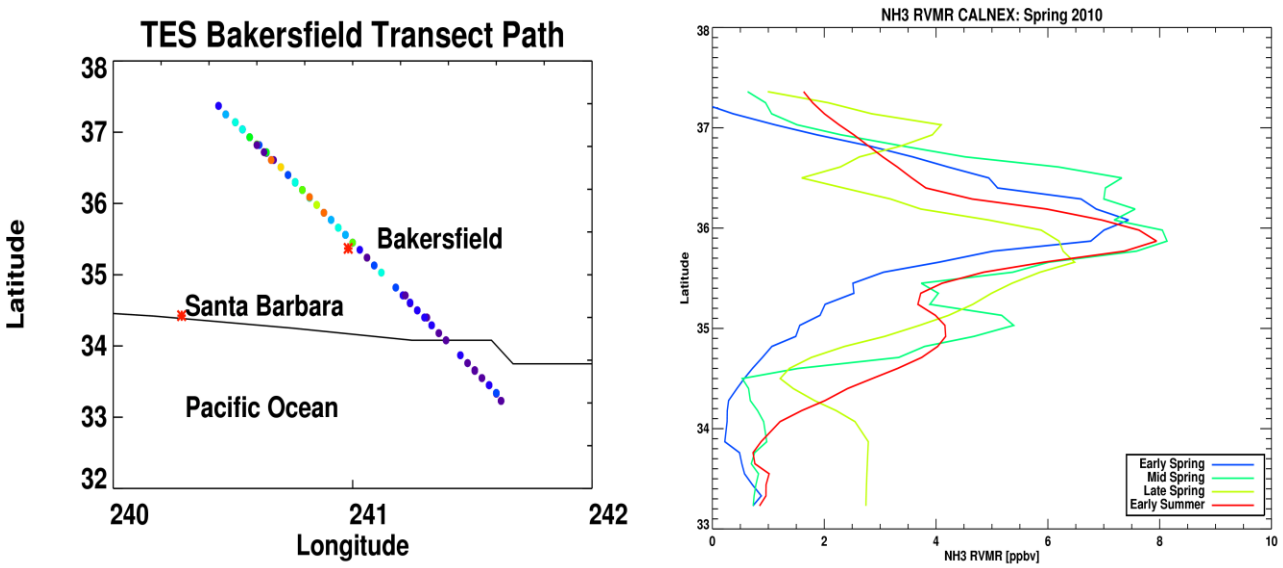


**Figure 14-4** Track of TES transects over Bakersfield during CalNex 2010 (left); 30 day means at each scan location of TES $NH_3$ (right).

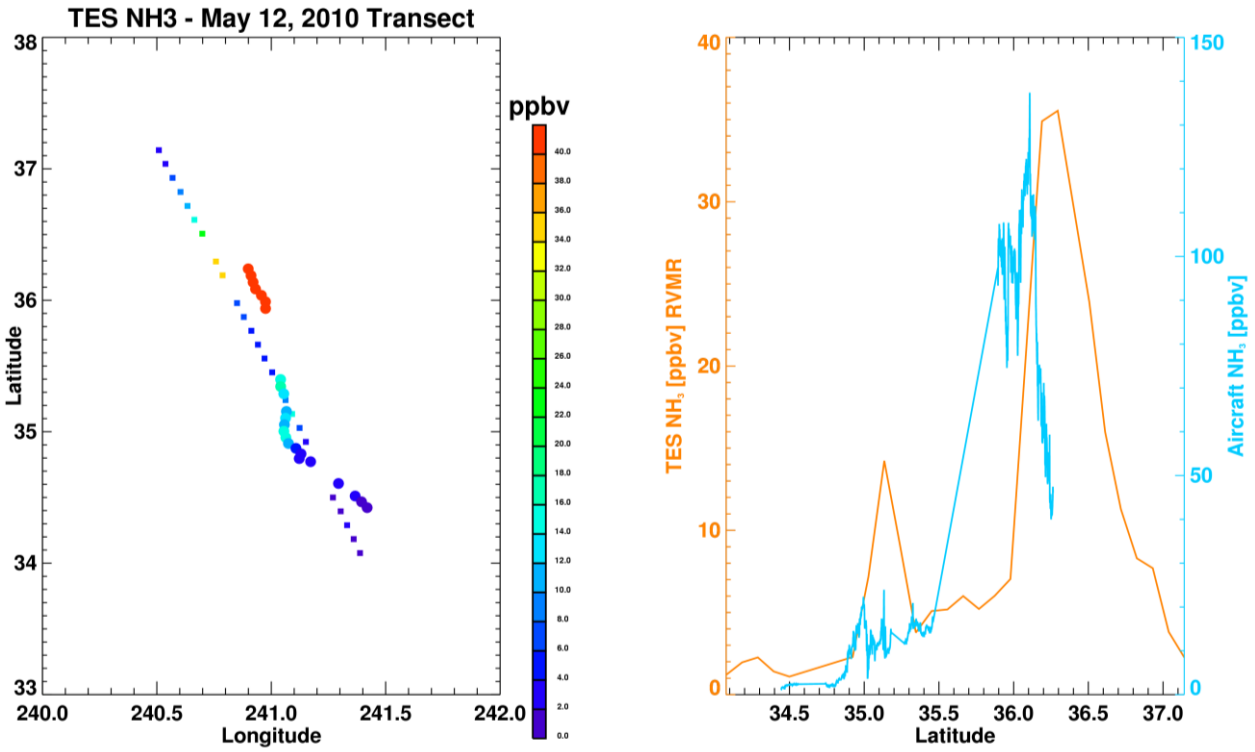


**Figure 14-5** TES $NH_3$ (squares) and aircraft (circles) $NH_3$ from the flights on May 12, 2010; TES data taken at 13:15 local time, aircraft data taken at 17:15 local time (left). TES and aircraft $NH_3$ as a function of latitude (right).

## 14.3 Conclusions

TES can detect spatial variability and seasonal trends in $NH_3$. The TES $NH_3$ signals appear well correlated with in situ measurements when averaged over time and/or space over regions with not ideal observing conditions, such as eastern China or North Carolina. When there are high concentrations, warm temperatures and few clouds, as in the San Joaquin Valley, it is possible to compare non-averaged TES signals with in situ measurements and show that both present similar spatial variability.

## 14.4 References

### 14.4.1 TES $NH_3$ references

[1] Beer, R., M.W. Shephard, S.S. Kulawik, , S.A. Clough, A. Eldering, K.W. Bowman, S.P. Sander, B.M. Fisher, V.H. Payne, M. Luo, G.B. Osterman, J.R. Worden (2008), First satellite observations of lower tropospheric ammonia and methanol, *Geophys. Res. Lett.*, *35*, L09801, doi:10.1029/2008GL033642, May 1, 2008.

[2] Clarisse, L., M.W. Shephard, F. Dentener, D. Hurtmans, K. Cady-Pereira, F. Karagulian, M. Van Damme, C. Clerbaux, P-F. Coheur (2010), Satellite monitoring of

ammonia: A case study of the San Joaquin Valley, J. *Geophys. Res., 115,* D13302, doi:10.1029/2009JD013291, July 10, 2010.

[3] Pinder, R.W., J.T. Walker, J.O. Bash, K.E. Cady-Pereira, D.K. Henze, M. Luo, G.B. Osterman, M.W. Shephard, Quantifying spatial and temporal variability in atmospheric ammonia with in situ and space-based observations (2011), *Geophysical Research Letters Vol. 38,* February 18, 2011.

[4] Shephard, M.W., K.E. Cady-Pereira, M. Luo, D.K. Henze, R.W. Pinder, J.T Walker, C.P. Rinsland, J.O. Bash, L. Zhu, V.H. Payne, L. Clarisse (2011), TES ammonia retrieval strategy and global observations of the spatial and seasonal variability of ammonia, *Atmos. Chem. Phys., 11,* 10743–10763, doi:10.5194/acp-11-10743-2011, October 31, 2011.

### 14.4.2 TES References

[5] Payne, V.H., S.A. Clough, M.W. Shephard, R. Nassar and J.A. Logan (2009), Information-centered representation of retrievals with limited degrees of freedom for signal: Application to methane from the Tropospheric Emission Spectrometer, *J. Geophys. Res., 114,* (doi:10:1029/2008JD010155) May 27, 2009.

### 14.4.3 General References

[6] Carmichael, G.R., M. Ferm, N. Thongboonchoo, J.H. Woo, L.Y.Chan, K. Murano, P.H. Viet, C. Mossberg, R. Bala, J. Boonjawat, P. Upatum, M. Mohan, S.P.Adhikary, A.B. Shrestha, J.J. Pienaar, E.B. Brunke, T. Chen, T. Jie, D. Guoan, L.C. Peng, S. Dhiharto, H. Harjanto, A.M. Jose, W. Kimani, A. Kirouane, J.P. Lacaux, S. Richard, O. Barturen, J.C.Cerda, A. Athayde, T. Tavares, J.S.Cotrina, E. Bilci (2003), Measurements of sulfur dioxide, ozone and ammonia concentrations in Asia, Africa, and South America using passive samplers, *Atmos. Environ., Vol. 37(9-10),* 1293–1308, doi:10.1016/S1352-2310(02)01009-9 September 10, 2003.

[7] Meng, Z.Y., W.L. Lin, X.M. Jiang, P. Yan, Y. Wang, Y.M. Zhang, X.F. Jia, and X.L. Yu (2011), Characteristics of atmospheric ammonia over Beijing, China, *Atmos. Chem. Phys., 11,* 6139-6151, 2011.

[8] Walker, J.T., D.R. Whitall, W. Robarge, and H.W. Paerl (2004), Ambient ammonia and ammonium aerosol across a region of variable ammonia emission density, *Atmos. Environ., Vol. 38(9),* 1235–1246, doi:10.1016/j.atmosenv.2003.11.027, 2004.

# Appendices

## A. Acronyms

| | |
|---|---|
| ACE | Atmospheric Chemistry Experiment |
| AER | Atmospheric and Environmental Research |
| AIRS | Atmospheric Infrared Sounder |
| AK | Averaging Kernel |
| AKVMR | Averaging Kernel weighted Volume Mixing Ratio |
| ALIAS | Aircraft Laser Infrared Absorption Spectrometer |
| AMSU | Advanced Microwave Sounding Unit |
| ASDC | Atmospheric Science Data Center |
| ARCIONS | Arctic Intensive Ozonesonde Network Study |
| ARCTAS | Arctic Research on the Composition of the Troposphere from Aircraft and Satellites |
| ARM | Atmospheric Radiation Measurement |
| ARM-SGP | Atmospheric Radiation Measurement – Southern Great Plains |
| ASHOE | Airborne Southern Hemisphere Ozone Experiment |
| AVE | Aura Validation Experiment |
| CalNex | California Nexus |
| CAMNET | Coordinated Air Monitoring NETwork |
| CASA | Carnegie Ames Stanford Approach |
| CFH | Cryogenic Frostpoint Hygrometer |
| $CH_4$ | Methane, Natural Gas |
| CMAQ | Community Multi-scale Air Quality |
| CO | Carbon Monoxide |
| $CO_2$ | Carbon Dioxide |
| CONTRAIL | CONdensation TRAIL |
| CR-AVE | Costa Rica Aura Validation Experiment |
| CTM | Chemical Transport Model |
| DACOM | Differential-Absorption Carbon Monoxide Monitor |
| DFM | Design File Memorandum |
| DOE | Department of Energy |

| | |
|---|---|
| DOF | Degrees of Freedom |
| DOFS | Degrees of Freedom for Signal |
| DPS | Data Products Specification |
| EOS | Earth Observing System |
| EPA | Environmental Protection Agency |
| ESDT | Earth Science Data Type |
| ESRL | Earth System Research Laboratory |
| FPH | Frost-Point Hygrometer |
| FTIR | Fourier Transform Infrared Spectrometer |
| FTP | File Transfer Protocol |
| FTS | Fourier Transform Spectrometer |
| GMD-ESRL | Global Monitoring Division of the Earth System Research Laboratory |
| GEOS | Global Earth Observing System |
| GEOS | Goddard Earth Observing System |
| GMAO | Global Modeling Assimilation Office |
| GSFC | Goddard Space Flight Center |
| GSI | Gridpoint Statistical Interpolation |
| GTS | Global Telecommunications Service |
| $H_2O$ | Dihydrogen Monoxide (Water) |
| HDF | Hierarchical Data Format |
| HDO | Hydrogen Deuterium Monoxide (“Heavy Water”) |
| HIAPER | High-Performance Instrumented Airborne Platform for Environmental Research |
| HIPPO | HIAPER Pole-to-Pole Observations |
| HIRDLS | High Resolution Dynamics Limb Sounder |
| HIRS | High Resolution Infrared Sounders |
| HIS | High-Resolution Interferometer Sounder |
| HITRAN | HIgh-resolution TRANsmission molecular absorption database |
| hPa | Hectopascal, a unit used for air pressure |
| HYSPLIT | Hybrid Single-Particle Lagrangian Integrated Trajectory |
| IDL | Interactive Data Language |
| IEEE | Institute of Electrical and Electronics Engineers |
| IGRA | Integrated Global Radiosonde Archive |

| | |
|---|---|
| INTEX | International Chemical Transport Experiment |
| IONS | INTEX Ozonesonde Network Study |
| ISM | Integrated Spectral Magnitude |
| JPL | Jet Propulsion Laboratory |
| K | Kelvin |
| L1B | Level 1B |
| L2 | Level 2 |
| LBLRTM | Line-by-Line Radiative Transfer Model |
| LT | Lower Troposphere |
| MACPEX | Mid-Latitude Airborne Cirrus Properties EXperiment |
| MATCH | Model of Atmospheric Transport and Chemistry |
| MISR | Multi-angle Imaging SpectroRadiometer |
| MLS | Microwave Limb Sounder |
| MODIS | Moderate Resolution Imaging Spectroradiometer |
| MOHAVE | Measurements of Humidity in the Atmosphere Validation Experiments |
| MOPITT | Measurement Of Pollution In The Troposphere |
| MOZAIC | Measurement of OZONE on Airbus In-service Aircraft |
| MOZART | Model for OZone And Related chemical Tracers |
| $N_2O$ | Nitrous Oxide |
| NASA | National Aeronautics and Space Administration |
| NCAR | National Center for Atmospheric Research |
| NCEP | National Centers for Environmental Prediction |
| NDACC | Network for the Detection of Atmospheric Composition Change |
| NESR | Noise Equivalent Spectra Radiance |
| NH | New Hampshire |
| $NH_3$ | Ammonia |
| NOAA | National Oceanic & Atmospheric Administration |
| $O_3$ | Ozone |
| OD | Optical Depth |
| OEM | Optimal Estimation Method |
| OMI | Ozone Monitoring Instrument |
| PAVE | Polar Aura Validation Experiment |

| | |
|---|---|
| PBL | Planetary Boundary Layer |
| PCS | Pointing Control System |
| PGE | Product Generation Executive |
| PI | Principal Investigator |
| PM | Particulate Matter |
| POLARIS | Photochemistry of Ozone Loss in the Arctic Region in Summer |
| QCLS | Quantum Cascade Laser Spectrometer |
| RMS, rms | Root-Mean-Square |
| ROI | Reynolds Optimally Interpolated |
| RTVMR | Representative Tropospheric Volume Mixing Ratio |
| RVMR | Representative Volume Mixing Ratio |
| Run ID | TES run identification number |
| SCIAMACHY | Scanning Imaging Absorption Spectrometer for Atmospheric Cartography |
| SGP | Southern Great Plains |
| SHADOZ | Southern Hemisphere Additional Ozonesondes |
| SO | Special Observation |
| SRF | Spectral Response Function |
| SST | Sea Surface Temperature |
| STRAT | Stratospheric Tracers of Atmospheric Transport |
| TATM | Temperature |
| TES | Tropospheric Emission Spectrometer |
| TOA | Top Of Atmosphere |
| TOPP | Tropospheric Ozone Pollution Project |
| TSUR | Surface Temperature |
| UT | Upper Troposphere |
| UTC | Universal Time Coordinated |
| VMR | Volume Mixing Ratio |
| WACCM | Whole Atmosphere Community Climate Model |
| WAVES | Water Vapor Validation Experiments |
| WOUDC | World Ozone and Ultraviolet Radiation Data Centre |
| WP-3D | Lockheed Research Aircraft used by NOAA |